

University of Southampton Research Repository

Copyright © and Moral Rights for this thesis and, where applicable, any accompanying data are retained by the author and/or other copyright owners. A copy can be downloaded for personal non-commercial research or study, without prior permission or charge. This thesis and the accompanying data cannot be reproduced or quoted extensively from without first obtaining permission in writing from the copyright holder/s. The content of the thesis and accompanying research data (where applicable) must not be changed in any way or sold commercially in any format or medium without the formal permission of the copyright holder/s.

When referring to this thesis and any accompanying data, full bibliographic details must be given, e.g.

Thesis: Michael Callum Thompson (2025) "Model Predictive Valve Control to Assist in Tracking a Lung Pressure Profile", University of Southampton, Faculty of Engineering and Physical Sciences (FEPS), School of Electronics and Computer Science (ECS), PhD Thesis, pagination.

Data: Michael Callum Thompson (2025), Model Predictive Valve Control to Assist in Tracking a Lung Pressure Profile.

UNIVERSITY OF SOUTHAMPTON

Model Predictive Valve Control to Assist in Tracking a Lung Pressure Profile

by

Michael Callum Thompson 

ORCID: 0000-0002-3254-6804

Supervisors: Prof. Christopher Freeman, Dr. Neil O'Brien, Dr. Ann-Marie
Hughes

A thesis submitted for the degree of Doctor of Philosophy

in the

Faculty of Engineering and Physical Sciences
School of Electronics and Computer Science


February 2025

UNIVERSITY OF SOUTHAMPTON

ABSTRACT

FACULTY OF ENGINEERING AND PHYSICAL SCIENCES
SCHOOL OF ELECTRONICS AND COMPUTER SCIENCE

Doctor of Philosophy

by Michael Callum Thompson 
ORCID: 0000-0002-3254-6804

In the UK, an estimated 88,000 people have a brain tumour, and typically are unaware of its presence until symptoms occur. Currently there is no mass screening available due to limitations in diagnostic techniques. Measuring changes in intracranial pressure could be revolutionary for diagnosing many cerebral pathologies. A strong link between intracranial and inner ear pressure is known to exist. Thus the indirect measurement of intracranial pressure, via tympanic membrane displacement, is a potential low-cost, accessible solution. However, natural physiological pressure fluctuations distort this association. Forced expiration during tympanic membrane displacement has the potential of reducing this distortion.

Lung pressure profiling is a recognised procedure in which a person generates specific lung pressures at specific times. These pressures are measured by using a hand-held breathing apparatus. A lung pressure profile reference is provided for a person to track during forced expiration. The pressures, and changes in pressures, when tracking the reference should result in corresponding changes in intracranial pressure. These intracranial pressure changes would be observed in tympanic membrane displacement. However, a person may not be able to accurately track the reference using the current clinical research breathing apparatus.

This thesis develops a solution to the tracking problem by assisting participants to precisely track pressure profile references, achieved by controlling airflow during forced expiration. This stabilises intrathoracic pressure, significantly reducing the physiological pressure fluctuations. The thesis develops and evaluates the first model to replicate a person's lung pressure profile tracking response. The airflow controller uses a novel model predictive control framework to adjust a model parameter in order to assist the person's tracking response. A clinically-feasible identification approach is then derived. Results with 10 participants confirm that lung pressure profile reference tracking is improved by an average of 22% compared to the current clinical research approach.

Contents

| | |
|---|-------------|
| Declaration of Authorship | xiii |
| Acknowledgements | xv |
| Abbreviations | xvii |
| Nomenclature | xix |
| 1 Introduction | 1 |
| 1.1 Research Aims and Objectives | 6 |
| 1.2 Contributions and Publications | 6 |
| 1.3 Thesis Structure | 7 |
| 2 Biological Background | 9 |
| 2.1 Introduction to Intracranial Pressure | 9 |
| 2.2 Intracranial Pressure, Blood Pressure and Lung Pressure Correlation . . . | 11 |
| 2.2.1 Afferent (Arterial) Flow | 12 |
| 2.2.2 Efferent (Venous) Flow | 13 |
| 2.3 Link between ICP and Lung Pressure | 15 |
| 2.4 Non-invasive Diagnostics using Tympanic Membrane Displacement | 17 |
| 2.5 Summary | 18 |
| 3 Respiratory Control Background | 19 |
| 3.1 Medical Ventilation | 19 |
| 3.2 Control Methods | 21 |
| 3.2.1 Proportional-Integral-Differential Control | 21 |
| 3.2.2 Fuzzy Logic Control | 22 |
| 3.2.3 Adaptive Control | 22 |
| 3.2.4 Iterative Learning Control | 23 |
| 3.2.5 Machine Learning Control | 24 |
| 3.2.6 Model Predictive Control | 25 |
| 3.2.7 Hybrid Control | 26 |
| 3.2.8 Application of Controllers to Lung Pressure Profile Testing | 27 |
| 3.3 Human Breathing Models | 30 |
| 3.3.1 Medical Imaging | 30 |
| 3.3.2 Gas Exchange | 31 |
| 3.3.3 Modelling using System Analogues | 33 |
| 3.3.3.1 Mechanical | 34 |

| | | |
|----------|---|-----------|
| 3.3.3.2 | Electrical | 35 |
| 3.3.4 | Application of Models to Lung Pressure Profile Testing | 38 |
| 3.4 | Summary | 39 |
| 4 | Problem Specification | 41 |
| 4.1 | Tympanic Membrane Displacement and Lung Pressure Measurements | 41 |
| 4.2 | Control During Lung Pressure Profile Testing | 42 |
| 4.2.1 | Specifications | 43 |
| 4.2.2 | Lung Pressure Profile Tests | 43 |
| 4.2.3 | Modified Experimental Setup | 45 |
| 4.3 | Controller and Model | 46 |
| 4.3.1 | Nested Loops | 48 |
| 4.4 | Summary | 49 |
| 5 | Model Predictive Valve Control using RLC Model Structure | 51 |
| 5.1 | Problem Description | 51 |
| 5.1.1 | Model Summary | 58 |
| 5.2 | Development of Model Predictive Valve Control | 58 |
| 5.2.1 | State-Space Model | 59 |
| 5.2.2 | State Estimation | 61 |
| 5.2.3 | Summary of Controller | 62 |
| 5.3 | Model Parameter Identification | 62 |
| 5.4 | Simulation Results and Discussion | 65 |
| 5.4.1 | Model Parameter Selection and Simulation | 65 |
| 5.4.2 | Control | 66 |
| 5.4.3 | Identification | 70 |
| 5.5 | Summary | 70 |
| 6 | Model Predictive Valve Control with Modified Model Structure | 73 |
| 6.1 | Problem Description | 73 |
| 6.1.1 | Forced Respiration Dynamics | 74 |
| 6.2 | Modified Model Predictive Valve Control (MPVC) | 78 |
| 6.3 | Modified Parameter Identification | 81 |
| 6.4 | Simulation Results and Discussion | 82 |
| 6.4.1 | Model Structure Selection and Simulation | 82 |
| 6.4.2 | Control | 84 |
| 6.4.3 | Identification | 86 |
| 6.5 | Experimental Application | 88 |
| 6.5.1 | Comparative Control Methods | 88 |
| 6.5.2 | Valve Control System | 90 |
| 6.5.3 | Procedure | 90 |
| 6.5.4 | Identification Data Collection | 91 |
| 6.5.5 | Control Application | 92 |
| 6.5.6 | Pressure Profiles | 93 |
| 6.6 | Practical Results and Discussion | 94 |
| 6.6.1 | Model Identification | 94 |
| 6.6.2 | Control | 97 |

| | |
|--|------------|
| 6.7 Summary | 102 |
| 7 Conclusions and Future Work | 105 |
| Appendix A Specification Document | 107 |
| Appendix B Conventional MPC Framework | 111 |
| References | 115 |

List of Figures

| | | |
|------|---|----|
| 1.1 | Cerebral Compliance | 2 |
| 1.2 | Reported deaths between 2001 and 2014 with deaths associated with neurological conditions | 3 |
| 1.3 | Percentage of deaths corresponding to neurological conditions | 3 |
| 1.4 | Clinical research apparatus | 5 |
| 2.1 | Cerebral Compliance (repeat of Figure 1.1) | 10 |
| 2.2 | Primary Blood vessels between lungs, heart and brain and thoracic pressure and heart compliance correlation | 12 |
| 3.1 | Clinical research apparatus (repeat of Figure 1.4a) | 20 |
| 3.2 | Fluidic/mechanical models of the lungs | 32 |
| 3.3 | Fluidic, mechanical, and electrical equivalent models | 34 |
| 3.4 | Electrical equivalent models of lung dynamics | 36 |
| 3.5 | Image of spirometry test | 38 |
| 4.1 | Clinical research apparatus (repeat of Figure 1.4a) | 44 |
| 4.2 | Examples of lung pressure profile tracking using the current clinical setup | 45 |
| 4.3 | Modified apparatus for this thesis | 46 |
| 5.1 | Simple block diagram of control and model tracking system | 52 |
| 5.2 | Closed loop system of respiratory pressure control dynamics | 53 |
| 5.3 | Fluidic model and electrical equivalent circuit to model respiratory pressure control dynamics | 54 |
| 5.4 | Mesh analysis circuit of electrical equivalent circuit | 55 |
| 5.5 | Lung pressure profile tracking system with controller and Kalman Filter | 62 |
| 5.6 | Simulated tracking response with no valve assistance | 66 |
| 5.7 | Simulated step tracking response comparing MPVC with no valve assistance | 67 |
| 5.9 | Colour map showing tracking error norm as a function of prediction horizon and number of possible resistance values | 69 |
| 5.10 | MPVC compared to non-assisted system tracking of a square wave reference | 69 |
| 5.11 | Simulated tracking response with no valve assistance with identified model comparison | 71 |
| 5.12 | Simulated model response with added noise compared to identified model response | 72 |
| 6.1 | Modified electrical equivalent circuit model | 75 |
| 6.2 | Modified closed-loop system dynamics | 76 |

| | | |
|------|--|----|
| 6.3 | Lung pressure profile with modified tracking system, controller, and Kalman Filter | 80 |
| 6.4 | Modified model simulations | 84 |
| 6.5 | Modified model simulations 2 | 85 |
| 6.6 | Modified controller simulation | 86 |
| 6.7 | Identification without noise results | 87 |
| 6.8 | Identification with minor noise results | 87 |
| 6.9 | Identification with moderate noise results | 88 |
| 6.10 | Resistance-tuning controller | 90 |
| 6.11 | Experimental lung pressure profile tracking response result | 94 |
| 6.12 | Experimental identification results | 95 |
| 6.13 | Model fitting accuracies results | 96 |
| 6.14 | Model comparison and control results | 98 |
| 6.15 | Control results | 99 |

List of Tables

| | | |
|-----|--|-----|
| 3.1 | Comparison of control methods | 28 |
| 3.2 | Fluidic, mechanical, and electrical equivalent parameters generalised to $\psi = R\zeta$ | 34 |
| 3.3 | Comparison of lung models | 39 |
| 4.1 | Specifications | 43 |
| 6.1 | Table of medians and means from the metrics in Figures 6.15a-6.15e . . . | 100 |
| 6.2 | Table of ranges and number of data points, with outliers in brackets, from the metrics in Figures 6.15a-6.15e | 101 |

Declaration of Authorship

I, Michael Callum Thompson, declare that this thesis titled “Model Predictive Valve Control to Assist in Tracking a Lung Pressure Profile” and the work and results presented in this thesis are my own, and have been generated by me as the result of my original research. I confirm that:

1. this work was done wholly or mainly while in candidature for a research degree at this University;
2. where any part of this thesis has previously been submitted for a degree or any other qualification at this University or any other institution, this has been clearly stated;
3. where I have consulted the published work of others, this is always clearly attributed;
4. where I have quoted from the work of others, the source is always given. With the exception of such quotations, this thesis is entirely my own work;
5. I have acknowledged all main sources of help;
6. where the thesis is based on work done by myself jointly with others, I have made clear exactly what was done by others and what I have contributed myself;
7. parts of this work have been published in: [1], [2], and [3](submitted)

Signed:.....

Date:.....

Acknowledgements

My supervisor throughout has been Professor Christopher Freeman; his unfailing continuous support and encouragement at all times have been of inestimable value. My deepest thanks are due to him.

I acknowledge the help given to me by the following people and thank each of them most sincerely.

Drs Ann-Marie Hughes, Neil O'Brien, Robert Marchbanks and Anthony Birch for their guidance, advice and expert knowledge.

A big thanks to all participants for giving up their time in order to further the understanding of control in lung pressure profile testing.

My thanks are due to friends who have supported me throughout these four years of great highs and lows.

The financial support of the Engineering and Physical Sciences Research Council is gratefully acknowledged.

To everyone who had even the smallest influence upon my work I thank you for helping make this all possible.

A special thanks to my family, in particular Dr Isobel Vincent for her editorial skills and her great care and patience throughout.

Abbreviations

| | |
|--------------|--|
| <i>ICP</i> | Intracranial pressure |
| <i>CSF</i> | Cerebrospinal fluid |
| <i>CT</i> | Computed tomography |
| <i>MRI</i> | Magnetic resonance imaging |
| <i>TCD</i> | Transcranial doppler ultrasonography |
| <i>TMD</i> | Tympanic membrane displacement |
| <i>UHS</i> | University Hospital Southampton |
| <i>CCFP</i> | Cerebral and cochlear fluid pressure analyser |
| <i>LPP</i> | Lung pressure profile |
| <i>MPC</i> | Model predictive control |
| <i>CBF</i> | Cerebral blood flow |
| <i>VM</i> | Valsalva manoeuvre |
| <i>CPP</i> | Cerebral perfusion pressure |
| <i>MAP</i> | Mean arterial pressure |
| <i>CVP</i> | Central venous pressure |
| <i>ITD</i> | Impedance threshold device |
| <i>IJV</i> | Internal jugular veins |
| <i>PID</i> | Proportional-integral-differential |
| <i>ILC</i> | Iterative learning control |
| <i>PI</i> | Proportional-integral |
| <i>RC</i> | Resistor-capacitor |
| <i>RIC</i> | Resistor-inductor-capacitor |
| <i>PWM</i> | Pulse-width modulation |
| <i>LTi</i> | Linear time-invariant |
| <i>LTV</i> | Linear time-variant |
| <i>MPVC</i> | Model predictive valve control |
| <i>ARMAX</i> | Auto-regressive moving average exogenous model |
| <i>LPV</i> | Linear parameter varying |
| <i>MFA</i> | Model fitting accuracy |

Nomenclature

Chapter 5 Nomenclature

| | |
|----------------------------------|---|
| r | Pressure profile reference (cmH ₂ O) |
| y | Measured output (cmH ₂ O) |
| V | Valve resistance (cmH ₂ O/L/s) |
| k | Sample instant |
| G | Dynamics of respiratory tract/breathing apparatus |
| $K(q)$ | Diaphragm/intercostal dynamics |
| $H(q)$ | Motor control feedback |
| q | Sample shift operator |
| w | External noise |
| $F(q)$ | Noise filter |
| Q | Airflow (L/s) |
| P | Pressure (cmH ₂ O) |
| R | Airway resistance (cmH ₂ O/L/s) |
| L | Airway inertance (cmH ₂ O/L/s ²) |
| C_a | Lung compliance (L/cmH ₂ O) |
| T_s | Sampling time (s) |
| e | Tracking error |
| J | Stage cost |
| N | End time instance |
| Q_i/R_i | Model predictive control cost weights |
| \mathcal{V} | Set of admissible valve apertures |
| A_k, B_k, C_k, D_k | System state-space matrices |
| $\{a_i, \bar{a}_i, b_i\}$ | Fixed coefficients of dynamics |
| $\{\sigma_i, \varpi_i, \chi_i\}$ | Fixed coefficients of dynamics |
| \hat{x} | State vector estimate |
| M | Kalman gain matrix |
| S | State error covariance matrix |
| I | Identity matrix |
| R_m | Measurement noise covariance |
| Q_p | Process noise covariance |
| $^\top$ | Matrix transpose |

| | |
|--|---|
| v | Filtered external noise |
| $\{\alpha_i, \bar{\alpha}_i, \beta_i\}$ | Fixed coefficients of dynamics |
| θ | Identification parameter vector |
| $\{\tilde{r}_i, \tilde{y}_i\}_{i=1, \dots, N}$ | Sampled experimental input-output data |
| $\{p_i, \bar{p}_i, c_i, h_i\}$ | Fixed scalar coefficients |
| m | Prediction horizon |
| $ \mathcal{V} $ | Number of possible values of V in set \mathcal{V} |

Chapter 6 Nomenclature

| | |
|----------------------------------|--|
| K | Diaphragm/intercostal dynamics |
| G | Dynamics of respiratory tract/breathing apparatus |
| r | Pressure profile reference (cmH ₂ O) |
| t | Continuous time variable |
| P | Pressure measured across the valve (cmH ₂ O) |
| T | End time (continuous)(s) |
| V | Valve resistance (cmH ₂ O/L/s) |
| P_l | Pressure generated by the respiratory muscles (cmH ₂ O) |
| Q | Airflow (L/s) |
| H | Feedback dynamics |
| FP | Feed-forward predictive dynamics |
| V_{max} | Maximum valve resistance (cmH ₂ O/L/s) |
| V_{min} | Minimum valve resistance (cmH ₂ O/L/s) |
| A_K, B_K, C_K, D_K | State-space matrices of K dynamics |
| A_H, B_H, C_H, D_H | State-space matrices of H dynamics |
| $A_{FP}, B_{FP}, C_{FP}, D_{FP}$ | State-space matrices of FP dynamics |
| R | Airway resistance (cmH ₂ O/L/s) |
| C_a | Lung compliance (L/cmH ₂ O) |
| L | Airway inertance (cmH ₂ O/L/s ²) |
| A_G, B_G, C_G, D_G | State-space matrices of G dynamics |
| T_s | Sampling time frequency in discrete time (s) |
| x_G | State vector of G dynamics |
| k | Sample instant (discrete time) |
| I | Identity matrix |
| N | End time (discrete) |
| $A_{KG}, B_{KG}, C_{KG}, D_{KG}$ | State-space matrices of KG dynamics |
| $A_{cl}, B_{cl}, C_{cl}, D_{cl}$ | Closed-loop state-space matrices |
| \bar{V} | Sequence of valve resistance values (cmH ₂ O/L/s) |
| J | Model predictive valve control cost |
| P_{max} | Maximum pressure generated across the valve (cmH ₂ O) |

| | |
|----------------|---|
| vc | Vital capacity (L) |
| \mathcal{V} | Set of valve resistances for controller to select (cmH ₂ O/L/s) |
| Φ | Model predictive control weighting coefficient |
| Ψ | Model predictive control weighting coefficient |
| m | Predictive control horizon |
| \hat{x} | Estimated state-space |
| M | Kalman gain matrix |
| S | State error covariance matrix |
| λ_m | Measurement noise covariance matrix |
| \top | Matrix transpose |
| μ_p | Process noise covariance matrix |
| $\bar{\Phi}$ | Φ multiplied by identity matrix |
| $\bar{\Psi}$ | Ψ multiplied by identity matrix |
| Γ | State prediction matrix |
| Ξ | Input prediction matrix |
| γ | State prediction matrix variable |
| ξ | Input prediction matrix variable |
| \tilde{V} | Valve resistance sequence (cmH ₂ O/L/s) |
| \tilde{r} | Sample reference sequence (cmH ₂ O) |
| θ | Parameter vector |
| K_p | Respiratory proportional control coefficient |
| K_i | Respiratory integral control coefficient |
| $\hat{\theta}$ | Identification parameter vector |
| R | Airway resistance (cmH ₂ O/L/s) |
| e | Lung pressure profile tracking error (cmH ₂ O) |
| e_Q | Valve resistance airflow error (L/s) |
| V_{e0} | Resistance offset (cmH ₂ O/L/s) |
| K_{pe} | Proportional coefficient of valve controller |
| K_{ie} | Integral coefficient of valve controller |
| k_{ec} | Sample instant when error changes sign for controller |
| κ | Proportional current gain coefficient of valve resistance-tuning controller |
| ρ | Pulse-width modulation duty cycle signal |
| K_v | Valve flow coefficient |
| η | Static non-linear function of $\kappa\rho$ |
| Q_r | Desired flow rate of valve (L/s) |
| \tilde{Q} | Measured airflow through valve (L/s) |
| K_ρ | Proportional control loop gain for valve resistance-tuning controller |

| | |
|------------|--|
| r_{id} | Identification reference value (cmH ₂ O) |
| V_{id} | Identification valve resistance value(cmH ₂ O/L/s) |
| Δr | Lung pressure profile minimum reference change (cmH ₂ O) |

Chapter 1

Introduction

Pressures in various parts of the human body can be measured and provide useful indicators of health. One of the most common is blood pressure, but other examples include the eye, bladder, middle ear, and the thoracic cavity. There is a dynamic interplay between these various body pressures, for example, both respiratory and circulatory pressures can impact intracranial pressure (ICP), i.e. the pressure within the skull. A simple example to demonstrate how respiratory, circulatory, and brain pressures are linked is the action of standing up quickly from sitting or lying down, which may briefly cause lightheadedness. This sensation quickly subsides as the dynamic pressures and blood flow to the brain readjust to the new body position.

The smooth functioning of such homeostatic mechanisms are compromised by pathologies such as tumours or haemorrhages. In the case of intracranial pathologies the effects on normal ICP can be catastrophic due to the rigid nature of the skull.

ICP must remain in a balanced state: too high a pressure and the brain tissue, blood vessels, and nerves will be dangerously compressed; too low a pressure and cells and capillaries may collapse. High and low cranial pressures have similar symptoms in that the person can experience headaches, dizziness and in some cases visual problems and nausea. Both, in more extreme cases, can lead to a stroke/ischemic event, where blood supply is cut off to parts of the brain causing permanent tissue damage if not dealt with quickly.

ICP is able to remain consistent due to physical mechanisms that alter the pressure dynamics of the intracranial space. This is facilitated by blood flow regulation both in and out of the brain as well as volume control of the cerebrospinal fluid (CSF). These are controlled to maintain pressure balance whilst still providing adequate oxygen, electrolytes, and protection for the brain to function optimally. If, for example, a brain tumour is small, these mechanisms are able to maintain normal ICP by expelling blood and CSF from the intracranial cavity. However, when the tumour becomes too large

these mechanisms break down and ICP rises (see Figure 1.1).

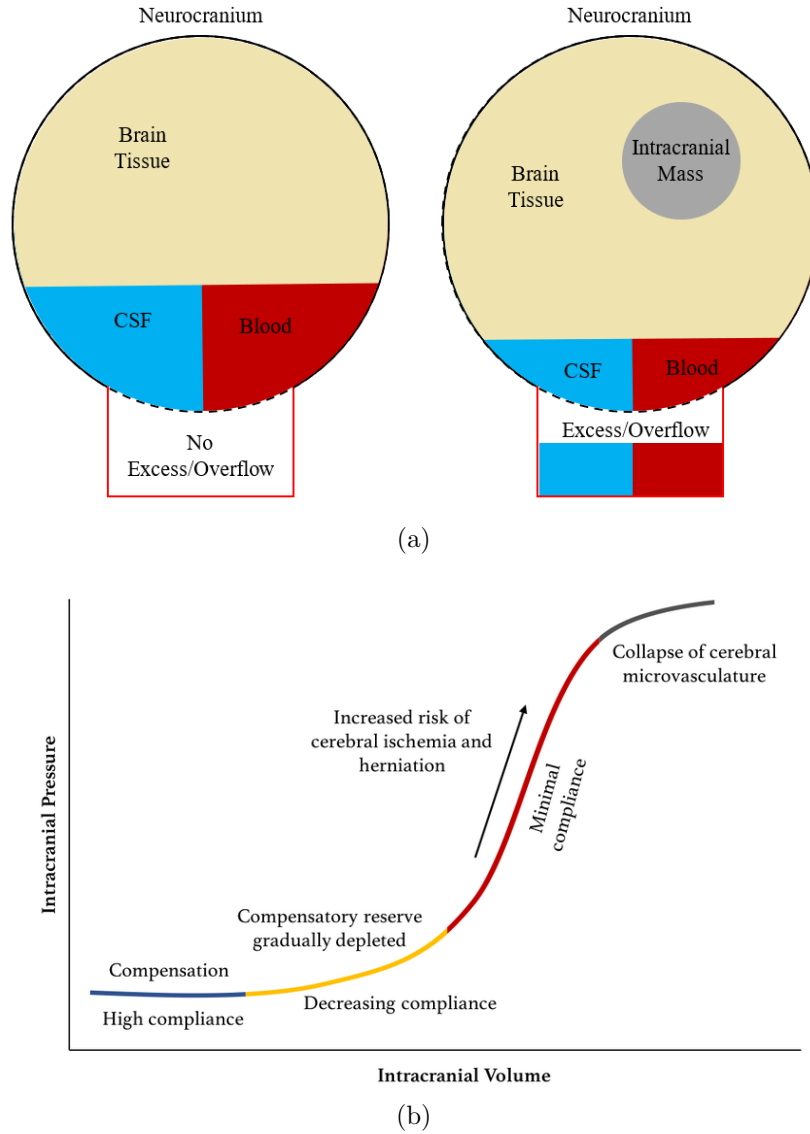


Figure 1.1: (a) Diagram showing how an intracranial mass (such as a tumour) causes CSF and blood to drain into the lymphatic or venous systems respectively due to auto-regulatory mechanisms
 (b) Graph showing how ICP changes with intracranial volume (i.e. intracranial mass size) [4].

Between 2001 and 2014 there were 366,728 deaths reported in people aged 20 and over, with a neurological condition stated as a cause of death [5]. The number of deaths steadily increased year on year, from 23,051 in 2001 to 31,925 in 2014. The trend in deaths related to neurological conditions is counter to the trend for all-cause deaths, which have fallen by 6%. Neurological deaths in 2014 accounted for 7% of overall deaths in England. Of the 366,728 deaths recorded, 74,725 deaths were related specifically to cranial tumours. Figures 1.2 and 1.3 show the statistical graphs of all neurological

conditions in the time period of 2001 and 2014. These data show that neurological conditions are a significant cause of death in the UK.

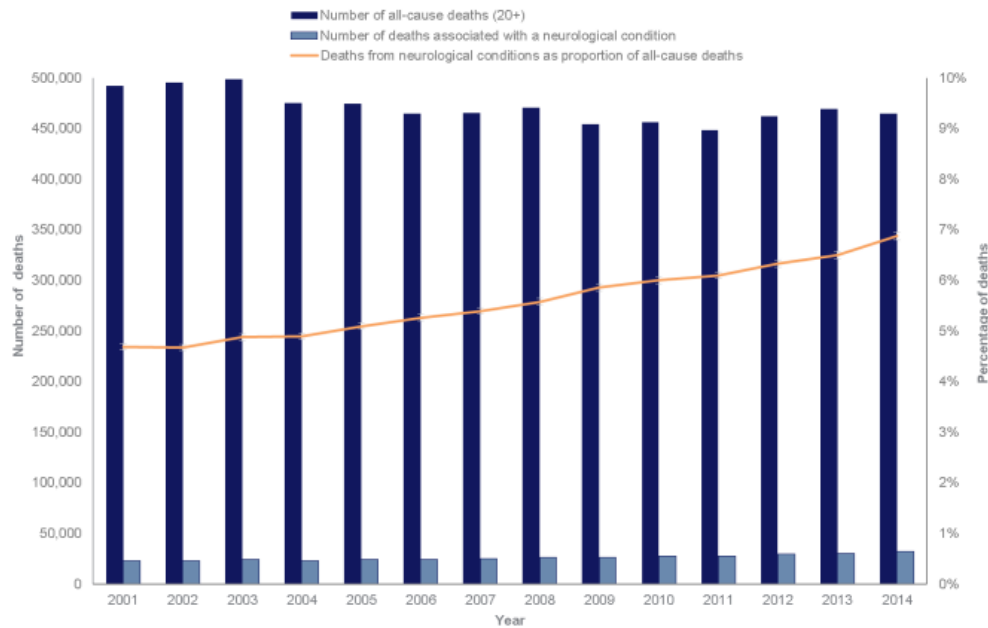


Figure 1.2: Recorded deaths, persons aged 20 and over, England, 2001 to 2014 [5].

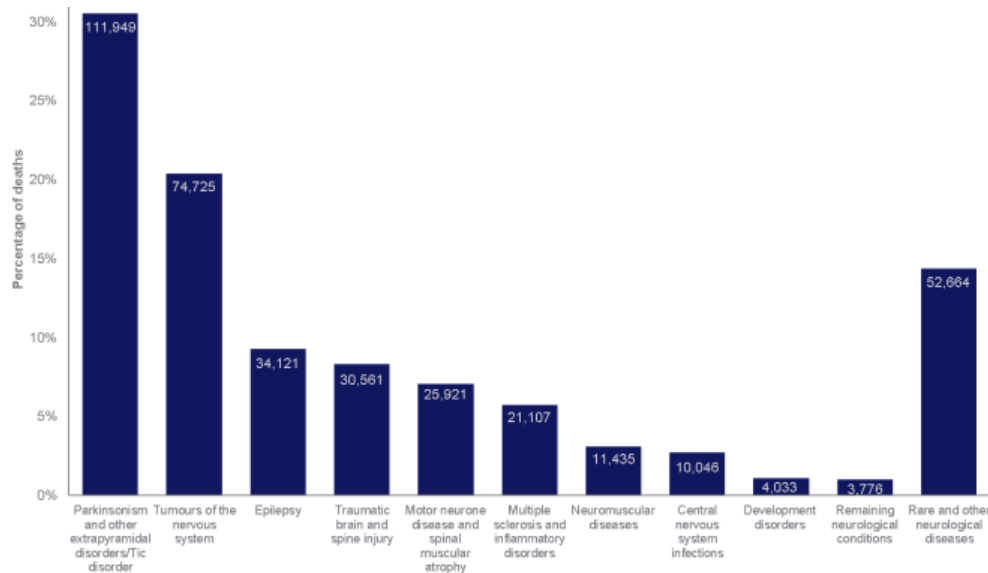


Figure 1.3: Proportion and number of all deaths associated with a neurological conditions groups, persons aged 20 and over, England, 2001 to 2014.

Note: Some people can have more than one neurological condition mentioned; they will therefore be counted in more than one of the presented groups [5].

Research is constantly revolutionising medicine in areas such as diagnostics. In 1971 the first computed tomography (CT) imaging scan of a patient's brain was performed

resulting in a huge step forward in medicine and diagnostics. It provided the first images of the brain without the need to perform invasive surgery. In the early 1980s magnetic resonance imaging (MRI) scans were introduced. MRI scans provide better observation of soft tissue and do not use ionising radiation like CT scans, so are considered safer. Diagnostic tools and procedures are constantly evolving, but very few of these have easy patient accessibility and still require a referral from a general practitioner (GP).

So, the next step in medical diagnostics technology for brain pathologies would be to develop more accessible and user-friendly tools. Methods to measure ICP are very accurate but are mostly invasive such as cranial bolt, intraventricular catheter and subdural/epidural sensors. These methods are highly accurate because they directly measure intracranial pressure. Non-invasive methods (indirect) include Transcranial Doppler Ultrasonography (TCD), MRI/CT scans and Ultrasound-Guided Eyeball Compression. TCD measures blood flow velocities, changes in the velocity can indicate changes in ICP; MRI/CT scans can provide indirect measurements/estimates of ICP based on the intracranial compliance; and eye compression applies gentle pressure to the eye and measures the response using ultrasound to estimate ICP. However, these techniques can only provide estimates for ICP, or have lower patient accessibility. The more accessible tools have to be used in conjunction with other tools in order to diagnose intracranial pathologies.

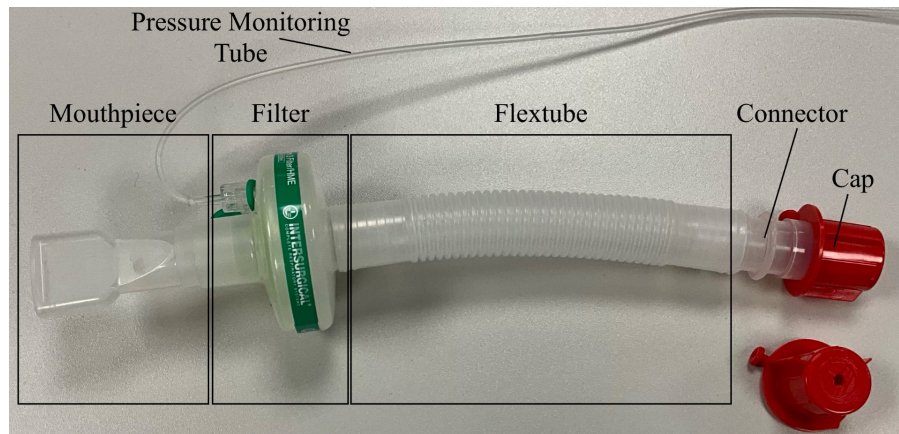
Tympanic membrane displacement (TMD) was first proposed in 1980 as a procedure that could be used to indirectly measure ICP by a team at University Hospital Southampton (UHS). TMD measures very small movements of the eardrum caused by an audio stimulus. The magnitude and direction of these movements are influenced by the pressure in the middle ear, which in turn reflects the pressure in the intracranial space (i.e. ICP), as the middle ear and intracranial space are connected via the cochlear aqueduct and other pathways. Over the last 40 years research has looked at how different criteria affect TMD measurements, from sitting posture to respiration and blood pressure (see Section 2.4). These natural variations in body pressure, although observable and identifiable in TMD, lower the precision to be able to directly relate the displacement to ICP.

Blood pressure varies in response to cardiac output (i.e. the volume of blood the heart pumps through the circulatory system) and can change based on oxygen supply. This means breathing and airway pressures alter cardiac output. During inhalation, airway pressure builds up and cardiac output increases in response to the renewal of oxygen in the lungs. Similarly, during exhalation, cardiac output decreases. Venous blood from the brain has very little resistance during its return to the heart. This means cerebral venous blood pressure (i.e. the venous blood pressure in the brain) and corresponding venous pressures in the neck down to the superior vena cava and the heart, can be used as a determining factor for ICP. Specific lung pressure and sitting postures can have a significant affect on venous blood pressure and thus ICP. This leads to the possibility

of measuring specific lung pressures to study venous return from the brain and, more significantly, ICP.

This programme of research has been carried out under the supervision of a team at UHS whose research has focused on venous return, ICP, and lung pressure measurements. One of their current projects is looking into measuring TMD using a cerebral and cochlear fluid pressure (CCFP) analyser whilst also measuring specific lung pressures. Lung pressure profile (LPP) tests require a patient to accurately follow a pressure reference by forced expiration through a breathing tube. The aim of this dual approach is to clarify the causal link between changes in lung pressure and changes in inner ear pressure, and thus ICP.

The current clinical research setup used for LPP testing is shown in Figure 1.4. The red cap has an orifice for consistent air leakage to prevent patient glottis closure. The cap can be completely removed to assist the patient in attaining a rapid pressure drop at the end of a LPP test.



(a)



(b)

Figure 1.4: (a) Clinical research apparatus for lung pressure profile testing
(b) Image showing the setup to measure lung pressure while patient follows a pressure reference.

1.1 Research Aims and Objectives

It is not possible for a patient to always achieve accurate pressure reference tracking with the currently available clinical research breathing apparatus. It is therefore the aim of this thesis to develop and evaluate an improved system to control airway pressure during LPP testing. This will enable more accurate tracking of pressure references, thereby improving analysis of TMD measurements. This will be achieved by replacing the manual cap removal method with a proportional valve to precisely control air flowing from the tube. An automatic control method is required to actuate the valve to facilitate tracking. Since maximum accuracy is crucial in this application, the control scheme requires a model of the underlying system. Lung modelling techniques must therefore be developed to replicate the human response during LPP reference tracking. Finally, identification methods are required to find the associated parameters, and must be suitable for clinical deployment.

The main objectives for this research can therefore be summarised as follows:

- To determine a mathematical model that can accurately replicate a human response - this allows a controller to be designed that is capable of prediction to improve LPP reference tracking accuracy. A simpler model means fewer parameters and thus reduces the possibility of over-fitting during identification;
- To establish an identification technique that calculates the model parameters using data sets collected before experimental application - each patient will naturally have different model parameters and so will require a bespoke controller to provide optimal assistance;
- To create a controller that can regulate the resistance of the system - most controllers provide an input to a system in order to influence the output. However, the resistance of the system is a direct parameter of the system model meaning a novel method of control must be developed.

1.2 Contributions and Publications

The contributions of this programme of research are as follows:

- A model of the human respiratory system during forced expiration incorporating the physiological parameters of the lungs and airways (i.e. resistance, inertance, and compliance), the diaphragm and intercostal muscle dynamics, and voluntary motor control feedback;

- A control methodology, using a model predictive control framework, which manipulates the resistance of a proportional valve in order to assist a patient during LPP reference tracking;
- An identification procedure that is efficient and easy to use for clinical application which identifies the model parameters that best fit a set of measured input and output data.

In this thesis, two attempts are made, for the first time, at modelling human respiratory pressure control:

- The first provides a mathematical model that solely relies on the assumption that passive electrical equivalent circuit components could be used to replicate a person's response to a LPP. This showed excellent reproducibility in simulation to identify parameters of a noiseless tracking response but struggled when process noise was added;
- The second adapts the above model with the addition of a variable driving force (variable voltage equivalent to human respiratory muscle control) with internal control components that could be identified from measured data. This shows promising results with both a noiseless and a noisy tracking response and as such was used in a controlled practical environment on 10 participants.

Technical results from this thesis will appear in the following publications:

- M. C. Thompson, C. T. Freeman, N. O'Brien, A.-M. Hughes, T. Birch and R. Marchbanks, "Model predictive valve control of lung pressure profile tracking," in *2022 Australian & New Zealand Control Conference (ANZCC)*, pp. 132–137, IEEE, 2022.[1]
- M. C. Thompson, C. T. Freeman, N. O'Brien, A.-M. Hughes, R. Marchbanks, and A. Birch, "Model predictive valve control for lung pressure profile tracking assistance," in *2024 IEEE Conference on Control Technology and Applications (CCTA)*, pp. 624–630, IEEE, 2024.[2]
- M. C. Thompson, C. T. Freeman, N. O'Brien, A.-M. Hughes, T. Birch and R. Marchbanks, "Model Predictive Valve Control to Assist Lung Pressure Profile Tracking," in *IEEE Transactions on Control Systems Technology*, 2025. (accepted for publication).[3]

1.3 Thesis Structure

Chapter 2 reviews literature confirming a correlation between ICP and lung pressure, suggesting that measuring lung pressure could provide useful data and its effects on

TMD. Chapter 3 reviews literature applying control methods that have been employed for medical ventilation and compares their strengths and weaknesses. It then reviews literature related to modelling of lung dynamics and compares the different models proposed and how and why they were used based on their key features.

Motivated by the paucity of research investigating the effects of controlling airflow during LPP tests, Chapter 4 discusses the current setup used for clinical research and the ways in which this thesis adapts it to improve the quality of patient LPP reference tracking.

Chapter 5 presents a novel model concept which combines lung physiology, voluntary muscle dynamics and feedback to replicate a human response to a LPP test whilst integrating a variable resistance valve. This model relies on the passive electrical equivalent circuit component dynamics to form a basic model of respiratory control. A control concept is presented applying model predictive control (MPC) of airflow by actuating a proportional valve. An identification technique is proposed to accurately and efficiently produce valid parameters for the controller based on initial reference tracking data. It compares the tracking ability of the controlled system model to an non-assisted system in simulation.

Chapter 6 modifies the model with the addition of a variable driving force (i.e. dynamic human respiratory pressure control). The controller is adapted to rely more on the pressure control of the person during LPP tests and only assists at significant points. The identification is modified to a more general solution which does not assume any form of the noise. Simulation results validate the model, controller, and identification procedure. Experimental studies were performed with 10 healthy participants. The ability of each of the following is demonstrated:

- the model to replicate a human response to a LPP test;
- the identification procedure to provide accurate model parameters;
- the controller to improve the tracking abilities of the participants.

Chapter 7 outlines the key findings from a more holistic point of view and discusses the challenges and considerations for future work to expand upon this research.

Chapter 2

Biological Background

This chapter introduces the biological background that underpins this thesis and motivates the research. It introduces intracranial pressure (ICP) and explains why it is an important biological indicator and how it is influenced by some of the body's key processes. In particular, it is closely associated with pulmonary pressure generated during forced expiration. The challenges of measuring ICP are investigated and the paucity of non-invasive methods is highlighted. A potential solution is described and it is shown how control of lung pressure holds the key for a future non-invasive solution.

2.1 Introduction to Intracranial Pressure

The neurocranium is the part of the skull that encases and protects the brain; by the very nature of its rigidity, its capacity is fixed. The neurocranial constituents comprise the parenchyma, cerebrospinal fluid (CSF), and intracerebral blood (roughly 80%, 8% and 12% respectively). Parenchyma, in this case, refers to all of the brain tissue including grey and white matter, dura mater, and blood vessel tissue. The CSF surrounds the brain and provides protection and cushioning, as well as providing and removing metabolites.

The Monro-Kellie doctrine [6, 7] states that the total volume of these constituents is homeostatically regulated. The fixed capacity of the skull means that if the volume increases or decreases, the pressure (i.e. ICP) will also increase or decrease concomitantly. The ability to adjust neurocranial constituent volume is known as cerebral compliance. This is achieved using homeostatic mechanisms which maintain ICP within a physiologically safe range (7-15 mmHg [8]). These mechanisms drain CSF and blood from the neurocranium to ensure the brain tissue does not get compressed [9]. ICP must remain consistent, as high or low pressures (possibly caused by a significant change in the physiology of the brain, such as a tumour or haemorrhage) can be life-threatening if untreated (see Figure 2.1).

Figure 2.1a is a simple depiction of how blood and CSF can be displaced from the neurocranium in response to the emergence of an abnormal intracranial mass (e.g. tumour). The blood and CSF are drained via the venous system and the spinal cord respectively. The drainage means that ICP is minimally affected thus avoiding possible issues from hypertension. Figure 2.1b shows how these drainage mechanisms help to maintain a consistent ICP; compensatory reserve refers to the volume of blood and CSF that can be safely drained without consequences. As the tumour increases in volume, more blood and CSF are drained. At a certain point, no more blood/CSF can be drained without causing damage to the brain due to lack of oxygen supply. The remaining non-fluid contents of the neurocranium cannot be drained (i.e. the parenchyma and the tumour) and therefore ICP will increase (as the tumour grows). Eventually, a high enough pressure can cause herniation, strokes, etc.

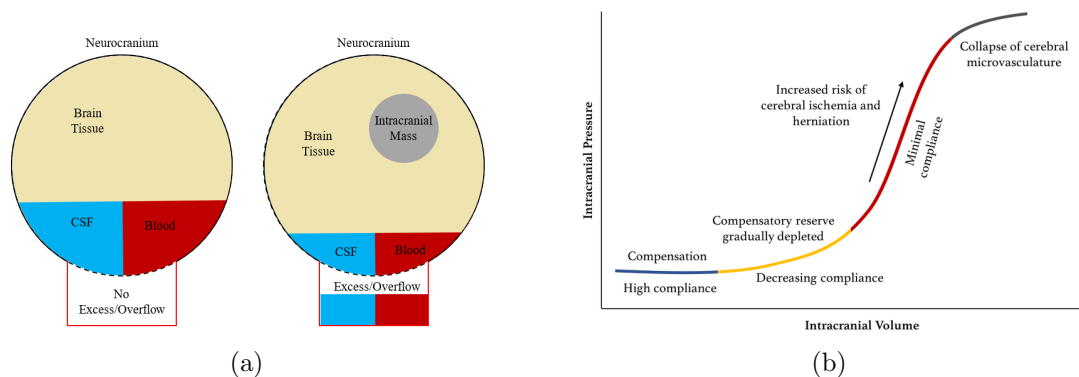


Figure 2.1: (a) Diagram showing how an intracranial mass (such as a tumour) causes CSF and blood to drain into the lymphatic or venous systems respectively due to auto-regulatory mechanisms
(b) Graph showing how ICP changes with intracranial volume (repeat of Figure 1.1).

There is roughly the same volume of blood in the intracranial cavity as there is CSF (~100-130ml). CSF can be relatively quickly moved around and, in the case of increased ICP, is diverted from the brain and into the spinal cord. Over time it is reabsorbed to relieve the CSF pressure. Reducing blood volume in the brain can be a quick response but there still needs to be an adequate supply to ensure the brain gets enough oxygen. A main focus of this chapter will be to review the different effects of arterial and venous flow to and from the brain.

Cerebral blood flow (CBF) refers to the amount of blood travelling through the brain per unit time. CBF regulation refers to the control of blood flow both in and out of the brain. To illustrate, when a healthy human stands up quickly, the change in body position causes a sudden drainage of blood from the cerebral veins, thus causing a drop in ICP. This causes a lightheaded feeling (dizziness). However, the sensation quickly subsides due to two CBF regulatory mechanisms. First, the large internal jugular veins

collapse to rapidly decrease blood flow from the brain to the heart; second, the arteries from the aorta dilate to increase blood flow from the heart to the brain.

2.2 Intracranial Pressure, Blood Pressure and Lung Pressure Correlation

Physiologically, circulation is affected by respiration and therefore, indirectly, so is ICP. This section introduces the effects that lung pressure and corresponding arterial and venous pressures have on ICP. Both the arterial and venous flow are discussed and how differing physiological conditions affect ICP regulatory mechanisms.

The Valsalva Manoeuvre (VM) is a recognised breathing technique in which a person closes their glottis, or pinches their nose and closes their mouth, and attempts to forcefully exhale without releasing any air (a similar sensation to lung pressure build-up before coughing but held for a longer period of time). The sensation of increased head pressure in response to raised pulmonary pressure (such as coughing) is well recognised in the literature. The physiological inference is that there is a correlation between lung pressure and cerebral pressure via blood flow pathways. A simple example is when a person inhales, more blood is pumped from the heart to oxygenate it, this leads to a higher blood pressure to the brain as well; when a person exhales, the opposite occurs and blood pressure drops.

Figure 2.2 presents the main blood vessels and flow between the lungs, heart, brain, and body, and how lung pressure affects the maximum volume of blood the heart holds before contraction. The carotid arteries are the main pathways of blood flow from the heart to the brain; the jugular veins are the main pathways for venous drainage from the brain to the heart. Figure 2.2b shows the effect thoracic pressure has on heart compliance. Heart compliance is a measure of how easily the heart can expand, thus how much blood it can hold before contraction. The heart compliance is analogously represented by the flexible membrane between the thoracic cavity and the heart in Figure 2.2b. During inspiration, the respiratory muscles contract which reduces the pressure in the thoracic cavity. This causes the lungs to inflate and the heart compliance to increase allowing a larger volume of blood to flow into the heart per beat. During expiration, the respiratory muscles relax, increasing pressure in the thoracic cavity, causing the lungs to deflate and heart compliance to decrease.

The rest of this section reviews the arterial and venous contributions to ICP regulation and discusses whether observations of specific blood flows to/from/around the brain could be used for identifying cranial pathologies.

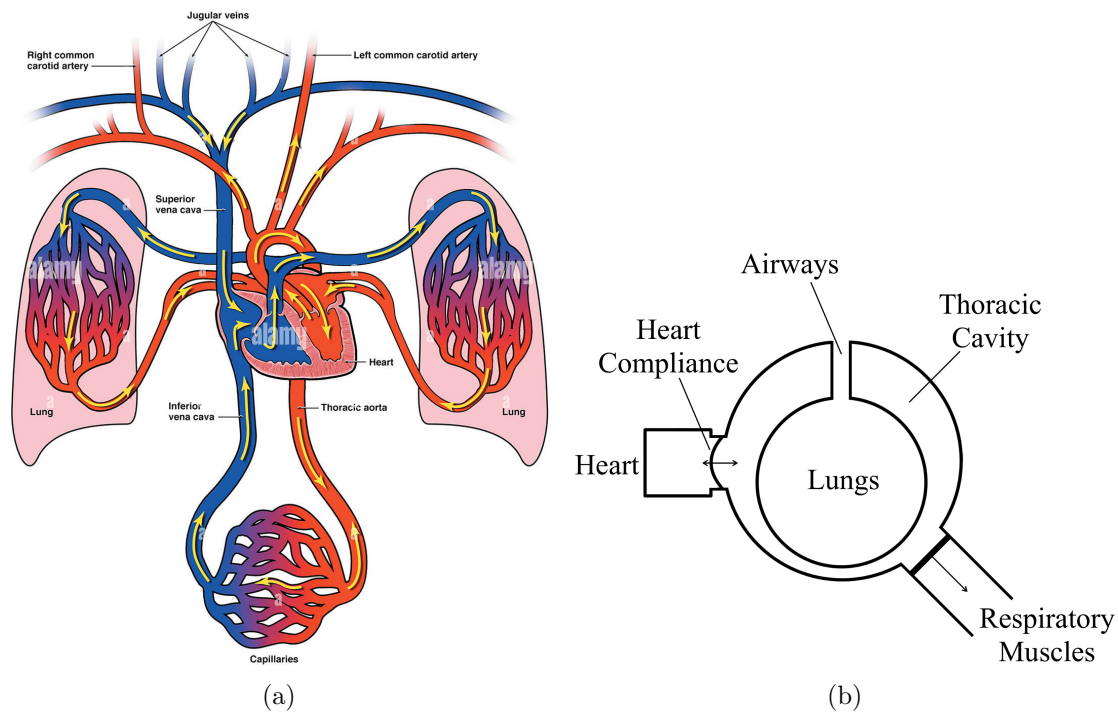


Figure 2.2: (a) Primary blood vessels of the circulatory system [10]
 (b) How thoracic and lung pressure affects heart compliance.

2.2.1 Afferent (Arterial) Flow

The VM has been studied to better understand the effect the lungs have on cerebral pressure and specifically on autoregulation (i.e. the regulation of arterial flow to the brain) [11–13]. Tiecks et al [11] assessed the effects of impaired carotid blood flow on autoregulation by monitoring CBF using a Transcranial Doppler (TCD) recording system. Two key measures that they used were CBF and cerebral perfusion pressure (CPP). CPP is the pressure gradient that drives blood flow to the brain; if this value is too low, not enough oxygen will be delivered to the brain causing an ischemic event (i.e. a stroke). They found that autoregulatory measures were significantly different in patients with impaired carotid blood flow compared to patients with normal vascular activity. This shows that the carotid arteries are a key component of autoregulatory processes in response to increased ICP from raised lung pressure. However, the carotids are not part of the brain anatomy, therefore their impairment will not provide an indication of brain abnormalities.

Zhang et al [12] evaluated the differences between the mechanical and nervous effects of the VM on CBF, by use of a nerve block agent. They discovered that autoregulation was unable to prevent a substantial fall in CBF due to a reduction in blood pressure during the VM. It is clear from these results that the nervous system is an integral part of normal cerebral autoregulatory function. Both these papers highlight the fact that raised ICP can be caused by pathologies external to the brain such as blood clots,

blocked blood vessels, and nerve damage. However, these papers studied conditions which, under normal circumstances, would show other symptoms unrelated to brain physiology.

The effects of arterial pressures on autoregulation, specifically when cranial pathologies were present, were studied by Prabhakar et al [13]. They analysed the effects of the VM on ICP, CPP, and mean arterial pressure (MAP) ($\text{MAP} = \text{CPP} + \text{ICP}$) on anaesthetised patients with cerebral pathologies. A passive VM was carried out by squeezing a bag in a closed breathing circuit to maintain an airway pressure of 20 cmH₂O above peak inspiratory airway pressure for 10 seconds. They found that ICP increased and MAP decreased during the VM, creating a considerable decrease in CPP. This shows that the reduction of MAP in order to reduce ICP, which would be effective in a healthy individual, is not sufficient when a cranial tumour is present. The research also shows that specific patient-generated lung pressures could be utilised when measuring ICP in order to determine the size of a cranial tumour.

These papers highlight the significance of arterial blood flow/pressure and its relation to ICP. Prabhakar et al [13] showed that a rise in ICP caused a decrease in MAP, proving that an inverse relation exists. However, MAP is affected by multiple variables including lung pressure, heart rate, stroke volume, and oxygen requirements from all parts of the body. This means that although MAP can be used as an indicator to the possibility of a cranial pathology, it is not a guarantee.

Venous drainage is another regulatory process which ensures that ICP would remain stable in the case of an intracranial mass being present. To avoid ICP rising, excess deoxygenated blood can be drained from the brain (Figure 2.1a). This shows that venous flow from the brain is as important as arterial flow to the brain. As such, research studying how lung pressure affects venous flow (and thus ICP) is reviewed next.

2.2.2 Efferent (Venous) Flow

The above papers have revealed the effects of lung pressure on afferent cerebral blood flow and ICP. Research has also studied the importance of efferent cerebral blood flow via venous drainage. In 1896, Hill [14] established that both arterial and venous pressure affect ICP but *“the venous side to a far greater degree than the arterial side, because it is on the arterial side that the resistance lies”*. Hill is referring to the fact that cerebral veins do not contain any valves or muscle tissue whereas cerebral arteries contain muscle to control the blood pressure and flow to the brain. This leads to his further observation that *“The intracranial pressure in all physiological conditions is the same as the cerebral venous pressure”*.

In the previous subsection it was shown that an increase in lung pressure caused an increase in ICP due to cranial compliance and autoregulation. Lung pressure has also been

studied for its effects on venous return and corresponding ICP changes. Hansen et al [15] attempted two methods to reduce ICP by reducing central venous pressure (CVP). This research was proposed in an attempt to address the risk of spaceflight-associated neuro-ocular syndrome. This is a condition that can affect astronauts during long missions due to natural drainage of blood from the brain being disrupted in the microgravity environment (gravity helps in venous drainage from the brain). The two research methods involved were: bilateral thigh cuffing, and breathing through an impedance threshold device (ITD). An ITD creates a higher resistance during the inhalation phase to generate a higher negative intrathoracic pressure. ICP was measured in four healthy participants through Ommaya Reservoirs (these implants had been used to successfully treat previous medical conditions). Additionally, CVP was measured by a PICC (peripherally inserted central catheter). The research showed that breathing through an ITD for five minutes reduced both CVP (6 ± 2 vs. 3 ± 1 mmHg) and ICP (16 ± 2 vs. 12 ± 1 mmHg) compared to no observed change during free-breathing conditions. Inflating the thigh cuffs to 30mmHg for two minutes caused no significant change in CVP (5 ± 4 vs. 5 ± 4 mmHg) or ICP (15 ± 3 vs. 14 ± 4 mmHg). This study confirms that thoracic pressure has a significant effect on CVP and thus ICP. It also shows that changes in blood pressure/flow in the legs do not have a significant impact on CVP or ICP.

As stated above, gravity impacts the drainage of blood from the brain. In a similar way, posture (e.g. sitting upright or lying down) affects blood drainage. A very simple example is to observe the distribution of water in a half-filled bottle when it is upright compared to on its side. Gisolf et al [16] studied the influence of posture and CVP on the distribution of cerebral venous outflow using a mathematical model. They measured the cerebral blood flow velocity and CVP of 10 healthy subjects. Measurements were taken during rest to use as a baseline and during a VM in both supine and standing positions. They found that the physical data correlated with the model simulation ($R^2 = 0.97$). In supine position the internal jugular veins (IJV) are the primary pathway from brain to vena cava. In standing position the IJV collapse and flow is shunted via other venous routes. However, a marked increase in CVP while standing (caused by performing the VM) completely re-opens the jugular veins.

This study demonstrates that blood pressure control mechanisms from the brain to the heart respond to pressure gradients. The greater the gradient, the higher the blood velocity. During the VM, CVP is high due to high thoracic pressure. This in turn reduces the pressure gradient between the vena cava and the brain's venous return pathways. To counter this, the IJV re-open to facilitate gravitational flow from the brain to the vena cava. The implications of this research are threefold: first, posture determines natural venous flow from the brain; second, high thoracic pressure reopens the venous pathways from the brain that naturally collapse when upright; and third, lung pressure has a direct effect on ICP via venous flow.

Similarly, Holmlund et al [17] performed a more focused study looking at how IJV collapse helps to regulate ICP in an upright seated position. They measured ICP, venous pressure and IJV cross-sectional area in 11 healthy subjects in 7 positions from supine to sitting (0-69°). They established that their model accurately replicated postural ICP changes with no difference between predicted and measured values for all angles. This confirmed that postural ICP changes are dependent on both CVP and IJV collapse.

This section has reviewed the effects of lung and intrathoracic pressure changes on blood flow to and from the brain and the corresponding impact on ICP. The next section provides a summary of the above reviewed papers linking the relationship between lung pressure and ICP. The research mainly used invasive techniques for the findings so a summary of the drawbacks of invasive and the advantages of non-invasive diagnostics are also presented in the next section.

2.3 Link between ICP and Lung Pressure

It is clear from the above studies that lung pressure has an effect on ICP. Both Gisolf [16] and Holmlund [17] showed that posture and lung pressure have a significant effect on cranial venous return and its pathways, and therefore on flow resistance. Higher lung pressures close off natural pathways thus the IJV re-open to ensure continuous blood flow from the brain.

Additionally, lung pressure has a cascade effect on stroke volume (i.e. the volume pumped from the ventricle per heart beat) as follows:

- stroke volume is dependent on cardiac pre-load (amount of blood in the ventricle before contraction);
- cardiac pre-load is affected by the volume of blood in the atria before atrial contraction;
- the volume of blood that fills the right atrium is dependent on the volume and pressure in the vena cava;
- the blood volume and pressure in the vena cava are dependent on venous pressure gradients to the vena cava as well as thoracic chamber pressure;
- an increase in lung pressure causes an increase in thoracic chamber pressure and vice versa thus lung pressure has an effect on stroke volume.

This has a two-fold effect on ICP:

- *Afferent flow* - higher thoracic chamber pressure reduces stroke volume and thus blood flow to the brain as well as the rest of the body. To ensure the brain receives an adequate oxygen supply, the arteries to the brain dilate causing more blood to flow to the region. Higher blood flow creates a higher blood volume, thus pressure, causing ICP to increase.
- *Efferent flow* - higher thoracic chamber pressure creates a higher pressure in the vena cava by compressing it, thus constricting it. This lowers the pressure gradient between vena cava and natural venous return pathways from the brain. If the IJV are collapsed a build-up of blood volume, thus pressure, occurs in the brain, increasing ICP.

In a healthy human, both mechanical and electrical cerebral blood flow regulatory mechanisms (such as IJV collapse/reopening and vasoconstriction/vasodilation respectively) ensure that thoracic chamber pressure has a limited effect on ICP.

All the research studies cited above have shown that lung pressure plays a significant role in cerebral blood flow regulation (both afferent and efferent) and ICP. However, many of them have either used invasive techniques to measure ICP, such as catheters and Ommaya Reservoirs, or have studied anaesthetised patients with known pathologies.

Invasive techniques can come with complications. Patients may experience pain, bleeding, infection and possibly permanent tissue damage. To minimise these risks, invasive procedures become very resource-intensive: specialised equipment must be manufactured to a strict standard; professional personnel have to perform the procedures; patients may also take a long time to recover and even longer if any problems occurred during/after the procedure.

Modern medicine is moving towards non-invasive diagnostic techniques which have many advantages including:

- no recovery time
- do not necessarily need to be performed in a clinical/sterile environment;
- do not necessarily need a professional to perform them thus wider accessibility;
- less patient discomfort;
- shorter overall procedure time-frames thus greater ease of access (e.g. could be performed in an appointment);
- improved patient safety;
- earlier detection via screening programmes;
- continuous monitoring.

Accurate non-invasive measurement of ICP would greatly improve the possibility of early detection of cerebral pathologies. For example, screening appointments would allow for wider patient accessibility.

The following section reviews research that used tympanic membrane displacement (TMD) as a non-invasive technique to indirectly measure ICP. It discusses the effect of cochlear fluid pressure on TMD and how that can be related to ICP and the current issues with TMD measurements due to physiological factors.

2.4 Non-invasive Diagnostics using Tympanic Membrane Displacement

Non-invasive techniques for diagnosing intracranial pathologies include imaging, electroencephalography, magnetoencephalography, and TCD. Most techniques are either expensive or time-consuming and are therefore less accessible or provide limited information. However, the possibility of accurately measuring ICP non-invasively would be a significant step forward in the diagnosis of intracranial pathologies. TMD appears to provide a way of indirectly measuring ICP due to the relation between inner ear pressure and ICP [18, 19].

Techniques have been developed to diagnose cranial pathologies non-invasively in conscious patients. Marchbanks et al [18] demonstrated that TMD was highly sensitive and revealed that changes in ICP brought about changes in cochlear fluid pressure. The same research group (Reid et al [19]) then went on to compare the effects of abnormal ICP on cochlear fluid pressure. The TMD data of patients with known neurological conditions (including hydrocephalus and intracranial tumours) associated with abnormal ICP were compared with healthy subjects. They showed that there were significant differences in the TMD between patients with raised ICP and normal ICP, thus confirming that TMD is a useful non-invasive technique for the diagnosis of cerebral pathologies.

Campbell-Bell et al [20] studied the effect of sitting posture angle on evoked TMD measurements finding that the pressure in the ears was significantly different in the supine position compared to the sitting position. They recruited 191 subjects aged between 20 and 80 years old (with a mean age of 43.8 years) and used a cerebral cochlear fluid pressure (CCFP) analyser to measure TMD in both sitting and supine positions. They found that in a seated position, the mean TMD was 132 nl in the left ear and 97 nl in the right; whereas in a supine position the mean TMD was 37 nl in the left ear and -15 nl in the right. The lower the numerical value, the greater the pressure in the middle ear. These data show there is a distinct relation between TMD and ICP.

El-Bouri et al [21] examined the frequency domain of spontaneous TMD measurements (i.e. those unrelated to auditory input) and specifically the power spectral densities.

They took data from 11 patients and measured spontaneous TMD, ICP and arterial blood pressure. Their data showed that the most common frequencies of tympanic membrane oscillations coincided with the respiratory and circulatory cycles, i.e. breathing and heart rate have an observable effect on ICP.

2.5 Summary

This chapter has highlighted research that shows lung pressure changes have a direct dynamic influence on ICP and CBF regulation. Section 2.4 has shown that TMD measurements have determined a clear correlation between inner ear pressure and ICP. However, due to disturbance factors such as respiratory and circulatory changes, currently TMD alone is not yet precise enough to be used as a diagnostic tool for cerebral abnormalities which affect ICP. Additional measurements, such as blood pressure and flow and lung pressure, could improve the precision of TMD.

Many of the above papers used techniques which involved lung pressure changes to induce ICP changes [11–13, 15–17]. If, for example, specific lung pressures could be measured during the VM, this would have a twofold effect on TMD measurements. First, the respiratory cycle component of the measured TMD signal would be non-existent as breathing rate is not involved. Second, CBF regulatory effects could be observed - specifically, at what lung pressure an increase in ICP can be observed in the TMD signal. The best way to do this is by taking lung pressure profile (LPP) tests during TMD measurements. LPP tests require a patient to accurately follow a predetermined pressure reference by forced expiration through a breathing tube. The specific pressures and changes in pressure excite the blood flow regulatory mechanisms of the brain. However, the accuracy of profile tracking relies on the individual patient's ability. In other words, there will be discrepancy between the desired pressures and changes and the human tracking response.

Chapter 3

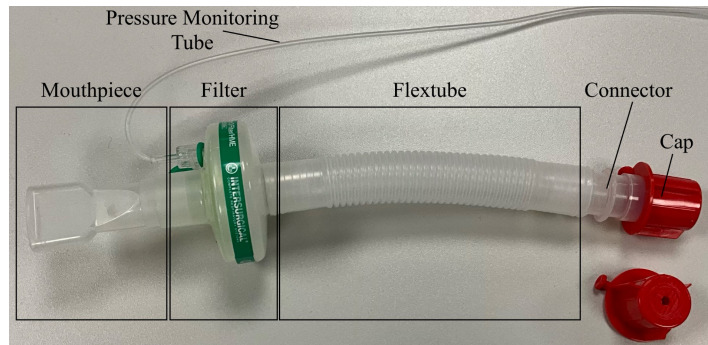
Respiratory Control Background

Chapter 2 showed that measuring TMD over a range of specific lung pressures could be used to determine the size of an intracranial mass (e.g. tumour). The problem is then how to achieve this range of lung pressures. The current solution used in hospitals is for the patient to follow a lung pressure profile (LPP). The standard apparatus used for LPP testing is shown in Figure 3.1a. The red cap has a hole to prevent glottis closure and can be removed by the clinician to quickly drop the lung pressure as necessary. Figure 3.1b shows an example of a patient's experience. They are seated and given the apparatus and asked to track the pressure profile reference on a screen by blowing into the apparatus. It is a very simplistic setup and accurate tracking of the reference by the patient is difficult to perform when precise pressure changes are required.

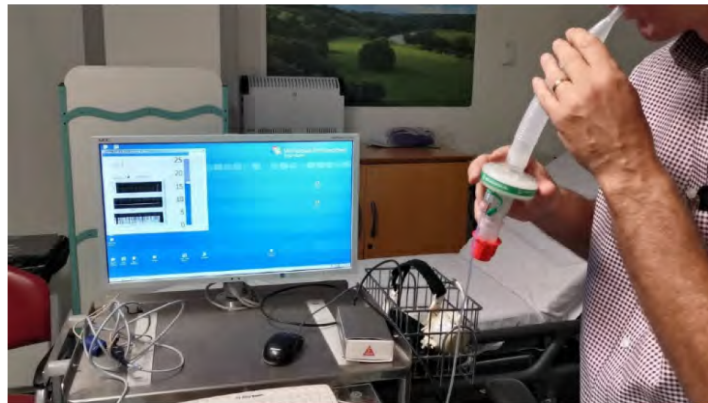
Introducing a controller that can adjust pressure would help reduce reference tracking error, therefore providing more accurate data for concomitant TMD measurements. Currently, there is no work that applies any form of control during reference tracking of a LPP. However, the basic principles of control techniques may be viable from other similar applications. For example, a situation that utilises external control with breathing, whilst also applying strict constraints for safety, is medical ventilation (can also be called artificial respiration/ventilation). The following section reviews control of medical ventilation in order to ascertain suitable approaches that may be utilised to assist tracking of LPPs.

3.1 Medical Ventilation

Medical ventilation attempts to replicate the process of conscious breathing. This involves using physiological parameters such as airway resistance and lung compliance as well as employing safety constraints such as levels of inflation or blood oxygen saturation. During natural respiration, chemoreceptors respond to changes in oxygen and



(a)



(b)

Figure 3.1: (a) Apparatus used to measure lung pressure
 (b) The setup used to measure lung pressure while a patient follows a pressure reference (repeat of Figure 1.4).

carbon dioxide levels in the blood and transmit this information to the central nervous system. The central nervous system then triggers a response in the body to breathe in/out in order to return the oxygen/carbon dioxide levels to a homeostatic state.

Where natural respiration is compromised, for example under general anaesthesia, respiratory assistance can be provided in the form of medical ventilation. A flexible tube is inserted into the trachea (via the mouth) and the other end is attached to the ventilator. The ventilator provides adequate air supply to the patient whilst avoiding hypoxia (lack of oxygen) or over-inflation which, if not dealt with quickly, can cause permanent tissue damage. A variety of control systems are utilised in medical ventilation to assist in maintaining normal airflow to the lungs. These controllers are chosen based on their implementation. For example, if a fast response is required, then the controller needs a significant gain factor; or if the system has constraints and needs to include the human breathing instinct, then the controller needs to be able to respond appropriately to remain within the system limits.

3.2 Control Methods

Many types of controllers have been applied in medical ventilation research. This section provides an overview of the different approaches that have been taken in order to improve the control task. Medical/mechanical ventilation can be observed in literature as far back as 1907 with the ‘Pulmotor’ [22] and 1928 by use of the ‘iron lung’ [23]. Over the last 100+ years many methods of improving this system have been researched. In more recent years the emphasis has been on applying controllers that ensure patient comfort, safety and oxygen requirements are met. The most common control types and their application to medical ventilation are reviewed next.

3.2.1 Proportional-Integral-Differential Control

Proportional-integral-differential (PID) is one of the most common types of control system due to its simplicity and wide applicability [24], including in medically-assisted ventilation [25–31]. PID control uses the process output signal reference error (difference between desired reference and measured output of the system) and corrects it based on proportional, integral and derivative calculations.

Tehrani et al [25] used the principals of natural breathing (i.e. levels of O_2/CO_2) to develop a closed-loop medical ventilation system that mimics a natural pattern of breathing. They used a dual control system: the first system used inputs of O_2/CO_2 levels and respiratory compliance and airway resistance to allow for effective emptying of the lungs during expiration; the second system used PID to automatically adjust oxygen concentration in the patient’s inspired gas and used arterial oxygen saturation as feedback. Testing was performed using mechanical lung studies, computer simulations and animals as test subjects. The results showed that the controller adjusted breathing frequency and tidal volume in a clinically-appropriate manner in response to changes in respiratory mechanics. The controller was also able to return blood gases to the normal physiological range within 25s after an induced disturbance. This shows that PID can provide appropriate ventilatory control even with induced disturbance. However, this application has a relatively slow feedback loop due to changes in oxygen levels.

Lua et al [26] presented a proportional assist ventilation method using a proportional solenoid valve to control air supply to patients suffering from respiratory disabilities. They developed a proportional control scheme which adjusted flow rate according to pressure in the lungs and airways in order to provide adequate oxygen supply. This was compared to the conventional method at the time (in 2001) which supplied either a preset amount of air or a given air pressure to the patient. They simulated applying both methods in vitro and compared the pressure and flow parameters. They showed that applying proportional assisted ventilation normalised the flow patterns of patients

with abnormal physiological parameters, and the controller could adjust its input in proportion to inspired volume/flow caused by the respiratory muscles. This demonstrates that proportional control of a valve can be used as a method to assist in pressure/flow adjustments and adapt to patient respiratory action. However, this could still be considered a linear single-input-single-output (SISO) (i.e. supplied air and airway pressure) system with a disturbance (inhaled air). It does however show that the PID parameters can be tuned to a faster feedback system with induced disturbance.

3.2.2 Fuzzy Logic Control

Fuzzy logic control is used to handle uncertainty/non-linearities in a system by using measured parameters to apply a specific input condition created by the parameters. The parameters are sorted into groups according to their value and the controller therefore does not need any form of model to handle varying conditions.

Nemoto et al [32] developed a Fuzzy logic algorithm to improve the weaning process from mechanical ventilation to natural respiration for ICU patients. The controller used physiological measurements of heart rate, tidal volume, breathing rate/frequency, and arterial oxygen saturation. They applied the controller retrospectively to 13 patients and compared its decision to the one made by the attending clinician. On average, the controller recommendations were within 2cmH₂O for 76% of the time, and within 4cmH₂O for 88% of the time. The clinicians also tended to be more aggressive in reducing the support level compared to the fuzzy controller's decisions. This shows that Fuzzy logic could be used to provide a smooth transition of control between pressure levels.

3.2.3 Adaptive Control

Traditional PID is a relatively simple form of control, has been applied in many different areas, is fast acting, and is highly effective on linear time-invariant systems. However, medical ventilation is inherently non-linear due to varying factors such as patient oxygen requirement, spontaneous breathing, and pressure stability. A linear PID controller cannot adapt to these changing conditions if they go beyond expected limits. More recent research has often implemented PID in conjunction with adaptive controllers for medical ventilation to improve performance and adapt to non-linearities of a system [27–29].

Reinders et al [27] introduced an adaptive controller to improve pressure support during mechanical ventilation. They presented a control strategy which estimated the hose resistance of a mathematical model of a patient-hose system to control the pressure supplied. This would avoid the need for calibration by hospital staff which would reduce setup time. The control approach was compared to two state-of-practice control

strategies; the first applied the same pressure as the target pressure; the second was an integral feedback controller. They applied all controllers in simulation across varying patient conditions as well as in an experimental case study. The data showed that the adaptive control significantly improved pressure tracking performance compared to the state-of-practice schemes.

Yan et al [28] compared traditional PID with fuzzy adaptive PID control of mechanical ventilation pressure. Fuzzy adaptive control uses Boolean logic to assign a value between 0 and 1 to the current conditions and boundaries are set based on previous data. They developed a fuzzy controller which adjusted the PID gains based on the error and the change in error. They then compared data from a traditional PID and the fuzzy adaptive PID controller by simulating their function based on a dual-lung model. The data showed that the response time of a traditional PID was faster but that the overshoot was also larger. The data also showed that a traditional PID became unstable if the system state suddenly changed which would become unsafe for a patient. In other words, traditional PID struggles to adapt to non-linear systems with varying conditions, but fuzzy PID control of airflow is smoother, so providing a safer and more comfortable ventilatory procedure.

Mehedi et al [29] developed an adaptive fuzzy sliding mode control system for pressure-controlled artificial ventilators. Their aim was to improve the accuracy and stability of airway pressure control. The control was based on two components: the first based on Fuzzy logic approximation of ideal feedback linearisation control; the second based on the sliding mode principle to minimize estimation error between the fuzzy control action and perfect feedback linearisation control. They applied the controller to a simulated ventilator system consisting of a blower-hose-patient setup and patient lung model with non-linear lung compliance. They compared the controller to traditional PID and sliding mode controllers. The fuzzy controller demonstrated significant improvement in tracking target airway pressure with faster convergence, less overshoot, and smaller tracking error.

The cyclical nature of respiration indicates that a learning controller could be introduced with a basic setup to work from. This would be similar to an adaptive control system in the sense that its parameters can be set at the start of applying control, and the learning aspect then adjusts these parameters over time to provide a more adequate control scheme with minimal tuning.

3.2.4 Iterative Learning Control

Iterative learning control (ILC) is a scheme normally used to improve control during a repetitive task. When used for mechanical ventilation it uses a baseline to then adapt the control. This baseline can take the form of: initial/end conditions (e.g. positive end-expiratory pressure or inspiratory positive airway pressure); initial parameters such

as breathing frequency/period; a patient model; or an initial control scheme such as PID (see Section 3.2.7).

Scheel et al [33] presented an ILC application to improve the performance of medical ventilation. The algorithm would adjust its control input based on previous iterations to attain reference values of positive end-expiratory pressure during expiration and inspiratory positive airway pressure (IPAP) during inspiration. The ILC algorithm was compared to a proportional-integral (PI) controller both in simulation and applied to a mechanical lung. They showed that ILC sequentially reduced the control error for every breathing period, and was able to provide the desired control accuracy which the PI could not. The ILC had a smaller overshoot and faster convergence speed.

De Castro and Tôrres [34] studied the use of ILC applied to tracking pressure profiles associated with a commonly-used ventilatory mode. The approach aimed to control airflow and pressure based on patient-specific requirements. They compared the results to the PI and a hybrid PI/ILC when applied to a simulation model of a mechanical ventilator. They concluded that although performance would improve with iterations, ILC was not suitable for their application due to tracking error in steady state and sizeable error in initial iterations. However, when ILC was combined with PI feedback control, the results showed great improvement in tracking and convergence, compared to both PI and ILC separately, including adjustment to a spontaneous shift in the model.

The possibility of using ILC with an initial controller baseline of PID is similar to an adaptive control scheme. The benefit would be that with ILC tuning the parameters could provide more adaptability to the varying conditions as shown by De Castro and Tôrres. The use of a model is also commonplace when applying control. Models can take many forms including collected and categorised data, mathematical equations, and analogous system equations. A model provides necessary information to the controller of how a system will most likely respond to tracking a reference.

3.2.5 Machine Learning Control

Machine learning control relies on previously collected large data sets to determine an optimised control input.

Neural networks is an area of machine learning that attempts to mimic the way a human brain would process information. The network receives a set of input data and makes step-by-step computations by chronologically applying functions to the data before creating an output. The functions and output are generated based on previous data given to the network. Perchiazzi et al [35] looked into the application of artificial neural networks to estimate the total positive airway pressure exerted on the alveolar walls at the end of expiration. An end-expiratory hold manoeuvre is normally used to measure this value. The hold means that the cyclic process of ventilation is disturbed for

an arbitrary length of time. This can be dangerous for patients with acute respiratory distress if performed too often. The study used pigs as models for human respiratory behaviour. It had two phases applied to 10 mechanically ventilated pigs: the first phase measured pressure and flow at the airway opening with different conditions to calculate parameters for the artificial neural network; the second phase trained and tested the neural network to estimate the positive end-expiratory pressure from the recorded data. The estimation data showed good concurrence with the measured values.

Reinforcement learning is another area of machine learning that has an ‘agent’. This agent learns to make decisions based on a reward system when interacting with its environment. Peine et al [36] presented a reinforcement learning algorithm which optimised ventilator settings for critically ill patients to improve patient outcome. The algorithm attempted to optimise settings for positive end-expiratory pressure, fraction of inspired oxygen, and ideal body weight-adjusted tidal volume. The algorithm was tested on 11,943 volume-controlled mechanical ventilation events from 61,532 ICU admissions, and further validated on a secondary dataset of 200,859 ICU stays. The results showed that the algorithm had a better performance return compared to clinicians’ standard care and provided a more patient-tailored approach to ventilatory care.

3.2.6 Model Predictive Control

The purpose of applying a controller to a system is typically to improve aspects such as: stability; performance; robustness; error correction; safety; and energy efficiency. A specific objective of many tracking controllers is to minimise the tracking error with respect to a reference using the least control input - this is termed optimal control and many of the above papers have implicitly utilised this principle. By assigning a weight to either tracking error or control input, a cost function can be established. For example, if reducing tracking error is more important, then a greater weighting coefficient can be applied to it. Optimal control is a method that seeks to minimise this cost function.

Model predictive control (MPC) specifically uses a model and cost function within its design structure to optimise its control input. Männel et al [37] presented a hierarchical control structure that implemented MPC to achieve adequate gas exchange by adjusting the minute volume ventilation within safe physiological limits. They used a physiological non-linear two-compartment patient model to assess the ability of the controller. The controller was assessed on its ability to track a minute volume reference in response to an increased metabolic production and its handling of patient respiratory activity. The data showed that MPC handled hard constraints on minute volume while still providing close to optimal support for the patient based on their breathing activity.

Acharya et al [38] developed an explicit model predictive controller to improve the airway pressure profile of a mechanical ventilator. The use of a Taylor series avoided the

application of an iterative method by linearising a non-linear system around a specific operating point. Simulations were performed to observe the pressure and flow responses in the patient's lungs as well as the ventilator response. The simulations tested the responses based on differing lung resistances and compliances to model different age/health factors in the respiratory system. The response was compared to a traditional PID controller. They found that explicit MPC was able to adapt to these changes without any further tuning of the control parameters.

3.2.7 Hybrid Control

Medical ventilation is a relatively consistent/iterative procedure and as such many types of controllers can be applied in a simple format. However, this can also limit the ability of the controller if conditions were to change, i.e. spontaneous breathing, oxygen supply/carbon dioxide removal, pressure/flow/volume variations or even a change in dependency e.g. the weaning process from mechanical to natural respiration. This has led to the development of hybrid control schemes. Recent research on medical ventilation spiked in response to the COVID-19 pandemic and therefore produced novel applications of control during medical ventilation. Hybrid control combines different modes of ventilation to improve patient care, comfort and safety. It can be used to adapt the control prioritisation (i.e. volume control, pressure control etc.) and can make dynamic adjustments based on the patient's condition such as variation in airway resistance or lung compliance to maintain adequate supply.

Hazarika and Swarup [30] studied the application of ILC and a hybridisation of ILC with PID to control flow rate of a ventilator during inspiration. ILC updates a control signal in order to correct for errors recorded in previous attempts. The researchers used an analogous electrical circuit to model a mechanical ventilator and applied ILC followed by the ILC-PID hybrid controller. The ILC provided successive reduced tracking error in every cycle. The application of ILC-PID reduced control effort, number of necessary iterations, and initial tracking error. Application of PID meant that the controller could withstand 15% parameter changes of the system, but also slowed the response compared to ILC alone.

Sakthiya Ram et al [31] used hybrid PID controllers to maintain oxygen levels in COVID-19 patients. Their aim was to assess the most efficient and safe feedback system to find the best controller for an automatic respiration system. They presented multiple algorithms to tune the parameters of a PID controller that regulated airway pressure to supply adequate oxygen. The PID control was hybridised with: genetic algorithm-based fractional order; Fmincon-pattern search algorithm; and MPC. They compared the effectiveness of these algorithms in MATLAB simulations incorporating possible conditions encountered during artificial respiration. All algorithms showed validity of

application, particularly the genetic algorithm, but exposed the limitations of inadequate patient data which potentially would lead to an imperfect respiration model.

3.2.8 Application of Controllers to Lung Pressure Profile Testing

PID utilises three basic principles of the reference tracking error to adjust pressure in the lungs during medical ventilation. A subset of these principles could be applied to LPP tests. Fuzzy logic control could be used for assistance during LPP tests, however the parameters of the controller still need to be tuned, and as such may struggle to provide adequate control if there is a larger disturbance in the system beyond what is expected.

Adaptive control can utilise basic models and provide accurate estimates of resistance to improve pressure tracking performance during medical ventilation. This means adaptive control could be used to assist during LPP tests. Hybrid controllers are able to provide control based on a hierarchical approach. For LPP tests, the controller would select the best type of control to provide assistance based on current requirements. Section 3.2.5 showed that machine learning algorithms can be used to estimate an output based on basic pressure and flow measurements when provided with an initial data set. Furthermore, they have been shown to improve control actions compared to a clinician's decision-making. This means a machine learning approach could be used for control during LPP tests if given a large enough data set to train the learning models.

The cost function used for MPC could be beneficial in assisting LPP reference tracking during forced expiration. The reliance of control and tracking ability could then be biased towards the patient. This would mean the controller performs small (or no) changes most of the time and only provides a large control input when there is a concomitant large reference error. Table 3.1 provides a brief summary of the advantages and disadvantages of each control method discussed and compatibility with regards to application to LPP testing.

Table 3.1: Comparison of control methods

| Control Method | Advantages | Disadvantages | Conclusions |
|--------------------|---|--|---|
| PID | Simple control method with wide applicability. Quickly reacts to disturbance in the system response. | Can struggle with non-linearities in the system if outside the range of expected function. May not be able to consider multiple constraints if they are interdependent. | Use for LPP testing is possible due to the simple pressure tracking task. Wide applicability means parameters could be tuned to patient requirements. However, minimum time and maximum airflow constraints may not always be adhered to. |
| Fuzzy logic | Can handle varying conditions. Non-linearities and numerous constraints can be considered. | Selecting correct boundaries for the logic system can be difficult and time consuming which can affect stability. | Adaptability of Fuzzy logic could allow for better tracking in LPP tests based on the required pressures and patient condition. Uncertainty would arise if the controller needed tuning for each patient. |
| Adaptive | Improvement upon PID as the parameters can be tuned during measurements. | Tuning difficulties similar to Fuzzy logic can affect stability. Complexity of control/system can create large computational load. | Adaptive control could handle non-linearities and disturbances. Complexity of the control scheme would require a large computational load which leads to increased costs of hardware. |
| Iterative learning | Can use a basic initial model/control scheme to develop algorithm. Constant adaptation during testing would improve tracking ability while reducing control input. | Relies on the repetitive nature of a task. Basic model still needs good accuracy for best control implementation. | Use of ILC for LPP tracking would require the tracking task(s) to be repetitive in nature. It is also unknown as to how long it would take to tune the ILC model and whether it would be universally applicable to any patient. |

| | | | |
|------------------|---|---|---|
| Machine learning | Predictive abilities with a large enough data set. Would be able to adapt to different patients without parameter changes made by program user. | Requires large data sets for best results. Larger data sets have a higher processing requirement. | Machine learning could be used for clinical LPP tests given a large enough data set which would give it universal applicability. However, this could increase costs due to the complexity of the controller and amount of data. |
| MPC | Predictive capabilities. Low processing requirement if prediction horizon is small. Better predictive ability as prediction horizon extends. | High processing requirement if prediction horizon is large. Optimal performance depends on model accuracy. | Predictive abilities of MPC could allow for improved control compared to PID on step changes in pressure and balance the control input compared to the patient input. Model accuracy and computational load need to be high priority in order to provide adequate control and keep costs low. |
| Hybrid | Multiple control schemes can be considered and so optimal performance is more likely as well as better resource usage and more robust to disturbance/noise. | Complexity can affect computational load, costs, and tuning challenges. | The ability to be able to switch between control schemes allows for adaptability to different circumstances/conditions. However, the complexity of the system and number of different control schemes available can affect the cost, and the performance if not tuned correctly. |

This section has reviewed literature that used approaches to controlling airflow/pressure provided by a medical ventilator applied in simulation, mechanical lung and clinical environments. Each controller was assigned a specific task based on a range of specific parameters such as adequate pressure or oxygen supply whilst adhering to strict constraints. Many of the controllers used some type of model to help optimise their control schemes. Models use a set of parameters/variables to allow a controller to mathematically predict possible future system outputs based on its possible inputs. For assistance

control in LPP testing, a suitable model could similarly provide benefit to achieve the intended objective. To aid in future construction of such a model, the next section reviews existing models of respiration.

3.3 Human Breathing Models

As stated, many of the previous medical ventilation controllers use some form of model to design the controller. The system model comprises the lung dynamics, i.e. the interaction between airway flow and alveoli pressure, and depends on the characteristics of the lungs (compliance, resistance etc.). No form of muscle/voluntary motor control was needed due to the patients being unconscious. During lung pressure profile testing, however, modelling the patient's voluntary control of the pressure will be necessary. Any model therefore will need to incorporate their muscle dynamics and voluntary control (i.e. conscious decision input). To date, there is little research into modelling the human respiratory system during forced expiration, thus most of the models examined next are related to medical ventilation.

Lung dynamics are a crucial part of the model needed in this research. Respiration provides a mechanism to deliver oxygen to the vascular system. During respiration the diaphragm/intercostal muscles contract to draw air through the trachea and bronchi and into the lungs. Gaseous exchange of oxygen and carbon dioxide occurs between the alveoli and surrounding blood vessels before the diaphragm/intercostal muscles relax and air is exhaled. In order to determine a suitable model to develop for forced expiration during lung pressure profile reference tracking, different types of lung models must be reviewed.

The rest of this section reviews human lung models. These models have been developed to study the various functions of the respiratory system. They fall in three main categories: imaging, gas exchange and analogous pressure-flow relationships.

3.3.1 Medical Imaging

Imaging models help to study the movement of lung tissue and air during respiration. This can help determine the overall health of the lungs and their dynamics as well as determine movement of a tissue mass, such as a tumour, to help in radiotherapy procedures.

Fuerst et al [39] used anatomical image models to estimate lung deformation during radiotherapy. Computed tomography (CT) scans produced images of the anatomical components of the thoracic cavity (e.g. diaphragm, lungs and intercostal muscles) at end-expiration and end-inspiration. These images had two purposes: 1 - to determine

the size of a tumour, 2 - to determine the shape of the lungs at minimum/maximum capacity and the position of the tumour at these stages of the respiratory cycle. The images were automatically segmented and combined with concurrent data from devices such as spirometers or abdominal pressure belts to create an anatomical model. The model was then used to predict the motion of the lungs and tumour during breathing thus improving the affect of radiotherapy whilst reducing treatment time.

Lin et al [40] used computational fluid dynamics and quantifiable regional features from imaging to model gas flow and particle transport in human lungs. They used this model to study three aspects of the lungs: airway structure; lung function; and flow characteristics. They reviewed their model by comparing it against images, airflow simulations and known physiological behaviour of lung function in different conditions. They concluded that the model offered an improved understanding of structure-function relations in the lungs by combining mathematical modelling with imaging techniques. It also allowed for subject-specific modelling which would lead to more bespoke diagnostics and treatments.

Imaging models are most commonly used for diagnostic and treatment procedures and as such do not have any explicit input/output variables. They could be used for determining muscle dynamics and strength, for control purposes, but this would require a lot of initial data from many patients to create a generalised model.

3.3.2 Gas Exchange

An alternative approach to studying respiratory processes is via a gas exchange model. Männel et al [37] used a gas exchange model to control the minute volume supply (i.e. the volume of air flowing in/out of the lungs per minute) of a medical ventilator. They achieved this by designing a controller that could adapt to patient disturbance (such as reflex breathing) and adjust minute volume accordingly within safe physiological limits. The controller would analyse and adjust model parameters such as respiratory rate, pressures, and amount of inspired oxygen to maintain sufficient oxygen supply and patient safety.

Ben-Tal [41] provided a mathematical framework to link between previously developed models with varying degrees of complexity. They also highlighted that simple models are easier to understand and provide insight to the system while detailed models provide more accurate quantitative information. These models are described below and shown in Figure 3.2.

Inflexible lung: this model assumes a rigid container such that airflow has some resistance flowing from the mouth to the lungs, and airflow in proportionally increases the pressure in the lungs. This model provides basic knowledge of lung function in that the

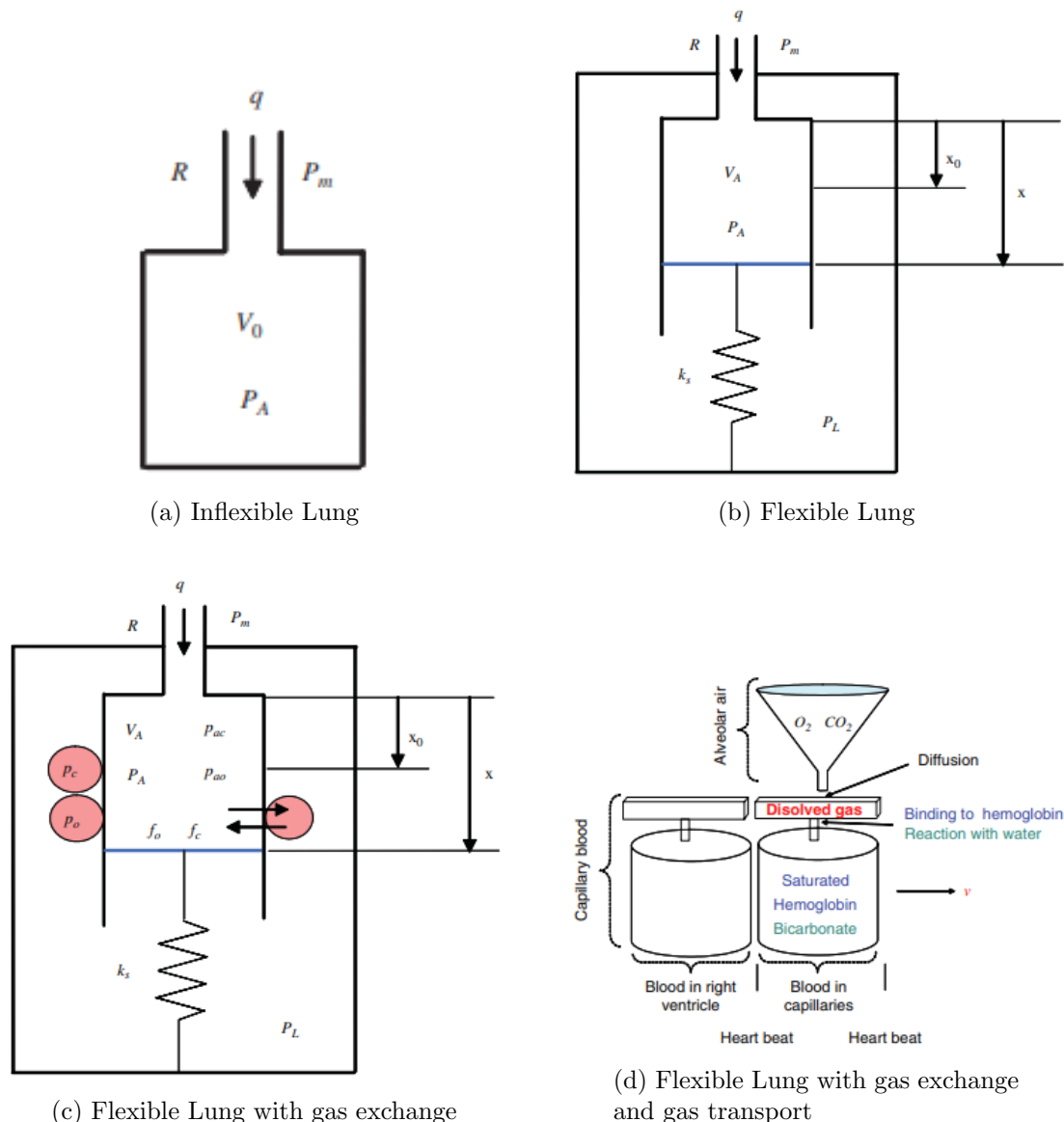


Figure 3.2: Mechanical models of the lungs taken from [41].

trachea/bronchi create air resistance and that there is a pressure-airflow-volume in the lungs.

Flexible lung: this model assumes a piston instead of a rigid container to model the lungs. The thoracic cavity is modelled as a container in which the pleural pressure changes due to movement of the respiratory muscles. The piston is connected to a spring that moves the piston with the pleural cavity. The other end of the spring is attached to the thoracic cavity. Spring compression represents lung expansion. This model expands upon the pressure-airflow-volume relation of the inflexible lung as it introduces an elasticity which moves air in and out of the lungs based on the pleural pressure.

Flexible lung with gas exchange: this model introduces gaseous exchange and partial pressures of oxygen and carbon dioxide. This uses an assumption of constant partial

pressures in the blood to calculate the rate of change of gas concentrations. These values are then used to determine the net flux of gas into the alveoli.

Flexible lung with gas exchange and gas transport: this model allows blood partial pressures to be variable. It presents a small container which represents dissolved gas, and a large container that represents the principal means by which oxygen and carbon dioxide are transported. The balance between the amount of oxygen that enters the capillaries from the lung and the amount of oxygen that binds to haemoglobin yields the rate of change in the partial pressure of oxygen. A similar equation is used for the reverse movement of carbon dioxide.

All of the above models were applied in numerical simulations. The results were used to validate the models, illustrate the advantage of moving between models, or provide new insights to the physiological system. The simulations were consistent with published experimental observations proving that each model provided the necessary information and expected output for their application.

In conclusion, gas exchange models are mainly used to study the expected changes in flow/pressure, partial pressures and volumes of the gases in the lungs. These models can be used to study how different environments/conditions can affect respiration. They can also be used as a diagnostic tool by comparing expected values given by the model and measured values from patients.

3.3.3 Modelling using System Analogues

Ben-Tal's flexible lung model presented a mechanical setup that related pressures, volumes, flows and a compressible chamber to represent the lungs, respiratory muscles and compliances. Other models have been used or developed to represent the relationship between external pressure and lung pressure [26, 28, 42–47]. These capture the dynamics of airflow using differential equations which embed the underlying physical relationships between key variables. The models are constructed using lumped parameter representations of the major components of lung function described as:

- compliance - the elasticity of the lung tissue (how much the lungs can expand and contract with air volume)
- resistance - the air resistance of the lungs and airways
- inertance - oscillatory motion of air due to differences in pressure

Models of lung dynamics are often represented in terms of an equivalent system such as is shown in Figures 3.2 and 3.3. Table 3.2 provides a summary of the equivalent characteristics between fluidic (i.e. the lungs), mechanical, and electrical systems.

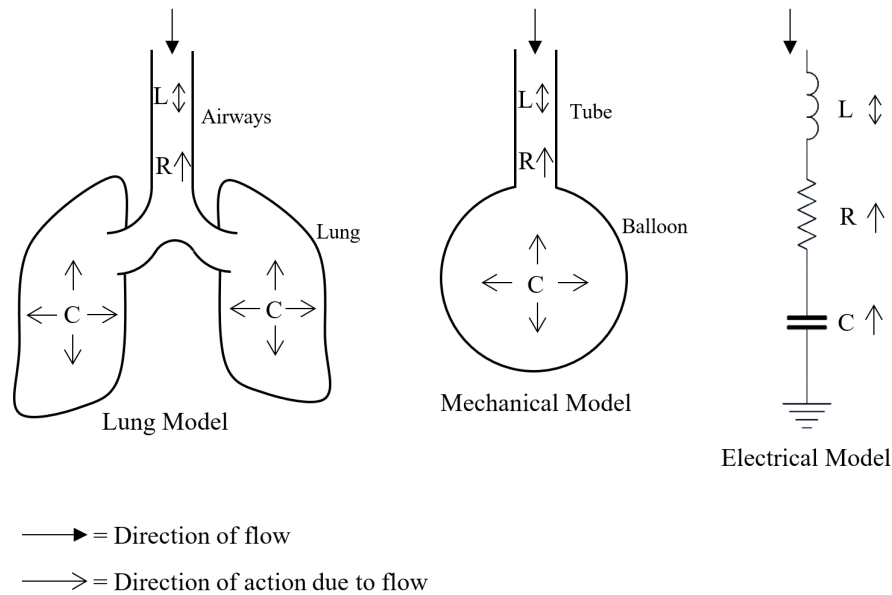


Figure 3.3: Left and Centre - Simple fluidic dual lung model and mechanical model of lungs respectively showing air inertance, air resistance and lung compliance. Right - Electrical model of lungs showing inductance, resistance and capacitance.

Table 3.2: Generalised system properties example. System resistance can be generalised to $\psi = R\zeta$

| System type | ψ (effort) | R (resistance) | ζ (flow) |
|-------------------------------|----------------------|-----------------------------|-----------------|
| Fluidic (Poiseuille's law) | Pressure difference | Fluid mechanical resistance | Volumetric flow |
| Mechanical | Force | Mechanical resistance | Velocity |
| Electrical | Potential difference | Electrical resistance | Current |

3.3.3.1 Mechanical

Ben-Tal presented two common forms of mechanical lung model that have been used in artificial respiration. These models are often used in commercial simulators to observe and compare dynamics to patient data or as a means to study, for example, how a controller would work in a clinical environment. Lua et al [26] utilised a commercial breathing simulator to mimic human spontaneous breathing for use during simulation testing. This simulator used the ‘two main lung model parameters’ of airway resistance and elastance (reciprocal of compliance). Their work focused on the application of control methods and is discussed in Section 3.2.1. The simulator itself is not analysed

as it is a commercial unit but it shows that basic parameters can be used to provide relatively accurate representations of human lungs.

Yan et al [28] described a dual lung model to determine the feasibility of their control schemes discussed in Section 3.2.3. The lung model used lung resistance and compliance, similar to Lua et al. Resistance is mainly caused by airway friction and was represented by throttle valves for each pipe to each model lung. The model lungs were considered as two variable-volume containers, thus the compliance was reflected by the volume change of these containers. This further validates the use of simplistic models to replicate the dynamics of the lungs.

Hunneken et al [42] derived a dynamical model of lungs to demonstrate the use of linear control and variable-gain control for mechanical ventilation. They derived the relationships between pressures and flows using the resistance and compliance dynamics of the lungs and tubing. The model provided the necessary data to validate the use of a variable-gain controller in medical ventilation as an improvement on linear controllers.

3.3.3.2 Electrical

Using Table 3.2, lung properties can be symbolised as electrical circuit components where voltage is analogous to pressure and current is analogous to airflow. More specifically, the pressure in the alveoli is analogous to the voltage across a capacitor, and the pressure at the airway entrance is analogous to the input voltage. Transfer functions and/or state-space equations can be derived from the electrical properties by relating the output to the input. The more detailed the model, the more complex its transfer function/state-space equations.

Diong et al [45] presented the most common models (see Figure 3.4) and compared their accuracies to establish how different pathologies affect airway resistance. The papers discussed below presented, used, and analysed the RC circuit as well as the models shown in Figure 3.4.

Schmidt et al [46] used the resistor-capacitor (RC) model (also presented in [28, 41, 42]) as well as the resistor-inductor-capacitor (RLC) model (Figure 3.4a) to determine lung mechanics (resistance, inertance and compliance). They stated that the RC model is commonly used for both tidal breathing and medical ventilation due to the low frequency of breathing. They then discussed the RLC model, which is beneficial in studying higher frequency dynamics. However, the one-compartment model cannot be used to examine differences in pulmonary dynamics between the left and right lung. They followed this with a description of the two-compartment RLC model where there is a central resistance as well as peripheral resistances with two compliances to represent each of the lungs. Finally they presented the Mead model shown in Figure 3.4f. This model gives further consideration of compliances of the airways, chest wall and extrathoracic components

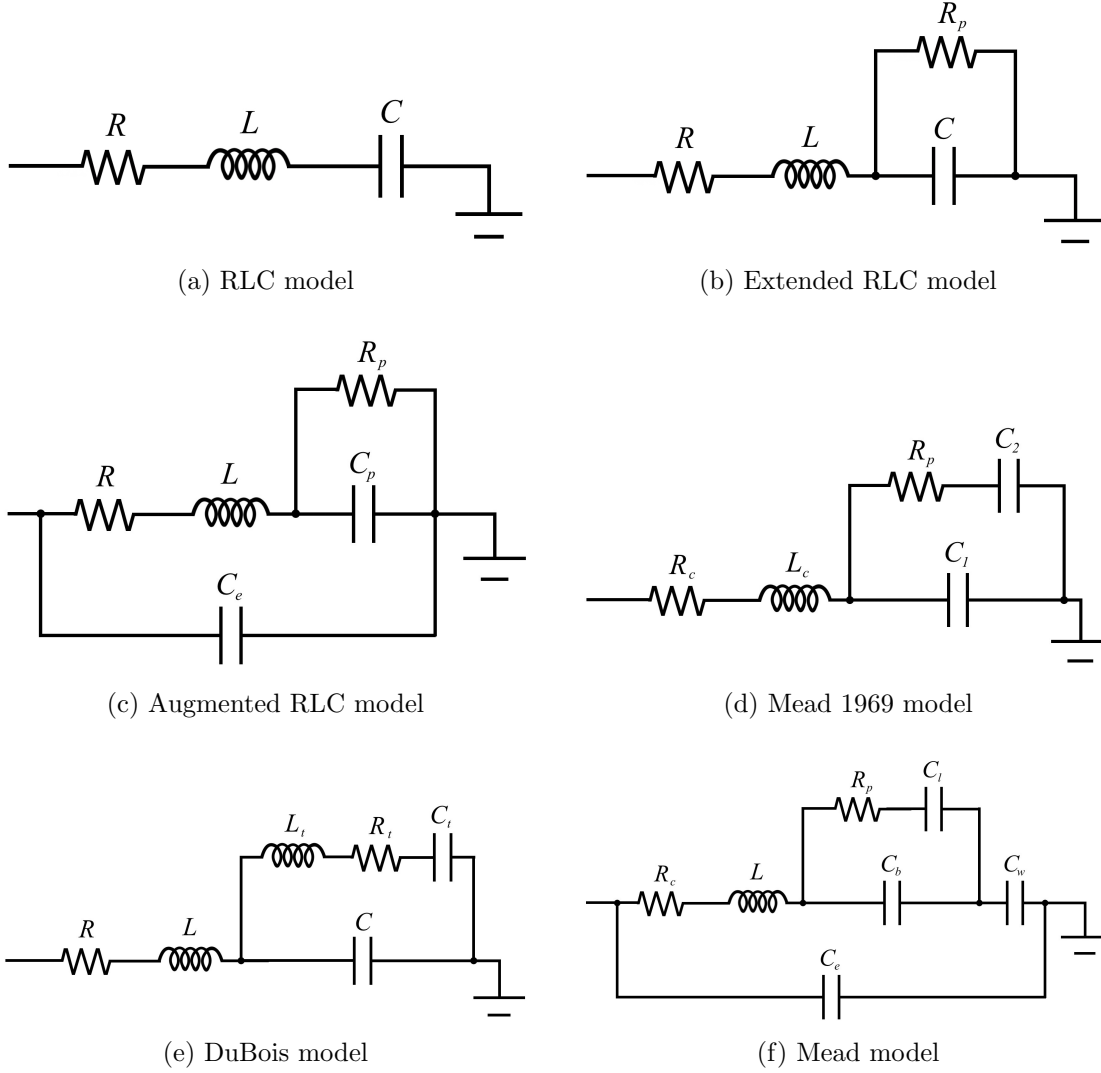


Figure 3.4: Example electrical equivalent models replicating the mechanical function of natural breathing [45].

(such as the mouth). This allows for observation of different influences on flow-pressure dynamics in the lungs. A more detailed model allows for different physiological factors, development, and diseases to be simulated in order to better understand the impact on lung function.

Diong et al analysed the extended RLC model (Figure 3.4b), and Rajagiri and Diong [48] analysed the augmented RLC model (Figure 3.4c). The extended RLC model adds peripheral resistance to the RLC model which allowed for frequency dependence observed in typical real impedance data. It provided a good fit in terms of model accuracy with a small error in reactance. However, even though the DuBois model had a larger error in reactance, it provided a better overall model fit to real data. The augmented RLC attempts an improvement upon the extended model by introducing an extrathoracic compliance. This attempts to increase the real part of the respiratory system's impedance at higher frequencies. It provided the best fit for compliance parameters

which benefited the research that they were performing. However, it only provided a good overall fit (like the extended RLC model) but was again outperformed by models such as Mead and DuBois.

To summarise the models discussed and shown in Figure 3.4:

- the RC model is the most simple model possible to reproduce the dynamics of the human lungs;
- the RLC model helps in simulating lung dynamics at higher frequencies where the RC model is less accurate;
- the extended RLC, augmented RLC, and Mead 1969 models provide additional components of compliance and resistance to provide a more accurate impedance of the respiratory system at higher frequencies;
- the DuBois and Mead models provide a high accuracy model of the respiratory system by introducing components external to the lungs such as thoracic cavity compliance (also added in augmented RLC) as well as peripheral inertance or extrathoracic compliance.

These models can be used to study the effects of many different aspects of the lungs including physical properties and pathologies across a range of frequencies.

A spirometry test is a commonly used procedure to study pulmonary function. The test involves taking a deep breath in and then exhaling forcefully into a small tube (called a spirometer, See Figure 3.5). The data from this can be used to:

- measure vital capacity (i.e. the maximum volume of air a patient can exhale);
- assess the force and speed a patient can exhale air. This can be used to monitor and diagnose respiratory conditions such as asthma, chronic obstructive pulmonary disease (COPD), cystic fibrosis and pulmonary fibrosis;
- assess the general health of a patient and their lungs before surgery [49].

Juroszek and Stanisławski [47] attempted to synthesise dynamic models to simulate experimental measurement data. The main idea was to replicate how a person might respond to a spirometry test to investigate the maximum change in air flow, referred to by the authors as the “pressure pulse excitation”. They achieved this by reverse engineering experimental pressure data during forced expiration, using a “black box” analogy, to generate duplicate simulation data. This allowed the excitation pulse to be determined. In their work they used a combination of RLC model components in differing configurations. Spirometry test modelling has a very similar application to



Figure 3.5: Example of patient using a spirometer taken from the NHS website[49].

lung pressure profiling as it involves forced expiration after a deep breath. However lung pressure profiling requires patients to track a pressure reference and can last longer than 20 seconds, whereas spirometry breathing apparatus has minimal resistive component and so each test lasts for only one or two seconds. This means that no pressure reference tracking is necessary.

A comprehensive search has found that no research has attempted to model the process of voluntarily tracking a lung pressure reference signal. This section has presented the most common models used for respiration. These basic lung models consider the underlying dynamics of the system such as resistance, compliance, and inertance. However, in order to model the entire closed-loop reference tracking system for LPP testing, additional components such as muscle dynamics and voluntary motor control of the lungs must be included. These will be discussed in subsequent chapters.

3.3.4 Application of Models to Lung Pressure Profile Testing

Section 3.3 has introduced human respiratory models commonly used in modern medicine. The models are used to help diagnose conditions that may affect respiration, replicate motion of the thoracic region during respiration to improve treatment, and determine how conditions affect different aspects of respiration such as airflow resistance or lung tissue compliance. Table 3.3 provides a brief summary of the strengths and weaknesses of each model and their applicability to LPP tests.

Table 3.3: Comparison of lung models

| Model | Advantages | Disadvantages | Conclusions |
|------------------|---|--|---|
| Imaging | Can be used to study the movement of the lungs and thus flow of air during respiration. Can help determine what may affect the respiratory dynamics. | High costs. Specialised equipment. Doesn't help determine the dynamics only what might affect them. | Imaging is very useful tool when analysing respiratory dynamics and what may affect them but does not have any explicit input/output variables. |
| Gas Exchange | Use multiple parameters such as minute volume, flow rate, pressure, partial pressures in the lungs. Can be used to predict upcoming changes in dynamics based on current conditions. | Higher accuracy leads to higher complexity and as such computational requirements. Predictions may not always be accurate. | Gas exchange models provide all the necessary variables for pressure control during LPP tests and how varying conditions can affect respiration. However, they are more often used for diagnostics or to ensure adequate oxygen supply and as such have higher complexity than necessary for LPP testing. |
| System Analogues | Models can be developed to be as simple or complex as necessary to model required parameters. Can be used to predict future responses. | Simpler models can reduce accuracy. Higher complexity creates more variables to identify which can increase computational load. | Analogous models allow for highly complex systems to be represented in lumped parameter form. More complex models provide more accurate replication of a system but also increase computational load. |

3.4 Summary

Chapter 2 reviewed the unequivocal link between changes in lung pressure and ICP. Some of the reviewed work focused on the effects of the Valsalva Manoeuvre (i.e. short periods of high lung pressure) and required invasive methods. It discussed that TMD is not yet

precise enough, but measurements taken coincidentally with specific lung pressures and changes in lung pressures may provide necessary data to improve this precision.

Humans cannot perfectly generate requested lung pressures and pressure changes for LPP testing, so some form of assistive controller will be needed. The review of control methods in this chapter has shown that focus has been on controllers for medical ventilation. The key purpose of these controllers is to adjust flow rates and pressures to supply adequate gas exchange in a physiologically safe manner. This means that the controllers have to handle system constraints and be able to adjust to patient requirements and circumstances (i.e. the non-linearity of the process model). However, to date, no research has been published that attempts to manipulate airflow in order to control lung pressure during voluntary forced expiration. Such a controller would need to be designed for a system that includes human breathing dynamics, muscle actuation properties and the voluntary control component.

The review of respiration models has shown that research has also focused on replicating natural breathing for use in medical ventilation. There are varying model types which are used based on their application. For example imaging is more useful for radiotherapy and electrical/mechanical equivalent models are more useful for ventilation. However, there are currently no models of voluntary lung pressure reference tracking. Replicating natural breathing means that multiple processes can be ignored such as muscle and motor control. These processes would need to be considered if voluntary respiratory changes in airflow or pressure (e.g. spirometry) were to be modelled. Such models would combine passive lung dynamics with muscle actuation and voluntary control of the central nervous system.

The next chapter will discuss how the controllers and models presented in this chapter could be applied to lung pressure profile reference tracking. It introduces exactly how and why LPP testing could be used alongside TMD in order to determine the size of an intracranial mass (such as a tumour). It also presents some of the specifications that LPPs would need to adhere to in order to be applied in a clinical setting.

Chapter 4

Problem Specification

Chapter 2 motivated improving the accuracy of lung pressure profile (LPP) testing. This in turn improves the accuracy of intracranial pressure (ICP) measurements via tympanic membrane displacement (TMD). Chapter 3 reviewed control schemes and models that could be applied to LPP testing. These controllers and models were mostly applied in medical ventilation as very little research has been conducted to control or model forced expiration. This chapter presents how TMD and concurrent LPP tests could be used to determine if a cranial mass (tumour) is present and its possible size. It also presents how LPP tests are currently performed and the inaccuracies that occur. It discusses relevant controllers and models that could be applied to LPP tests and provides constraints that must be applied to the selected controller(s).

4.1 Tympanic Membrane Displacement and Lung Pressure Measurements

LPP testing could provide critical data that would improve analysis of both evoked and spontaneous TMD data. The desired pressures and pressure changes would cause excitation of the blood flow regulatory mechanisms of the brain. This excitation would be observable in the TMD measurements. A simple lung pressure profile may comprise a step-change increase in lung pressure (e.g. from 0 to 50 cmH₂O), a hold of the pressure for a few seconds, and a release of that pressure (i.e. a step change from 50 to 0 cmH₂O). Tracking this profile would result in the following process in a healthy individual.

- Generating a pressure of 40-60 cmH₂O (high pressure sensation similar to the Valsalva Manoeuvre (VM)) in the lungs causes constriction of the vena cava thus increasing venous pressure up into the intracranial cavity;

- the ICP regulatory mechanisms adapt CSF volumes and blood flow to and from the brain to decrease ICP to a safe value;
- quickly dropping lung pressure to 0 cmH₂O causes an excess volume of venous blood to drain from the brain;
- the pressure regulatory mechanisms redirects blood and CSF back to the brain.

For an individual with a significant intracranial mass the following process would occur.

- Generating a pressure of 40-60 cmH₂O (high pressure) in the lungs causes constriction of the vena cava thus increasing venous pressure up into the intracranial cavity;
- the ICP regulatory mechanisms adapt CSF volumes and blood flow to and from the brain to decrease ICP - however, ICP may not fall within a safe range;
- quickly dropping lung pressure to 0 cmH₂O causes an excess volume of venous blood to drain from the brain;
- the pressure regulatory mechanisms redirect blood and CSF back to the brain.

The difference between a healthy individual and an individual with a intracranial mass is that ICP may not be considered a safe value during the high lung pressure stage. This would be detectable in the TMD measurements. The specific lung pressure at which high ICP can be detected in the TMD measurements could determine the relative size of the intracranial mass. The lower the lung pressure at which a high/raised ICP is detected at, the larger the intracranial mass.

4.2 Control During Lung Pressure Profile Testing

The control of airflow during LPP testing should assist a patient to track the pressure reference. The current approach when used for LPP testing in a clinical research setting does not allow for any assistance control. However, it does comply with multiple specifications that are required of it such as particular airflow and pressure ranges. This section introduces some of the key specifications for the setup and how they may be applied as constraints in a control setting. Examples of LPPs are presented and discussed to show how a patient can track a reference, and how implementing airflow/pressure control would help them improve their tracking ability.

4.2.1 Specifications

Appendix A presents the key specifications that must be met for an apparatus setup to be used for clinical LPP testing. Some of the specification points will be used as limits, constraints and/or objectives of the control schemes applied in this thesis as presented in Table 4.1.

Table 4.1: Table of specifications

| Specification | Reason | Constraint |
|--|---|--|
| The measurements should be near real-time | Target profiles are measured ideally at 100Hz - this ensures the patient is shown the exact pressure that they are generating | The pressure sensor must be accurate and not have an observable delay, the controller must be efficient enough to be able to provide adequate control whilst not slowing down the rest of the software |
| An ideal minimum flow rate of around 5 ml/s | To ensure the glottis remains open and the measured oral pressure is the same as in the lungs | Upper limit on valve resistance |
| Profiles should last at least 20 seconds | To coincide with TMD measurement profiles | Lower limit on measurement time period (relies on average airflow over measurement period) |
| Achievable pressures up to 60 cmH ₂ O | Patient should be able to generate pressures in a relatively comfortable manner | Upper limit on pressure reference and possible increase in lower limits of valve resistance at higher pressures |
| Lower pressure limit of 0 cmH ₂ O | The research objective is to model and control forced expiration | Lower limit on pressure reference |
| Lower limit on valve resistance | Fully open valve still has resistance | Lower limit on resistance of 20 cmH ₂ O/L/s |
| Maximum exhaled volume limit | Patients have a limited lung capacity and should not over-exert during forced expiration | Volume limit around 1 litre less than their vital capacity |

4.2.2 Lung Pressure Profile Tests

Before LPP tests begin, the patient is seated and shown a pressure waveform chart on a computer display. The x-axis displays time and the y-axis displays pressure. Two signals are plotted on the graph; one showing a reference pressure and one showing the measured pressure in the apparatus. When a patient blows into the apparatus, they will observe a corresponding change in the apparatus pressure signal.

The aim is for the patient to generate the same pressure in the apparatus as the reference; this is called LPP reference tracking. To reduce the impact of learning on the

response, the patient is only shown the current reference pressure in order to prevent them anticipating the future response. Patients can be requested to generate a constant pressure or follow sinusoidal/square wave or step-change pressure references for over 20 seconds, with values ranging between 0 and 60 cmH₂O (coinciding with the specifications in Table 4.1).

The red cap (as seen on the end of the breathing tube in Figure 4.1) provides consistent air leakage to prevent patient glottis closure. It can be removed manually during LPP testing to create a sudden drop in lung pressure. This terminates the measurement period since the test only involves forced expiration.

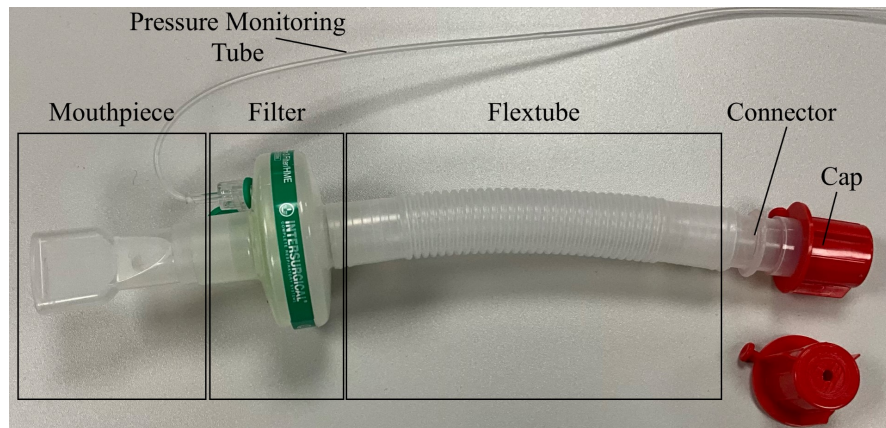


Figure 4.1: Repeat of Figure 1.4a).

Figure 4.2 shows examples of data, collected for this thesis, of how a person can track a pressure reference of a lung pressure profile. These data sets were all taken using the new setup with the valve shown in Figure 4.3 but replicating the current clinical setup with the red cap shown in Figure 4.1.

Figure 4.2a shows an example of moderate tracking ability where the participant has struggled to follow the reference changes, and also struggled to generate a pressure higher than 20 cmH₂O. This could be resolved by providing a higher airflow resistance in order to generate higher pressures. Figure 4.2b shows an example of good steady state tracking but with large overshoots on pressure reference changes. These overshoots could be minimised if the airflow resistance was adjusted. Figure 4.2c shows an example of what is considered good pressure reference tracking. There is very little overshoot or undershoot and the steady state error mostly remains within 2-3 cmH₂O. However, if airflow control was introduced, the ‘reaction time’ to each step change could be reduced, i.e. the resistance could change when the reference changed to initiate a more immediate response. The addition of the variable resistance valve would address all the issues above: providing higher resistances; reducing overshoot; reducing reaction time.

The timing of the red cap removal is neither consistent nor reliable, therefore, it motivates the approach taken in this thesis to replace the cap with a proportional valve. The

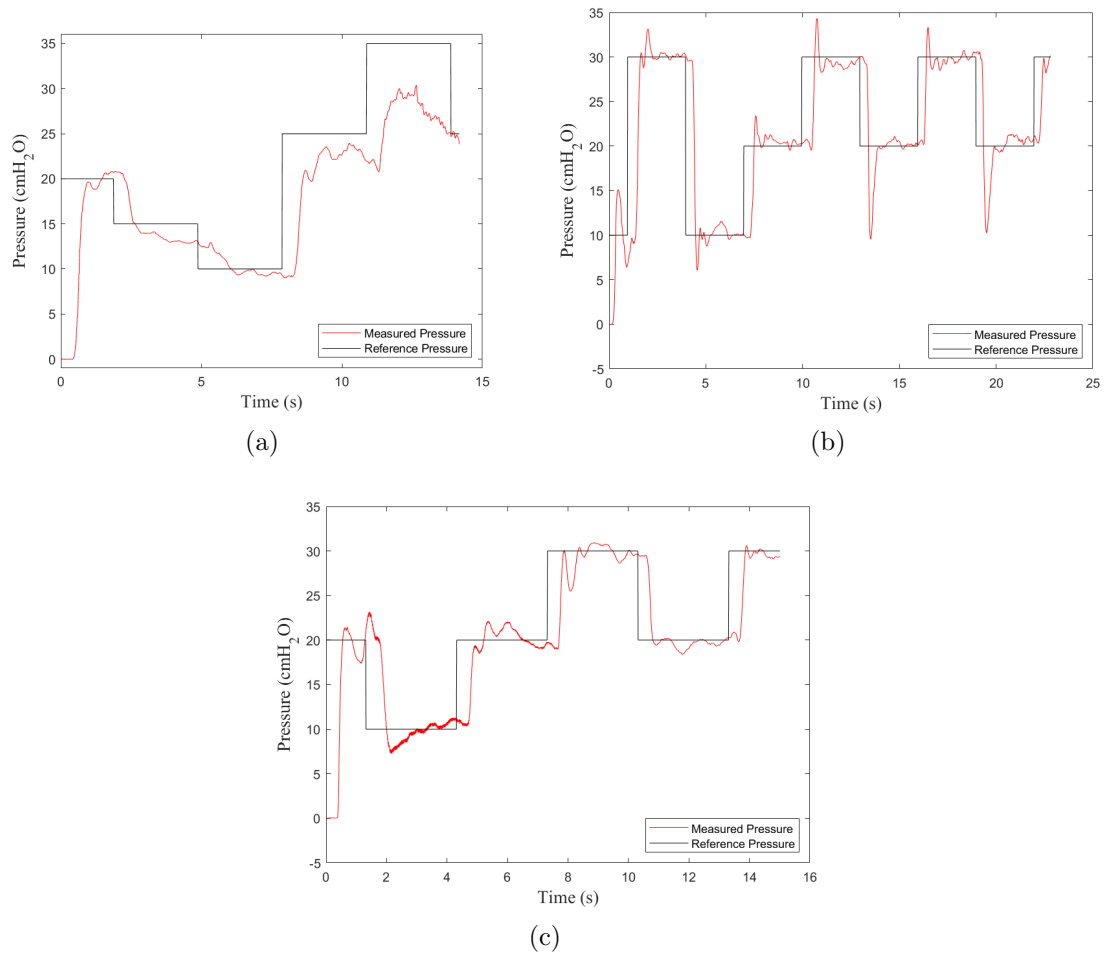


Figure 4.2: Examples of:

- (a) Moderate/poor tracking but struggling to reach higher pressures
- (b) Very good steady state tracking but significant overshoot on step changes
- (c) Very good overall tracking with small overshoot and good steady state tracking.

selected proportional valve must adhere to the same constraints as the original setup. The valve must have a fast input signal response and be able to create a large range of resistances.

4.2.3 Modified Experimental Setup

Figure 4.3 shows the modified setup. Compared to the standard clinical research setup shown in Figure 4.1, the flextube has been removed to reduce compliance. The modified setup has retained the mouthpiece, filter, and pressure monitoring tube as in Figure 4.1. To apply any form of control, the modified setup must have an airflow sensor and a variable valve. The airflow sensor must be added to enable accurate resistance calculations (using the linear relationship, $R = P/Q$), and the valve must be added

in order to control airflow. The modifications in this thesis have been chosen with a universal applicability of different control types in mind.

The airflow sensor needs to be able to precisely measure airflow between a range of 0 to 2.5 L/s. This airflow range covers all necessary valve resistances and pressure ranges of 20-1000 cmH₂O/L/s and 0-60 cmH₂O respectively. The selected sensor is a *Sensirion SFM3020 series* which has a flow range of -0.167 to 2.67 L/s with a typical accuracy $\pm 3\%$ of the measured value.

A variable pulse-width modulation (PWM) valve has been added to control airflow resistance. The valve needs to be able to precisely produce resistances between 20 and 1000 cmH₂O. The selected valve is a *Burkert 6024 series (12mm)* which can produce these resistances with a typical hysteresis value of $< 7\%$.

The pressure sensor is a *Panasonic PS-A series (6KPa)*. Its full range of pressure values is -5 to 65 cmH₂O. The measurement hardware and software are *National Instruments myRIO-1900 series* and *Labview 2019* respectively. All identification, control design, and analysis computations were performed in *MATLAB R2020b*.

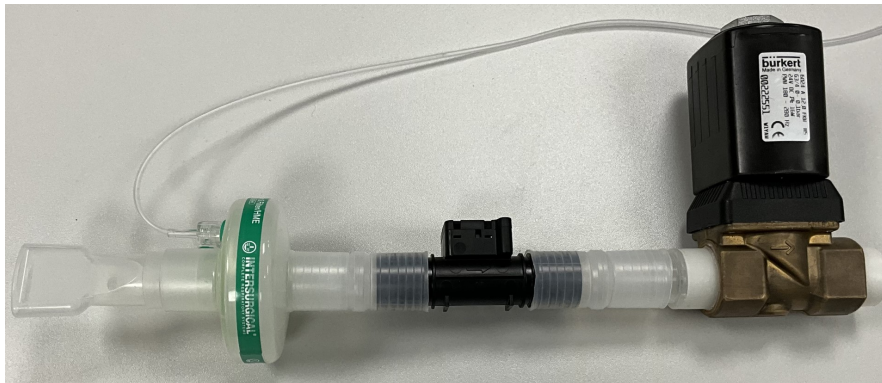


Figure 4.3: Breathing tube, pressure sensor, airflow sensor and variable valve used to measure lung pressure.

4.3 Controller and Model

The application of control of a parameter in a parameter-varying system is a complex endeavour. The control schemes presented in Section 3.2 can be adapted to be applied to pressure control during LPP testing. Controllers usually apply an additional input to the system in order to improve the output. When considering this for LPP reference tracking, this would be equivalent to an additional pump attached to the apparatus. A pump is not viable for this application for multiple reasons but mainly due to safety, response time, and practicality (a large pump would be needed to generate the pressures which limits its portability).

From the research findings in Chapter 3 and summary of advantages and disadvantages in Table 3.1, it is apparent that there are multiple controllers that could be implemented in LPP tracking assistance. Machine learning has many advantages for its use in LPP tracking assistance from a clinical perspective as it would be able to use large datasets in order to provide the best control. It would possibly not need tuning from patient to patient and only require basic metrics such as age, sex, and health status. However, for initial application and research it is not viable due to the necessity of collecting enough data in order to train the controller. This thesis is attempting to minimise costs for wider application, so the complexity and the storage necessary would increase costs. As a corollary, the complexity of adaptive control and hybrid control are also non-viable for the thesis due to storage/computing demands. Hybrid control also uses multiple control methods using data collected for each control type. As no data have been collected on any controller for application in LPP tracking assistance hybrid control is not considered in this thesis.

In clinical application, LPPs can be repetitive tasks such as maintaining a consistent pressure or square wave pressure profiles. However, some profiles are more randomised to elicit different responses. Iterative learning control (ILC) would not be viable as not all the reference profiles are repetitive tasks. Additionally, ILC would need a baseline control technique to start with in order to adapt the controller to improve its ability to assist the patient. ILC would be a viable next step once an initial baseline control method has been validated and the ILC can improve its performance by tuning the controllers parameters. As with machine learning and adaptive control, fuzzy-logic would require a large amount of data in order to tune the controller parameters for best performance. Fuzzy-logic is therefore not a viable control option for this thesis.

Proportional-integral-derivative (PID) control and its variations/combinations would be a viable option to use for this thesis due to the assistive nature of the control task. It is not a complex method and as such does not have significant storage or computational requirements. Proportional control would adjust the valve in such a way that it would increase valve resistance the lower the pressure the patient is generating below the target, and decrease the resistance the higher the generated pressure is above the target. PI control would be similar except with the pressure being over or under but the increase or decrease in resistance would accumulate over time until the target pressure is reached.

Model predictive control (MPC) is another viable option for application to assist during LPP tracking. The predictive capabilities of MPC means that, with an accurate model, it can provide appropriate control given that it knows the future target pressure and the expected response from the patient. A balance can be found which allows for a prediction horizon large enough to predict far enough ahead while minimising computational load thus the cost of hardware. MPC can also be developed to function within hard constraints and can adapt to changes in system dynamics. Based on this section's analyses of controllers, MPC is the main focus of controller development in this thesis.

As MPC is the chosen control approach, an appropriate model is required. Section 3.3 presented three key models that are commonly used in medicine to present lung dynamics. Table 3.3 presented the advantages and disadvantages of their applicability to LPP testing. Imaging models are overly complex for this application as they would produce data that do not provide any benefit to pressure control. Further reasons to not use imaging are that: it uses highly specialised equipment which leads to high costs and maintenance; it must be performed in a controlled environment; and it mostly uses X-rays for imaging purposes which therefore means that it cannot be used continually without causing significant harm to the patient.

Similarly to imaging models, gaseous exchange models would use/produce some data that would not be beneficial for control of lung pressure. The higher complexity of the model would also create larger computational loads in order to process accurate prediction. This leads to the conclusion that imaging and gaseous exchange models would not be adequate for use in MPC for LPP testing. System analogues such as mechanical and electrical models can provide a great benefit for MPC as the model can be as simple or as complex as is necessary. They can also be used to represent the most common dynamics of the lungs. Mechanical models of the lungs would also require analysis of fluid dynamics which would provide high model accuracy but also increase complexity. Assumptions can be made to mitigate this which are already intrinsic in electronic models such as laminar flow and no flow disturbance/turbulence. This motivates the use of electrical analogous modelling as it can provide linear pressure-flow-resistance correlations.

In order to provide adequate pressure assistance control during LPP testing, there must be a focus on the trade-off between model accuracy and ease of identification. The main components of resistance, inertance, and compliance are necessary to model the lung dynamics. However, even though additional components would provide more detail of lung airway branching (i.e. resistance of bronchi or compliance of alveoli), they also produce additional variables to be identified. This leads to the conclusion that the best model for this research is the basic RLC model shown in Figure 3.4.

4.3.1 Nested Loops

The application of control to human lung dynamics in medical ventilation is relatively simple in a sense that the only input of pressure or airflow is the ventilator itself as the patient is unconscious during the procedure. The considerations that must be made for LPP tracking tasks is that the patient is responsible for making pressure changes. The primary form of control for the tracking task is therefore the patient's cognitive ability and respiratory muscle strength. The role of the implemented MPC in this thesis is to act as a secondary internal control loop. This is to assist the patient in achieving the required pressures without compromising the patient's own control.

To ensure that the MPC applied to the valve does not have an adverse affect on the tracking task, constraints on valve resistance and flow can be implemented to ensure that the reliance of the tracking still remains on the patient. Both the patient and controller are provided with the reference pressure to adjust the valve resistance accordingly. The controller needs to be fast-acting, with a quicker response than the patient, in order to adjust the resistance of the valve based on the patient's control action. This also allows for the MPC to complement rather than compete with the patient's control action. The most important consideration for the controller to provide assistance is to use a model that accurately replicates the patient's response while minimising model complexity, in order to maximise performance.

An additional issue is the valve hysteresis mentioned in Section 4.2.3. The valve's resistance is based on a PWM signal which determines the current supplied. In order to provide assistive control the valve resistance selection of the MPC controller must be accurately provided by the valve itself. There are two ways to ensure this occurs, the first is to develop an algorithm which perfectly maps how the valve resistance will change based on its previous position, which could produce a near perfect resistance every time but would be time consuming to develop and could be computationally expensive. The second would be to develop an additional controller which adjusts the PWM signal to adapt the current supplied, thus the resistance can be constantly tuned by a further internal control loop to the MPC. This would need the same basic principles of function as the MPC to the patient's control in that the 'inner loop' would have to be faster acting whilst also being undetectable by the patient.

This highlights the necessary complexity of the developed system in order to provide assistive control to a patient during LPP testing. The next step would be to determine appropriate timings for each control loop in order to provide the best control.

4.4 Summary

This chapter has stated how specific lung pressures and pressure changes can be observed in TMD measurements. It has presented how a person may track a LPP. It has addressed the issues that result in imperfect LPP tracking and how control of airflow could mitigate these. Section 4.3 discussed the reviewed controllers from Section 3.2 with regards to their suitability for application to this research. It was decided that MPC was the most appropriate controller to use with comparative PID methods. The next step is to formulate the MPC control problem and develop a suitable model. Modelling would require an appropriate level of complexity in order to analysis the appropriate dynamics of the system, whilst maintaining simplicity to minimise unnecessary excess data and computational load. Electrical analogous models would provide the necessary data for MPC to predict the expected patient response to a LPP tracking task.

Chapter 5

Model Predictive Valve Control using RLC Model Structure

The last chapter motivated applying MPC and defined the basic objectives of the tracking task. This chapter formulates the MPC objective and develops a suitable model. The focus will be on a straightforward approach that yields a computationally efficient solution. As described in Chapter 4, the objective is to control the valve resistance as part of a linear parameter-varying system.

This chapter introduces a system model that comprises the underlying dynamics of the respiratory system. A control approach is then developed to minimise an objective cost function. Simulations of the system model and controller are analysed to determine its applicability. An identification technique is then presented using linear regression to provide parameters for the controller.

Recall that during lung pressure profile (LPP) testing, the pressure in the breathing tube will be sampled using a pressure monitoring tube connected to a pressure sensor. The pressure will then be displayed to the patient and operator (e.g. a clinician). A dual-user interface will be employed so the operator can create parameters for a pressure profile whilst also observing the measurements. The patient can only observe their LPP reference tracking up to the current time. Based on the measured pressure and target pressure, the controller will actuate the valve connected to the breathing tube.

5.1 Problem Description

Figure 5.1 shows a block diagram of how valve aperture would be manipulated where the system represents the patient using the device (i.e. having been given a reference they generate a pressure). The pressure reference is r and the measured output of the patient model is y . The controller uses the reference and measured pressures to determine the

best aperture of the valve, V , in order to assist in increasing or reducing the pressure produced by the person. Subscript k denotes the discrete-time sample instant.

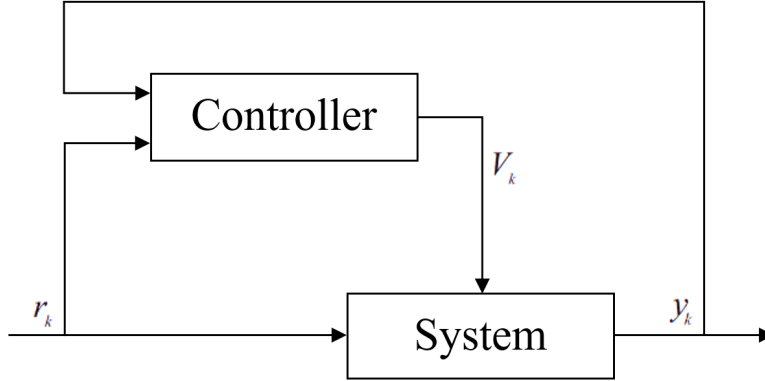


Figure 5.1: Block diagram of control process where the system corresponds to the human tracking the pressure reference, and the controller adjusts valve resistance V accordingly.

There are a variety of models of voluntary human sensorimotor control available (see, e.g. [50]). The most basic form of human motor control always involves feedback. For example, standing does not involve any form of preliminary motor input, however, balance mechanisms (proprioception) provide continuous feedback in order to remain upright. To model walking, a forward planning component must be added in order to actuate the appropriate muscles (i.e. for leg movement).

A forced expiration breathing model must incorporate muscle actuation and motor control. The feedback component represents the patient's attempts to mitigate the error between the desired and measured pressure. The feed-forward component represents voluntary motor control dynamics of the respiratory muscles during LPP tests. These components are shown in Figure 5.2, where:

- G is the dynamics of the respiratory tract and breathing apparatus;
- $K(q)$ is the diaphragm and intercostal muscle dynamics;
- $H(q)$ is the motor control feedback;
- $F(q)$ is the noise filter.

Additionally, q is the sample shift operator and external noise is denoted by the signal w . The filter $F(q)$ reduces the noise component using assumed system dynamics in order to improve the model identification procedure.

To expand on the above bullet points, G represents the effects on airflow due to the structure of the lungs. This corresponds to:

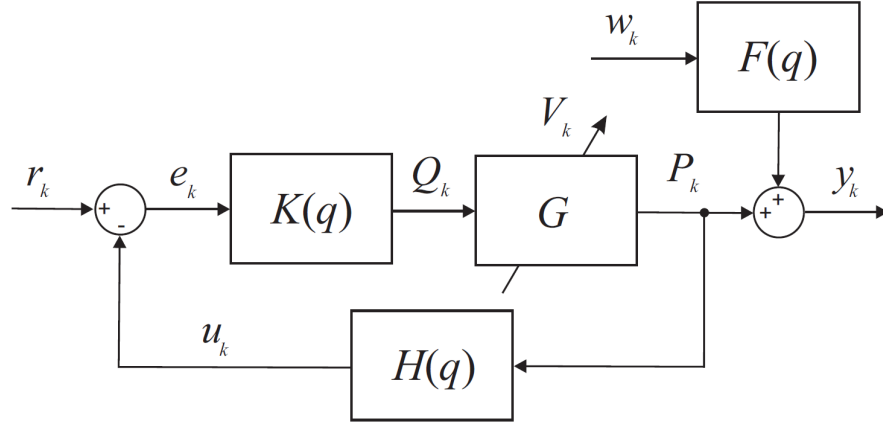


Figure 5.2: Voluntary pressure reference tracking system with valve resistance V_k . This depicts the ‘System’ in Figure 5.1.

- resistance to airflow - caused by physiology such as cilia or undulation from differing tissues and cartilage;
- compliance of the lungs - i.e. how the lungs have elastance during expansion and shrinkage while breathing;
- inertance - caused by the volume and pressure/density of the air in the lungs.

K represents the force from the musculature surrounding the thoracic cavity generating the pressure in the lungs during exhalation. H refers to the feedback the patient receives such as visual feedback from reference to generated pressures and tactile feedback from the valve resistance and their respiratory muscle contraction.

The derivation of K and H is dependent on the ability of a theoretical patient. The necessity of their own actions by contracting their respiratory muscles to generate the required pressure creates a controlled input. The contraction of muscles together with visual feedback to the patient as to whether the required pressure is being generated is a simple control loop (as shown in Figure 5.2). This loop comprises an observed input (the reference pressure), a generated pressure (depending on the patient control action and strength K and dynamics G), and an observed feedback that is acted upon (H gives a scaled error).

A model for system G is shown in Figure 5.3 and represents the physiology of the human lungs, where current source Q represents the effect of diaphragm movement (L/s), and P is the pressure difference (cmH₂O) measured across the variable valve resistance V . This builds on the RLC medical ventilation model presented in Section 3.3 by incorporating valve resistance into G as part of the conditions that air will experience when flowing from the lungs. The unit, cmH₂O, is conventionally used to measure pressure in medical ventilation. This model assumes laminar flow, with the Hagen-Poiseuille equation enabling valve resistance V to be related directly to the valve aperture. Components R ,

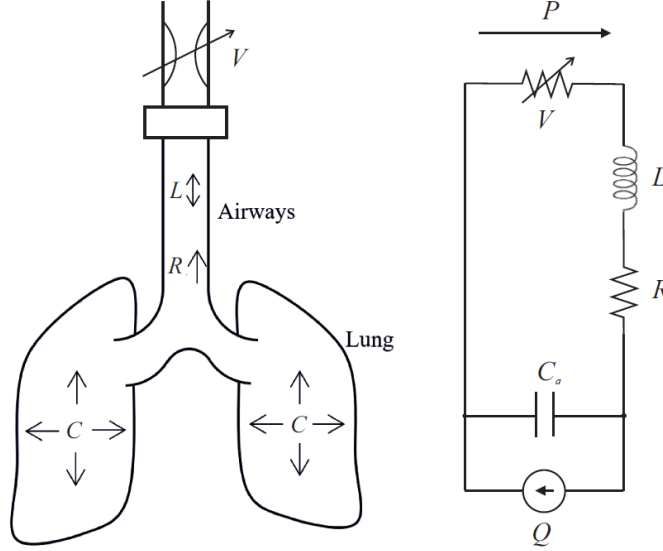


Figure 5.3: Left diagram - lung model showing air inertance L , air resistance R , valve resistance V and lung compliance C . Right diagram - equivalent electrical analogue.

L , and C (henceforth labelled C_a) are lumped parameter representations of airway resistance, inertance and compliance. These values are constants based on the physiology of the patient.

More complex lung representations that model downstream branching of the airways (i.e. bronchi resistance and alveoli compliance) are possible as reviewed in Section 3.3, and will all result in the same overall form. Having defined G as an analogue system, it is now possible to convert it into a difference equation form that is needed in later development. This is described below.

Definition 5.1 (System Description). The system has the form of Figure 5.2 where $K(q)$, $H(q)$, and $F(q)$ have linear time-invariant (LTI) dynamics and G takes the form of a lumped parameter lung model with valve resistance V_k at sample k . The transfer function of system G can be represented in the linear time-varying (LTV) form

$$P_k \left(p_0 + \frac{\bar{p}_0}{V_k} \right) + P_{k-1} \left(p_1 + \frac{\bar{p}_1}{V_{k-1}} \right) + P_{k-2} \left(p_2 + \frac{\bar{p}_2}{V_{k-2}} \right) = Q_k \quad (5.1)$$

Proof. The differential equation of the mesh in Figure 5.4 is

$$(V + R)Q_2 + L \frac{dQ_2}{dt} + \frac{1}{C_a} \int Q_2 = \frac{1}{C_a} \int Q_1 \quad (5.2)$$

Using analogous voltage and pressure equations the relation between pressure, airflow, and valve resistance is $P = Q_2 V$. Substituting that into the derivative of (5.2) gives

$$\frac{dP}{dt} + R \frac{dQ_2}{dt} + L \frac{d^2 Q_2}{dt^2} + \frac{1}{C_a} \times \frac{P}{V} = \frac{1}{C_a} Q_1 \quad (5.3)$$

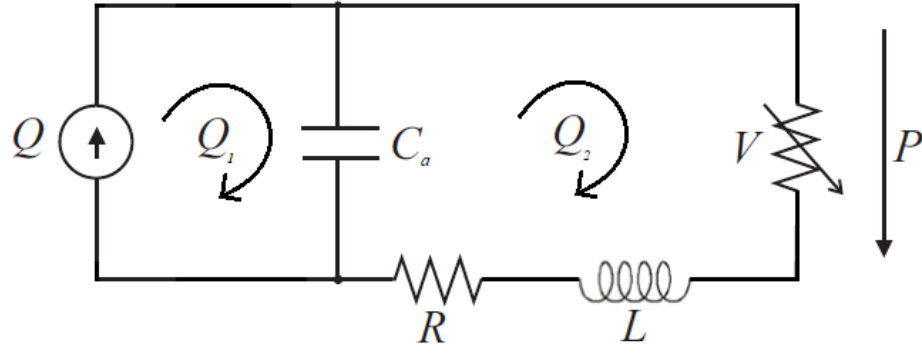


Figure 5.4: Mesh analysis diagram of electrical equivalent circuit in Figure 5.3.

given T_s is the sampling time and the Euler backward finite difference approximations

$$\begin{aligned}\frac{dP}{dt} &= \frac{P_k - P_{k-1}}{T_s} \\ \frac{dQ_2}{dt} &= \frac{1}{T_s} \left(\frac{P_k}{V_k} - \frac{P_{k-1}}{V_{k-1}} \right) \\ \frac{d^2Q_2}{dt^2} &= \frac{1}{T_s^2} \left(\frac{P_k}{V_k} - 2\frac{P_{k-1}}{V_{k-1}} + \frac{P_{k-2}}{V_{k-2}} \right),\end{aligned}$$

(5.3) can present the relation between P , V and Q_k (where Q_k is the value of Q_1 at each time instant k) in the form

$$\begin{aligned}Q_k &= C_a \left(\frac{P_k - P_{k-1}}{T_s} \right) + \frac{RC_a}{T_s} \left(\frac{P_k}{V_k} - \frac{P_{k-1}}{V_{k-1}} \right) \\ &\quad + \frac{LC_a}{T_s^2} \left(\frac{P_k}{V_k} - 2\frac{P_{k-1}}{V_{k-1}} + \frac{P_{k-2}}{V_{k-2}} \right) + \frac{P_k}{V_k}\end{aligned}$$

Expanding and collating P_k coefficients gives

$$Q_k = P_k \left(\frac{C_a}{T_s} + \frac{1 + \frac{RC_a}{T_s} + \frac{LC_a}{T_s^2}}{V_k} \right) + P_{k-1} \left(-\frac{C_a}{T_s} - \frac{\frac{RC_a}{T_s} + \frac{2LC_a}{T_s^2}}{V_{k-1}} \right) + P_{k-2} \left(\frac{\frac{LC_a}{T_s^2}}{V_{k-2}} \right)$$

The G dynamics can therefore be represented in the LTV form of (5.1)

$$P_k \left(p_0 + \frac{\bar{p}_0}{V_k} \right) + P_{k-1} \left(p_1 + \frac{\bar{p}_1}{V_{k-1}} \right) + P_{k-2} \left(p_2 + \frac{\bar{p}_2}{V_{k-2}} \right) = Q_k,$$

where

$$\begin{aligned}p_0 &= \frac{C_a}{T_s}, & \bar{p}_0 &= 1 + \frac{RC_a}{T_s} + \frac{LC_a}{T_s^2}, & p_1 &= -\frac{C_a}{T_s}, \\ \bar{p}_1 &= -\left(\frac{RC_a}{T_s} + \frac{2LC_a}{T_s^2} \right), & p_2 &= 0, & \bar{p}_2 &= \frac{LC_a}{T_s^2}\end{aligned}$$

□

For simplicity of later computation, system $K(q)$ is assumed to have the general LTI dynamics

$$Q_k = c_0 e_k + c_1 e_{k-1} + c_2 e_{k-2} + \cdots + c_n e_{k-n} \quad (5.4)$$

and similarly system $H(q)$ is assumed to have the LTI dynamics

$$u_k = h_0 P_k + h_1 P_{k-1} + h_2 P_{k-2} + \cdots + h_n P_{k-n} \quad (5.5)$$

where $\{c_i, h_i\}$ are fixed scalar coefficients.

The assumption of LTI dynamics of K and H means that the model is simpler for control application and parameter identification. Note that assuming finite impulse response (FIR) forms for $K(q)$ and $H(q)$ does not limit generality since both are assumed to be stable (and hence an infinite impulse response (IIR) form can be converted to an FIR form). Using Definition 5.1, the closed-loop assisted pressure tracking system in Figure 5.2 can be represented by the following minimum parameter LTV form.

Definition 5.2 (Closed-loop Dynamics). By substituting the G , K and H dynamics (5.1)-(5.5) into the signal relationships of Figure 5.2, the closed-loop system can be represented by the LTV dynamics

$$\sum_{i=0}^n b_i r_{k-i} = y_k \left(a_0 + \frac{\bar{a}_0}{V_k} \right) + y_{k-1} \left(a_1 + \frac{\bar{a}_1}{V_{k-1}} \right) + y_{k-2} \left(a_2 + \frac{\bar{a}_2}{V_{k-2}} \right) + \sum_{i=3}^n a_i y_{k-i} \quad (5.6)$$

Proof. From Figure 5.2, $e_k = r_k - u_k$, substituting into 5.4 gives

$$Q_k = c_0(r_k - u_k) + c_1(r_{k-1} - u_{k-1}) + c_2(r_{k-2} - u_{k-2}) + \cdots + c_n(r_{k-n} - u_{k-n})$$

Substituting 5.5 into this and equating to 5.1 gives

$$\begin{aligned} & P_k \left(p_0 + \frac{\bar{p}_0}{V_k} \right) + P_{k-1} \left(p_1 + \frac{\bar{p}_1}{V_{k-1}} \right) + P_{k-2} \left(p_2 + \frac{\bar{p}_2}{V_{k-2}} \right) \\ &= c_0 r_k + c_1 r_{k-1} + c_2 r_{k-2} + \cdots + c_n r_{k-n} \\ &\quad - c_0 (h_0 P_k + h_1 P_{k-1} + \cdots + h_n P_{k-n}) \\ &\quad - c_1 (h_0 P_{k-1} + h_1 P_{k-2} + \cdots + h_n P_{k-n-1}) \\ &\quad - c_2 (h_0 P_{k-2} + h_1 P_{k-3} + \cdots + h_n P_{k-n-2}) \\ &\quad - \cdots - c_n (h_0 P_{k-n} + h_1 P_{k-n-1} + \cdots + h_n P_{k-n-n}) \end{aligned} \quad (5.7)$$

Assuming no external disturbance ($w = 0$), y_k can substitute P_k . Collating coefficients of 5.7 gives

$$\begin{aligned} \sum_{i=0}^n c_i r_{k-i} = & y_k \left(p_0 + \frac{\bar{p}_0}{V_k} + c_0 h_0 \right) + y_{k-1} \left(p_1 + \frac{\bar{p}_1}{V_{k-1}} + c_0 h_1 + c_1 h_0 \right) \\ & + y_{k-2} \left(p_2 + \frac{\bar{p}_2}{V_{k-2}} + c_0 h_2 + c_1 h_1 + c_2 h_0 \right) \\ & + y_{k-3} (c_0 h_3 + c_1 h_2 + c_2 h_1 + c_3 h_0) + \cdots + y_{k-2n} (c_n h_n) \end{aligned}$$

The closed-loop system in Figure 5.2 can therefore be represented by the LTV dynamics

$$\sum_{i=0}^n b_i r_{k-i} = y_k \left(a_0 + \frac{\bar{a}_0}{V_k} \right) + y_{k-1} \left(a_1 + \frac{\bar{a}_1}{V_{k-1}} \right) + y_{k-2} \left(a_2 + \frac{\bar{a}_2}{V_{k-2}} \right) + \sum_{i=3}^n a_i y_{k-i}$$

where $\{a_i, \bar{a}_i, b_i\}$ are the fixed coefficients

$$a_i = \begin{cases} p_i + \sum_{j=0}^i c_j h_{i-j}, & i \leq 2, \\ \sum_{j=0}^i c_j h_{i-j}, & i \geq 3, \end{cases} \quad \bar{a}_i = \bar{p}_i, \quad i \leq 2, \quad b_i = c_i, \quad i \geq 0,$$

□

The next step is to develop a control scheme which can provide an assistance to the action of the control loop in Figure 5.2. As stated in Section 4.3.1, the addition of assistive control introduces the structure of nested loops, i.e. a control loop within a control loop. The control of the inner loop must be designed such that it does not hinder the main generated action and must have a faster response compared to the external loop. The adjustment of valve resistance should be able to be large enough to create an observable improvement in LPP tracking ability, whilst maintaining a dependence on the overall control of the patient and the pressure they generate. This leads to the assistive approach which can now be defined.

Definition 5.3 (Valve Assistance Problem). Consider the system shown in Figure 5.2 computed over a finite time period, $k = 1, 2, \dots, N$. The control problem is to select the sequence of valve resistance values $V = (V_1, V_2, \dots, V_N)$ such that the 2-norm of the tracking error is minimised, i.e.

$$\operatorname{argmin} J(V), \quad J(V) := \sum_{i=1}^N (r_i - y_i)^2 \quad (5.8)$$

As previously noted, this is fundamentally different to a conventional control problem since it involves changing a parameter within the system dynamics (i.e. the valve resistance V), rather than a control signal.

The control input could take on differing forms such as voltage to the valve or current through the valve solenoid coil. However, these are external variables to the system and are affected by factors such as hysteresis. Considerations must be made that take these factors into account and the possible development of a further nested loop. However, the direct impact of the valve is that a change in its resistance has a direct effect on the system dynamics in Figure 5.2.

5.1.1 Model Summary

Modelling human control requires underlying knowledge of how decisions are made during a control task. The fundamentals of human control are involved in, for example, movement and balance. First, muscles need to be activated to initiate movement or to correct target error (i.e. to prevent falling). Similarly, during LPP testing patients have to contract their respiratory muscles to generate the target pressure, this is represented by K in Figure 5.2. Second, feedback is provided by proprioceptors in order to remain balanced after initial muscle activation. In LPP testing, both visual and sensory feedback help a patient to maintain or change the pressure. This proprioception is represented by H in Figure 5.2

The model presented in this section incorporates multiple factors in LPP tracking that are essential to consider when providing assistive control in order to improve the tracking ability. Understanding how each control loop (i.e. human control and valve control) functions within the overall system helps to identify where a change in valve resistance would most benefit the patient. For example, a patient is more likely to have good steady state/pressure control but may not be so good when tracking a pressure reference change. It is important to produce an appropriate model so the valve resistance control assists at appropriate times during measurements.

5.2 Development of Model Predictive Valve Control

Conventional MPC actuates a control input signal in order to force the system output to attain a set-point or reference. Definition 5.3 requires reducing the difference between patient-generated lung pressure and the reference pressure. However, treating this as the only goal is not ideal as it does not consider the control input on the valve. In practice, this means that the valve resistance could rapidly oscillate which would distract the test subject and possibly impair their tracking ability. The following definition therefore

provides a practical control implementation, where the tracking error and control input must be appropriately balanced.

Definition 5.4 (Model Predictive Valve Control (MPVC)). Let cost function (5.8) be generalised to penalise the sample-to-sample change in valve resistance, giving

$$\operatorname{argmin} J(V), \quad J(V) := \sum_{i=1}^N (r_i - y_i)^2 Q_i + (V_{i-1} - V_i)^2 R_i \quad (5.9)$$

subject to dynamics (5.6), where Q_i and R_i are positive definite and positive semi-definite weights respectively. In addition, each $V_k \in \mathcal{V}$ with \mathcal{V} being a set of appropriate valve apertures.

The purpose of set \mathcal{V} is to simplify the control problem by providing a selection of discrete values rather than a continuous range. The objective of MPVC is therefore to compute the sequence of valve resistances V_1, V_2, \dots, V_N that minimise finite horizon cost (5.9). To make the computation tractable, MPVC replaces (5.9) with the receding horizon approximation (i.e. stage cost)

$$\operatorname{argmin} J(\bar{V}_k), \quad J(\bar{V}_k) := \sum_{i=k}^{k+m-1} (r_i - y_i)^2 Q_i + (V_{i-1} - V_i)^2 R_i \quad (5.10)$$

where m is the predictive horizon, and the stage valve resistance sequence on sample k is $\bar{V}_k = (V_k, V_{k+1}, \dots, V_{k+m-1})$. V_k is then applied to the current time index k and the computation is then repeated on the next sample index $k = k + 1$.

5.2.1 State-Space Model

Solving (5.10) requires computing closed-loop dynamics (5.6) which, in the absence of noise ($w = 0$), can be represented as the discrete time-varying state-space system

$$\begin{aligned} x_{k+1} &= A_k x_k + B_k r_k \\ y_k &= C_k x_k + D_k r_k, \quad x_0 = 0 \end{aligned} \quad (5.11)$$

To determine the state-space matrices $A - D$, closed-loop dynamics (5.6) must first be written in its shift operator (q) form

$$r_k \sum_{i=0}^n b_i q^{-i} = y_k \left(\left(a_0 + \frac{\bar{a}_0}{V_k} \right) + \left(a_1 + \frac{\bar{a}_1}{V_{k-1}} \right) q^{-1} + \left(a_2 + \frac{\bar{a}_2}{V_{k-2}} \right) q^{-2} + \sum_{i=3}^n a_i q^{-i} \right)$$

dividing both sides by $\left(a_0 + \frac{\bar{a}_0}{V_k}\right)$ gives

$$r_k \sum_{i=0}^n \varpi_i q^{-i} = y_k \left(1 + \sum_{i=1}^n \sigma_i q^{-i}\right) \quad (5.12)$$

where

$$\sigma_i = \begin{cases} \frac{a_i + \frac{\bar{a}_i}{V_{k-i}}}{a_0 + \frac{\bar{a}_0}{V_k}}, & i = \{1, 2\}, \\ \frac{a_i}{a_0 + \frac{\bar{a}_0}{V_k}}, & i \geq 3, \end{cases} \quad \varpi_i = \frac{b_i}{a_0 + \frac{\bar{a}_0}{V_k}}, \quad i \geq 0.$$

Introducing the system state vector parameter χ such that

$$\chi_k \left(1 + \sum_{i=1}^n \sigma_i q^{-i}\right) = r_k$$

and substituting into 5.12 gives

$$\chi_k \sum_{i=0}^n \varpi_i q^{-i} = y_k$$

These can be rearranged to

$$\chi_k = r_k - \sigma_1 \chi_{k-1} - \sigma_2 \chi_{k-2} - \cdots - \sigma_n \chi_{k-n} \quad (5.13)$$

and

$$y_k = \varpi_0 \chi_k + \varpi_1 \chi_{k-1} + \varpi_2 \chi_{k-2} + \cdots + \varpi_n \chi_{k-n} \quad (5.14)$$

respectively. Finally, substituting (5.13) into (5.14) gives

$$\begin{aligned} y_k &= \varpi_0 (r_k - \sigma_1 \chi_{k-1} - \sigma_2 \chi_{k-2} - \cdots - \sigma_n \chi_{k-n}) + \varpi_1 \chi_{k-1} + \cdots + \varpi_n \chi_{k-n} \\ &= \varpi_0 r_k + (\varpi_1 - \sigma_1 \varpi_0) \chi_{k-1} + (\varpi_2 - \sigma_2 \varpi_0) \chi_{k-2} + \cdots + (\varpi_n - \sigma_n \varpi_0) \chi_{k-n} \end{aligned} \quad (5.15)$$

If the state vector is $x_n = [\chi_{k-1} \ \chi_{k-2} \ \cdots \ \chi_{k-n}]^\top$, the state-space matrices, A_k and B_k , in (5.11) can be determined from (5.13), and C_k and D_k from (5.15) such that:

$$\begin{aligned} A_k &= \begin{bmatrix} -\sigma_1 & -\sigma_2 & -\sigma_3 & \cdots & -\sigma_{n-1} & -\sigma_n \\ 1 & 0 & 0 & \cdots & 0 & 0 \\ 0 & 1 & 0 & \cdots & 0 & 0 \\ 0 & 0 & 1 & \cdots & 0 & 0 \\ \vdots & & & \ddots & 0 & 0 \\ 0 & \cdots & 0 & \cdots & 1 & 0 \end{bmatrix} \\ B_k &= \begin{bmatrix} 1 & 0 & \cdots & 0 \end{bmatrix}^\top \\ C_k &= \begin{bmatrix} (\varpi_1 - \sigma_1 \varpi_0) & \cdots & (\varpi_{n-1} - \sigma_{n-1} \varpi_0) & (\varpi_n - \sigma_n \varpi_0) \end{bmatrix} \end{aligned}$$

$$D_k = \varpi_0$$

Solving cost function minimisation (5.10) on each sample k is a non-convex problem and therefore requires calculating the cost for all possible sequences of \bar{V}_k and selecting the lowest. This solution, \bar{V}_k^* , then yields the applied valve resistance on sample k of

$$V_k = [1, 0, \dots, 0] \bar{V}_k^*$$

5.2.2 State Estimation

Computing cost (5.10) requires simulating state-space system (5.11) starting from the current state x_k . In practical application, the system states will be unknown during measurements and therefore will need to be estimated. A Kalman Filter is used to approximate the state vectors of a system throughout the measurement period. It collates current system data with respective noise components (namely the input reference r , output y and the previous state vector estimate \hat{x}_k). The filter then uses this data to optimise its gain matrix (M_k) to reduce the noise components. The filtered data are used to adjust the system's state vector estimate. Using the state vector and other current system conditions, the estimator then predicts the next state vector. The time-variant nature of the system means a Time-Varying Kalman Filter is required. The equations presented in (5.16) show the function of the Time-Varying Kalman Filter and are adapted from Rhudy et al [51] using the state-space representation (5.11).

$$\begin{aligned} M_k &= S_k C^\top (C S_k C^\top + R_m)^{-1}, \\ \hat{x}_k &= \hat{x}_k + M_k (y_k - C \hat{x}_k), \\ S_k &= (I - M_k C) S_k, \\ \hat{x}_{k+1} &= A_k \hat{x}_k + B_k r_k, \\ S_{k+1} &= A_k S_k A_k^\top + B_k Q_p B_k^\top, \end{aligned} \tag{5.16}$$

with initial values $\hat{x}_0 = 0$ and $S_0 = B_0 Q_p B_0^\top$. Here S_k is the state error covariance matrix, R_m is the measurement noise covariance matrix, and Q_p is the process noise covariance matrix.

The overall MPVC system is shown in Figure 5.5. In practice, the computed valve resistance V_k is converted to the required valve aperture via the Hagen-Poiseuille equation $\left(\Delta p = \frac{8\mu L Q}{\pi R^4}\right)$, and signal y_k is the measured airway pressure.

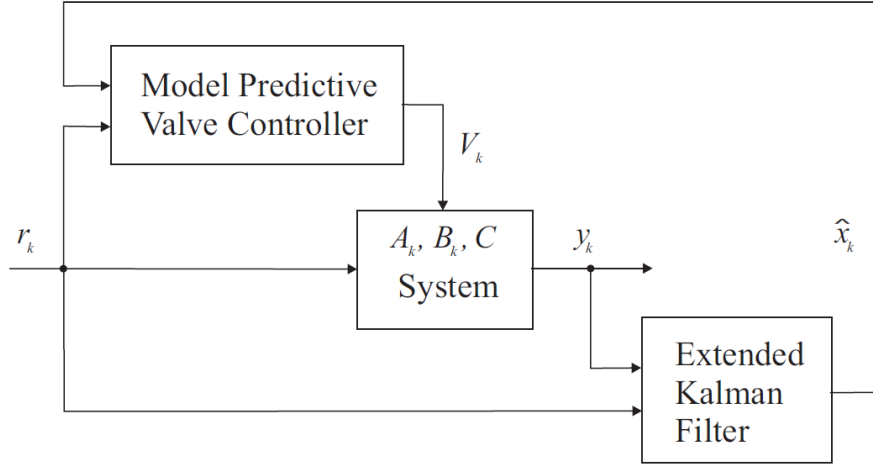


Figure 5.5: Block diagram of the MPVC system where r_k is the reference input and \hat{x}_k is the estimated system state.

5.2.3 Summary of Controller

The development of MPVC is to attempt to mitigate the tracking error during LPP testing. The controller uses a range of model parameters and variables to provide improvement in the tracking task whilst maintaining the primary reliance on the tracking ability of the patient. The black box modelling of the patient and the changing of a parameter within the system (i.e. the valve resistance) means that the states of the system must be estimated via a Kalman Filter with time-varying applicability. The controller then uses Equations 5.10, 5.11, and 5.16 in order to predict the current and future states to provide assistance control within the prediction horizon time frame. In order to provide adequate control, the model parameters must be identified using a procedure that can both handle noise in the system data and efficiently mimic the response of the patient if the procedure were to be used in a practical environment.

5.3 Model Parameter Identification

Before experimental data collection, an identification procedure must be performed that is efficient. The controller is implemented using (5.10) and (5.16), both of which depend on state-space model (5.11). The model parameters in (5.11) must therefore be identified. A standard way of identifying a model is to assume an auto-regressive moving average with exogenous input (ARMAX) model form which includes a representation of the external disturbance [52]. The model coefficients are chosen to minimise the disturbance, given a set of input and output data. Since the model is linear, this yields a global optimum solution. This approach will be applied to the current identification problem.

Definition 5.5 (Identification Problem). Consider the time-varying discrete closed-loop system shown in Figure 5.2 with components (5.1) - (5.5), and assume the ARMAX

disturbance form for filter $F(q)$ of

$$w_k = v_k \left(a_0 + \frac{\bar{a}_0}{V_k} \right) + v_{k-1} \left(a_1 + \frac{\bar{a}_1}{V_{k-1}} \right) + v_{k-2} \left(a_2 + \frac{\bar{a}_2}{V_{k-2}} \right) + \sum_{i=3}^n a_i v_{k-i} \quad (5.17)$$

where $v = y - P$. Then, given a set of sampled experimental input-output data $\{\tilde{r}_k, \tilde{y}_k\}$, $k = 1, \dots, N$, and corresponding valve resistance sequence $V = (V_1, V_2, \dots, V_N)$, the identification problem is to compute the parameter vector

$$\hat{\theta} = [\bar{\alpha}_0, \alpha_1, \bar{\alpha}_1, \alpha_2, \bar{\alpha}_2, \alpha_3, \dots, \alpha_n, \beta_0, \beta_1, \dots, \beta_n]^\top$$

where $\bar{\alpha}_i = \frac{\bar{a}_i}{a_0}$, $\alpha_i = \frac{a_i}{a_0}$ and $\beta_i = \frac{b_i}{a_0}$, such that the disturbance norm

$$\|w\|_2^2 = \sum_{k=1}^N w_k^2 \quad (5.18)$$

where $w = [w_1 \ w_2 \ w_3 \ \dots \ w_N]^\top$, is minimised.

Since all the resistance values, V_i , are known and (5.17) is linear in parameters $\{a_i, \bar{a}_i\}$, the solution can be computed using the method of least squares.

Theorem 5.6. *The solution to the Identification Problem is*

$$\hat{\theta} = ([\tilde{Y}, \tilde{R}]^\top [\tilde{Y}, \tilde{R}])^{-1} [\tilde{Y}, \tilde{R}]^\top \tilde{y} \quad (5.19)$$

in which

$$\tilde{Y} = \begin{bmatrix} -\tilde{y}_1/V_1 & 0 & 0 & 0 & 0 & 0 & \dots & 0 \\ -\tilde{y}_2/V_2 & -\tilde{y}_1 & -\tilde{y}_1/V_1 & 0 & 0 & 0 & \dots & 0 \\ -\tilde{y}_3/V_3 & -\tilde{y}_2 & -\tilde{y}_2/V_2 & -\tilde{y}_1 & -\tilde{y}_1/V_1 & 0 & \dots & 0 \\ -\tilde{y}_4/V_4 & -\tilde{y}_3 & -\tilde{y}_3/V_3 & -\tilde{y}_2 & -\tilde{y}_2/V_2 & 0 & \dots & 0 \\ -\tilde{y}_5/V_5 & -\tilde{y}_4 & -\tilde{y}_4/V_4 & -\tilde{y}_3 & -\tilde{y}_3/V_3 & -\tilde{y}_2 & \dots & 0 \\ \vdots & \vdots & \vdots & \vdots & \vdots & \vdots & \ddots & \vdots \\ -\tilde{y}_N/V_N & -\tilde{y}_{N-1} & -\tilde{y}_{N-1}/V_{N-1} & -\tilde{y}_{N-2} & \dots & \dots & \dots & -\tilde{y}_{N-n} \end{bmatrix}$$

$$\tilde{R} = \begin{bmatrix} \tilde{r}_1 & 0 & \dots & 0 \\ \tilde{r}_2 & \tilde{r}_1 & \dots & \vdots \\ \vdots & & \ddots & \vdots \\ \tilde{r}_N & \dots & \dots & \tilde{r}_{N-n} \end{bmatrix}$$

Proof. Substitute (5.17) into (5.6) to give

$$\begin{aligned} \sum_{i=0}^n b_i r_{k-i} &= (y_k - v_k) \left(a_0 + \frac{\bar{a}_0}{V_k} \right) + (y_{k-1} - v_{k-1}) \left(a_1 + \frac{\bar{a}_1}{V_{k-1}} \right) \\ &\quad + (y_{k-2} - v_{k-2}) \left(a_2 + \frac{\bar{a}_2}{V_{k-2}} \right) + \sum_{i=3}^n a_i (y_{k-i} - v_{k-i}) \end{aligned}$$

divide by a_0 and rearrange to give

$$\begin{aligned} w_k &= y_k \left(1 + \frac{\bar{a}_0/a_0}{V_k} \right) + y_{k-1} \left(\frac{a_1}{a_0} + \frac{\bar{a}_1/a_0}{V_{k-1}} \right) + y_{k-2} \left(\frac{a_2}{a_0} + \frac{\bar{a}_2}{V_{k-2}} \right) \\ &\quad + \sum_{i=3}^n \frac{a_i}{a_0} y_{k-i} - \sum_{i=0}^n \frac{b_i}{a_0} r_{k-i} \end{aligned}$$

which can be simplified to

$$w_k = y_k + \sum_{i=0}^n \frac{\bar{\alpha}_i}{V_{k-i}} y_{k-i} + \sum_{i=1}^n \alpha_i y_{k-i} - \sum_{i=0}^n \beta_i r_{k-i} \quad (5.20)$$

Computing for each time index $k = 1, 2, 3, \dots, N$,

$$\begin{aligned} w_1 &= y_1 + y_1 \frac{\bar{\alpha}_0}{V_1} - \beta_0 r_1 \\ w_2 &= y_2 + y_2 \frac{\bar{\alpha}_0}{V_2} + y_1 \alpha_1 + y_1 \frac{\bar{\alpha}_1}{V_1} - \beta_0 r_2 - \beta_1 r_1 \\ w_3 &= y_3 + y_3 \frac{\bar{\alpha}_0}{V_3} + y_2 \alpha_1 + y_2 \frac{\bar{\alpha}_1}{V_2} + y_1 \alpha_2 + y_1 \frac{\bar{\alpha}_2}{V_1} - \beta_0 r_3 - \beta_1 r_2 - \beta_2 r_1 \\ &\vdots \\ w_N &= y_N + y_N \frac{\bar{\alpha}_0}{V_N} + \dots + y_{N-n} \alpha_n - \beta_0 r_N - \beta_1 r_{N-1} - \dots - \beta_n r_{N-n} \end{aligned}$$

(5.20) can be presented in matrix form as

$$\begin{bmatrix} w_1 \\ w_2 \\ w_3 \\ \vdots \\ w_N \end{bmatrix} = \begin{bmatrix} \tilde{y}_1 \\ \tilde{y}_2 \\ \tilde{y}_3 \\ \vdots \\ \tilde{y}_N \end{bmatrix} + \begin{bmatrix} \tilde{y}_1/V_1 & 0 & \dots & 0 \\ \tilde{y}_2/V_2 & \tilde{y}_1 & \dots & 0 \\ \tilde{y}_3/V_3 & \tilde{y}_2 & \dots & 0 \\ \vdots & \vdots & \vdots & \vdots \\ \tilde{y}_N/V_N & \dots & \dots & \tilde{y}_{N-n} \end{bmatrix} \begin{bmatrix} \bar{\alpha}_0 \\ \alpha_1 \\ \bar{\alpha}_1 \\ \vdots \\ \alpha_n \end{bmatrix} - \begin{bmatrix} \tilde{r}_1 & 0 & 0 & \dots & 0 \\ \tilde{r}_2 & \tilde{r}_1 & 0 & \dots & \vdots \\ \tilde{r}_3 & \tilde{r}_2 & \tilde{r}_1 & \dots & \vdots \\ \vdots & \vdots & \vdots & \ddots & \vdots \\ \tilde{r}_N & \dots & \dots & \dots & \tilde{r}_{N-n} \end{bmatrix} \begin{bmatrix} \beta_0 \\ \beta_1 \\ \beta_2 \\ \vdots \\ \beta_n \end{bmatrix}$$

where \tilde{r} and \tilde{y} are measured inputs and outputs respectively. Therefore, the minimisation of the cost norm (5.18) can be written as

$$\min_{\theta_a, \theta_b} \|\tilde{y} - [\tilde{Y}, \tilde{R}][\theta_a, \theta_b]^\top\|$$

where $\theta_a = [\bar{\alpha}_0, \alpha_1, \bar{\alpha}_1, \alpha_2, \bar{\alpha}_2, \dots, \alpha_n]$, $\theta_b = [\beta_0, \beta_1, \dots, \beta_n]$. This has solution (5.19) since $\theta = [\theta_a, \theta_b]$. \square

If \tilde{r} is chosen such that \tilde{R} or \tilde{Y} are full rank, then the solution (5.19) will be a global minimiser. In practice, both \tilde{r} and valve resistance sequence V must be chosen as sufficiently exciting to activate all the closed-loop dynamics of interest.

Sections 5.1-5.3 have presented the mathematical approach for the model, controller and identification procedure. The next step is to simulate: the model and its response to a pressure reference; the controller and its ability to improve model tracking performance; and the identification procedure to validate its ability to determine the model parameters.

5.4 Simulation Results and Discussion

This section presents simulations of the lung model, controller and identification procedure to provide an insight into the feasibility of practical application.

5.4.1 Model Parameter Selection and Simulation

Model parameters for the closed-loop system of Figure 5.3 have been chosen to reproduce a person's tracking response to a LPP reference. The values $L = 18$ cmH₂O/L/s², $R = 34$ cmH₂O/L/s, $C_a = 0.1$ L/cmH₂O, $K(q) = 36$, and $H(q) = 1$ were calculated to mimic the experimental data in Figure 4.2b.

The range of valve resistance values for V were computed using Hagen-Poiseuille equation. These values produce the G dynamics coefficients in (5.1) as follows

$$\begin{aligned} p_0 &= \frac{1}{10T_s}, & \bar{p}_0 &= 1 + \frac{3.4}{T_s} + \frac{1.8}{T_s^2}, & p_1 &= -\frac{1}{10T_s}, \\ \bar{p}_1 &= -\frac{3.4}{T_s} - \frac{3.6}{T_s^2}, & p_2 &= 0, & \bar{p}_2 &= \frac{1.8}{T_s^2} \end{aligned}$$

These generate the overall closed-loop coefficients within the time-varying discrete system transfer function (5.6) of

$$\begin{aligned} a_0 &= 36 + p_0, & \bar{a}_0 &= \bar{p}_0, & a_1 &= p_1, & \bar{a}_1 &= \bar{p}_1, & a_2 &= p_2, \\ \bar{a}_2 &= \bar{p}_2, & a_i &= 0, & i &\geq 3, & b_0 &= 36, & b_i &= 0, i \geq 1, \end{aligned}$$

Figure 5.6 shows the results of the fixed valve resistance system ($|\mathcal{V}| = 1$), which mimics a real human response to a pressure reference (cf. Figure 4.2b). This has a tracking

error norm of $\|e\| = 71.7$, where $\|\cdot\|$ denotes the 1-norm

$$\|e\| = \sum_{k=0}^{k_{max}} |r_k - y_k|$$

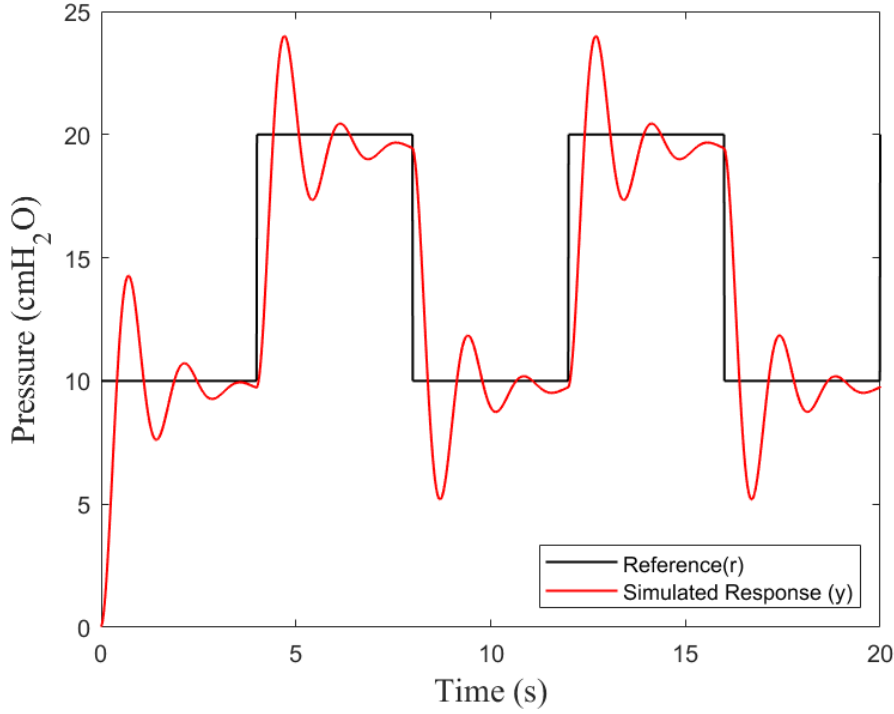


Figure 5.6: Simulated tracking response with no valve assistance.

5.4.2 Control

In order to maintain an adequate speed of MPVC computation, the solution must be calculated within the sampling time frame T_s . Additionally, an appropriate sampling time must be chosen such that a suitable number of calculations can be made. For example, a value of $T_s = 1\text{ms}$ is not useful if only one or a few computations can be made in that time period, and a value of $T_s = 1\text{s}$ is also not useful if many calculations can be made to provide the best control input but the valve control frequency is longer than the patient control frequency (as discussed in Section 4.3.1). A value of $T_s = 0.1\text{s}$ ensures both criteria are met. Following this, the prediction horizon m was limited to 10, i.e. predicting one second ahead ($T_s \times 10 = 1\text{s}$), and the number of possible resistance values to 11. This gives the permissible set of resistance values $\mathcal{V} = \{0, 10, \dots, 100\}$. Solving the non-convex MPC problem (5.9) then requires evaluating the stage cost J for all $|\mathcal{V}|^{m-1}$ possible valve resistance sequences. The controller then selects the lowest stage cost and applies the initial resistance value for the current time index k .

Smaller sets of resistance ranges were also investigated, and are denoted by their size, $|\mathcal{V}|$. Smaller prediction horizons were likewise investigated, with a minimum of $m = 2$. The choice of $|\mathcal{V}| = 1$ corresponds to a fixed valve resistance and is used to denote the simulated non-assisted human response. To give an example of the MPVC computational load: if $m = 3$ and $|\mathcal{V}| = 3$, the controller would have to simulate the system response to three possible valve resistances over two time indices ahead, thus giving nine (3^2) stage costs to evaluate per sample.

MPVC is applied using the control structure of Figure 5.5 where V_k is computed using (5.10). Figure 5.7 shows simulation results for MPVC ($m = 4$ and $|\mathcal{V}| = 2$) when tracking a step reference. This illustrates the improved effect on the tracking ability of the patient compared to the non-assisted case. The tracking error norm $\|e\|$ is 42.7.

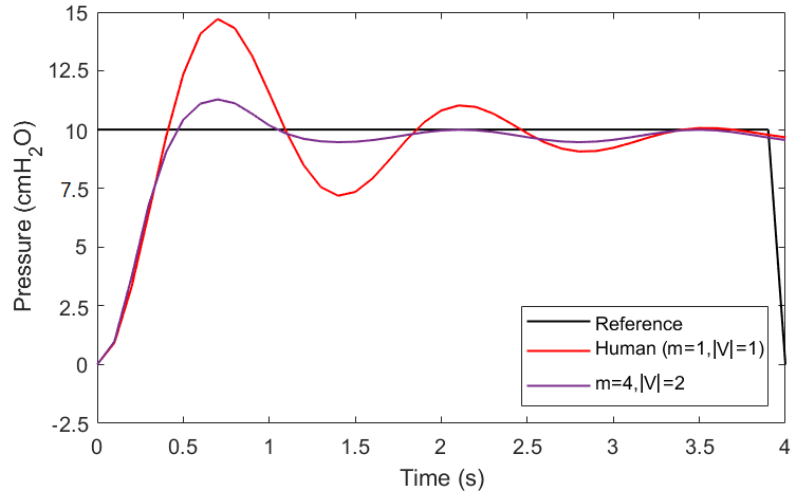


Figure 5.7: Simulated step tracking response comparing MPVC with no valve assistance.

Figures 5.8 and 5.9 show the impact of changing m and $|\mathcal{V}|$ on tracking capabilities of the resistance-controlled system. Cost function (5.10) is utilised by the controller to balance the minimisation of reference tracking error and control input. Figure 5.8a shows that tracking error is reduced even with the most basic form of MPVC. The overshoot is reduced and the system reaches a steady state before a step-change unlike the non-controlled system. Figure 5.8b shows further reduction in overshoot but takes the same time to reach steady state. This is due to the size of the prediction horizon. Figure 5.8c shows a significant reduction in both overshoot and settling time. However, a long prediction horizon and only two possible valve resistances results in use of either a high or low value of V . In practical application this would most likely lead to the patient running out of breath very quickly in order to reduce their overshoot error due to high airflow from a low valve resistance.

Figure 5.9 shows that increasing the prediction horizon past $m = 5$ has very limited effect on further improving tracking error. This is due to the MPVC being part of a

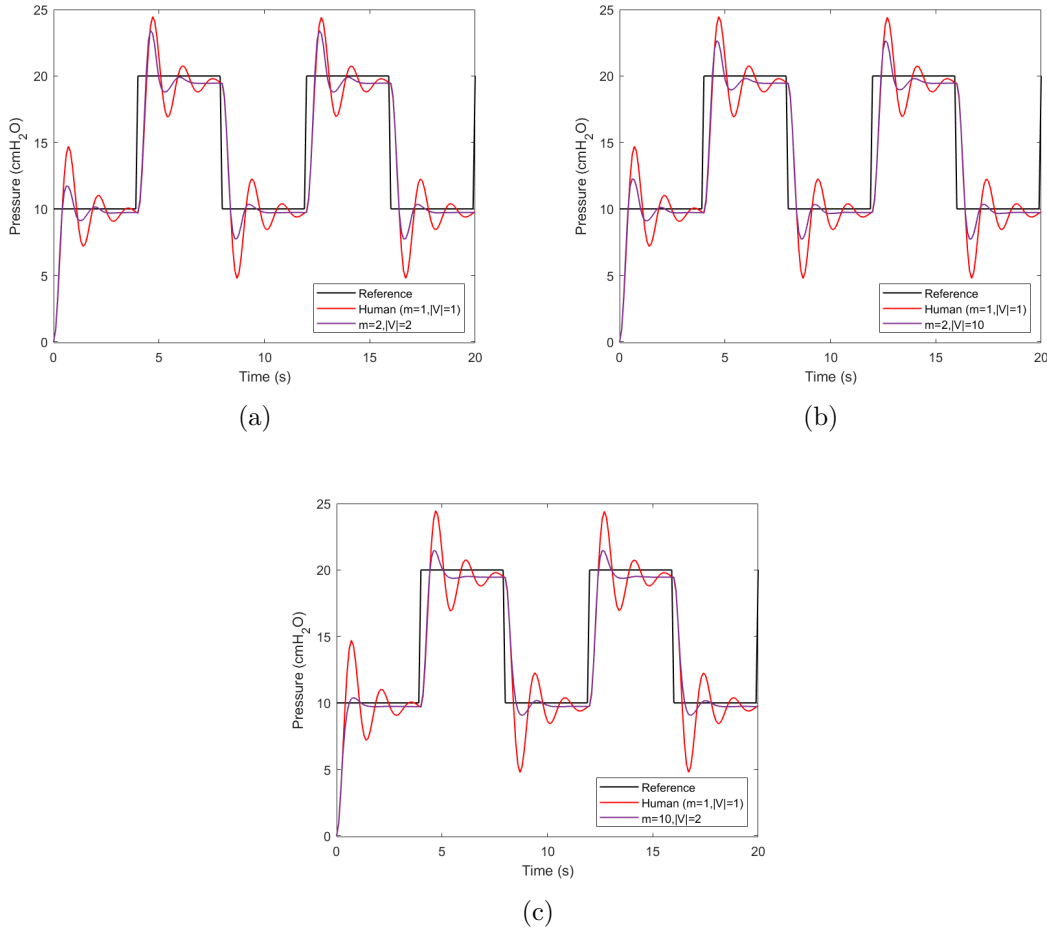


Figure 5.8: Simulated tracking response to a square wave reference with:

- (a) a prediction horizon of $m = 2$, and resistance set size of $|\mathcal{V}| = 2$
- (b) a prediction horizon of $m = 2$, and resistance set size of $|\mathcal{V}| = 10$
- (c) a prediction horizon of $m = 10$, and resistance set size of $|\mathcal{V}| = 2$

nested loop control scheme where the outer loop (i.e. the patient or, in this case, the simulation model) still provides the main form of control and the MPVC is providing assistance. The results show the inevitable compromise between tracking performance and computational load. However the selection of $m = 5$ and $|\mathcal{V}| = 5$ is seen to provide a suitable balance between tracking accuracy and computational load.

Figure 5.10 shows the result of controlling system resistance with $m = 5$ and $|\mathcal{V}| = 5$. The system has a similar tracking error to Figure 5.8c but a balance between prediction horizon and permissible valve resistance would be more useful in practical application. The slightly larger overshoot at the beginning is due to the smaller prediction horizon but the larger set of valve resistances would make pressure assistance more viable in terms of longevity of measurement period. Figure 5.10 highlights the effect of MPVC on the patient's reference tracking abilities compared to the non-assisted case in Figure 5.6. The tracking-error norm of the non-assisted system is 71.7 cmH₂O whereas the tracking error norm of the controlled system is 40.4 cmH₂O, corresponding to a 44% reduction.

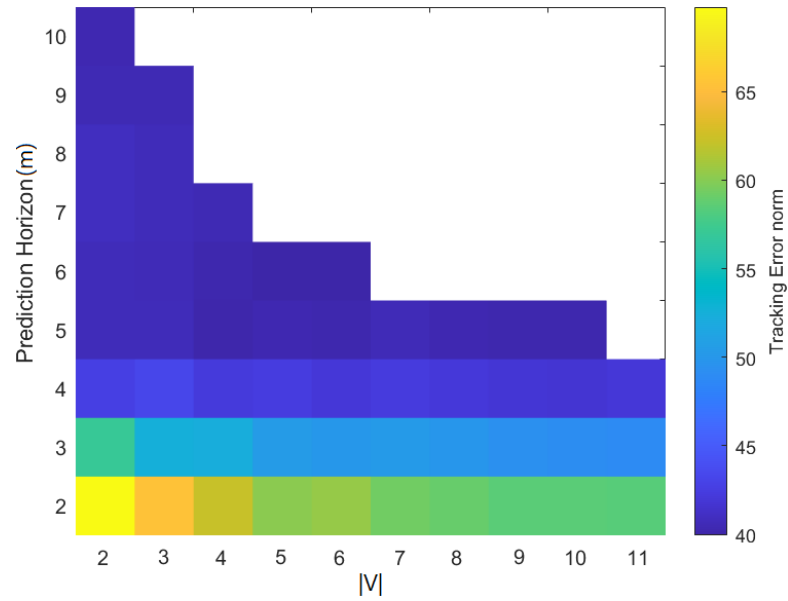


Figure 5.9: Colour map showing tracking error norm as a function of prediction horizon and number of possible resistance values.

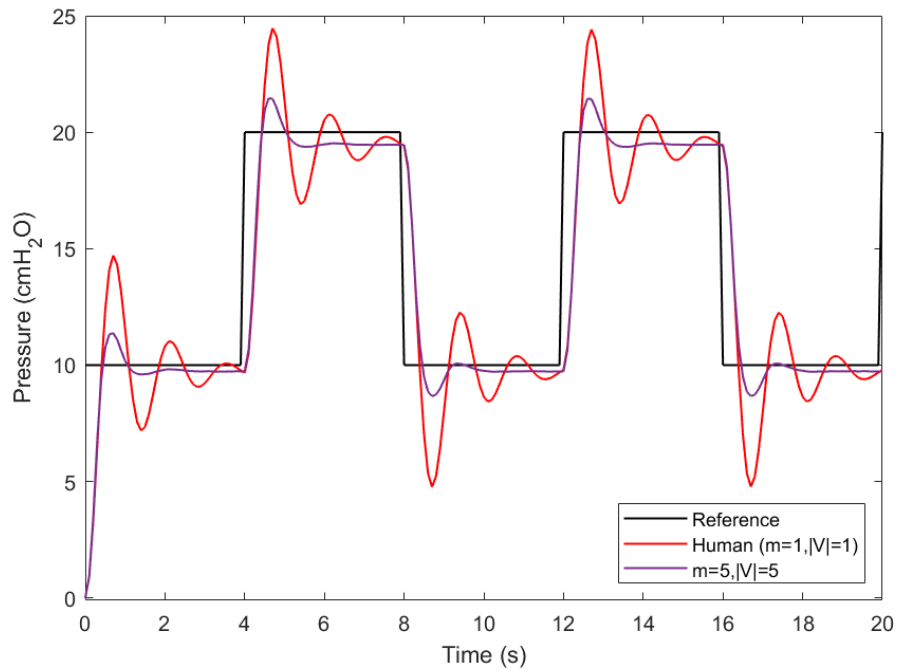


Figure 5.10: Simulation of MPVC compared to non-assisted system tracking of a square wave reference with a prediction horizon of $m = 5$, and resistance set size of $|\mathcal{V}| = 5$.

The result shown in Figure 5.10 demonstrates that MPVC can be used to significantly improve a human's tracking ability during lung pressure profiling. A key feature is that the assisted valve system has a much smaller overshoot compared to the non-assisted system. This improved tracking capability is expected to result in better TMD measurements from the patient when implemented in practical application.

5.4.3 Identification

The simulation results above show that the model produced a response similar to that of a person. Furthermore, the control results show that MPVC should be valid for use in practical application. The identification procedure initially shows encouraging results as seen by the perfect model replication of the simulated response in Figure 5.11. The identification initially validates the mathematical theory of the procedure as presented in Section 5.3 and proves that if \tilde{r} and V are suitably selected, then the parameter vector θ will be correctly identified. This was effective across a range of values of R , C_a , L , and K where the model was simulated to track varying references with varying valve resistances. The data were then used to reverse engineer the model parameters in θ .

The addition of Gaussian noise was used to simulate variation in human response as well as measurement noise from the pressure sensor. Figure 5.12a presents the simulated system output (red) which incorporates a small magnitude ($\leq 0.1\text{cmH}_2\text{O}$) of noise. The model output (blue) was simulated using the parameters resulting from the identification procedure. It is clear that the effectiveness of the identification procedure is not as good as the original noiseless data shown in Figure 5.11. The identified model in Figure 5.12a has a smaller overshoot and reaches a stable pressure much more quickly compared to the original model output. Recall that $F(q)$ is applied to the external Gaussian noise, and filters it using part of the system dynamics. This leads to an assumption that the noise in the system is dependent on the system dynamics and not random like Gaussian noise. However, in real-life even a predeterminable action (such as walking, for example) still has variation from step to step that is unpredictable. The identification was further compromised when a greater magnitude ($\leq 0.3\text{cmH}_2\text{O}$) of Gaussian noise was applied.

Additional simulations showed that this was a compound effect that occurred from the model design but was undetected due to the perfectly noiseless simulated data. Another inaccuracy that was discovered was changing the sample frequency from 10Hz to 100Hz (i.e. $T_s = 0.1\text{s}$ to $T_s = 0.01\text{s}$) changed the overshoot and oscillatory response. This shows a sensitivity to sampling time which may have been caused by higher frequency components due to the large inertance value in the model.

5.5 Summary

Control of lung and airway pressure is a crucial component of research into ICP and is needed to develop improved measurement and diagnostic approaches. The current clinical apparatus used for LPP testing provides limited pressure control (i.e. removal of the red cap). This chapter outlined specifications to improve the current setup. It developed a new model of lung dynamics which incorporated the physiological components, muscle actuation, and voluntary feedback control. Section 5.2, proposed a novel

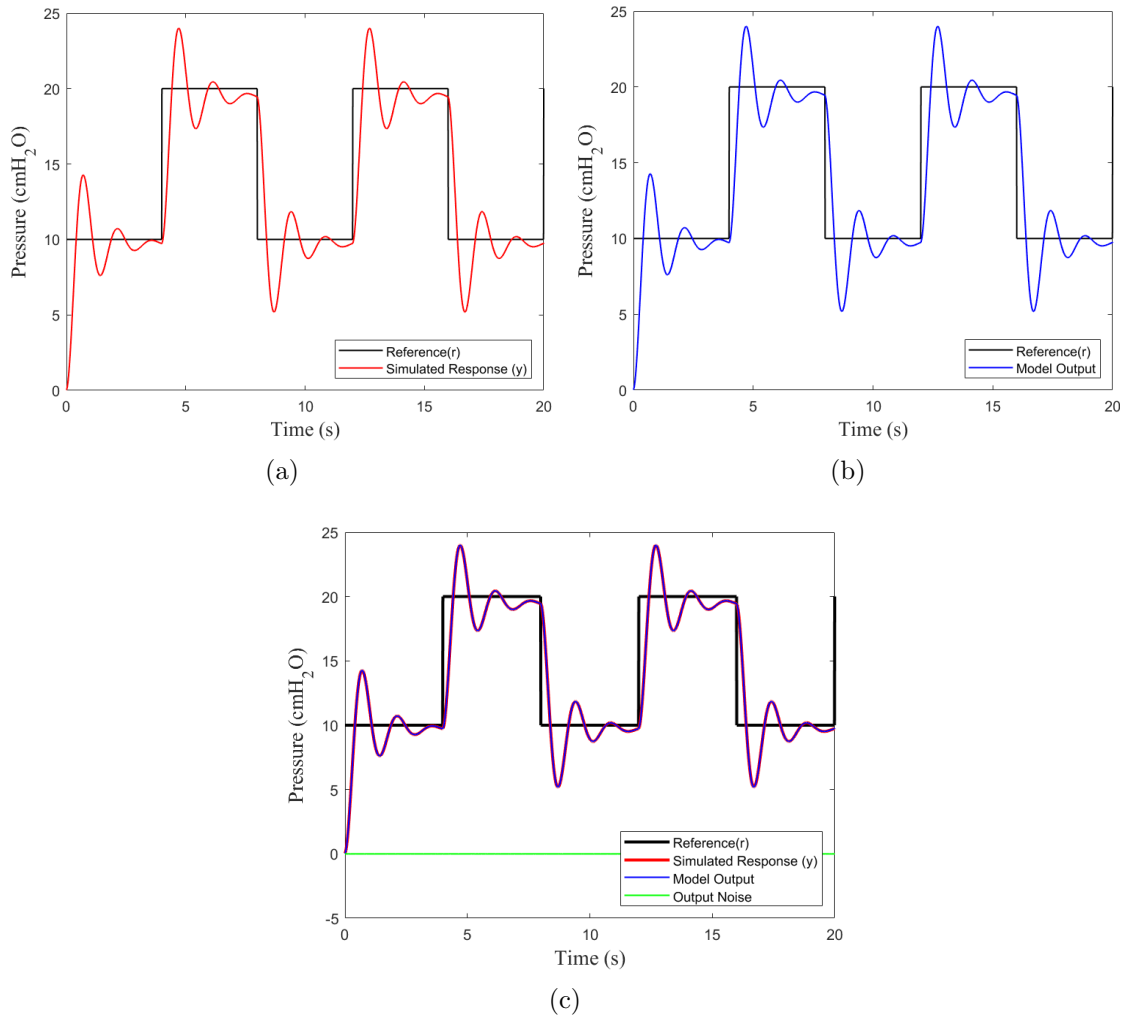


Figure 5.11: (a) Simulated tracking response with no valve assistance (Repeat of Figure 5.6)
 (b) Tracking response of identified model using Figure 5.11a data
 (c) Combined overlay of simulated and model response. Green line represents the output noise (equal to zero) applied to simulated response before identification process.

type of control which manipulated a valve's resistance to control airflow. Simulation results showed a significant reduction in tracking error when MPVC was applied compared to a non-controlled system. The parameters of the model need to be tailored to each individual to provide optimised control. Section 5.3 presented an ARMAX noise model to minimise disturbance thus optimising a least squares identification procedure.

The results showed that the identification procedure functioned correctly when the disturbance fitted the filtered form of the model. However, it did not handle more general disturbance data. Further testing showed that the resistance selections made during the control application shown in Figure 5.10 would not be suitable for use in practical application (low resistances would lead to very short measurement periods). The initial results showed promise for the model, controller and identification procedure. This leads

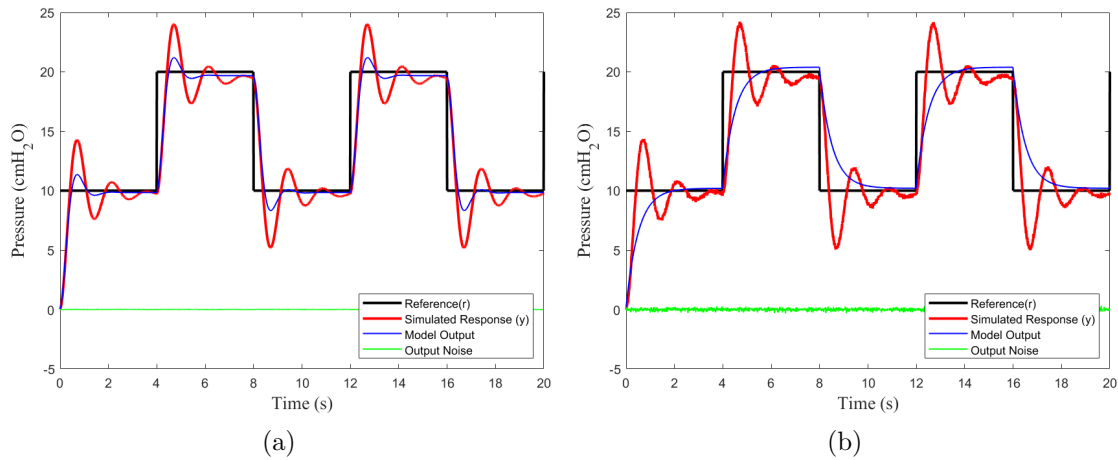


Figure 5.12: (a) Identified model (blue) compared to simulated data with minor Gaussian noise (red)
 (b) Identified model (blue) compared to simulated data with moderate Gaussian noise (red).

to the justification that an updated version of the model, control, and identification procedure is needed. Chapter 6 will develop a model structure that does not rely on a distinct form of disturbance.

Chapter 6

Model Predictive Valve Control with Modified Model Structure

In Chapter 5 a model was developed to mimic a person's lung pressure profile (LPP) tracking ability. This model used the most basic principles of inertance, resistance, compliance, and numerical gain to achieve this. Results were promising but showed that model modification was needed to make the parameter identification less sensitive to system disturbance.

The modifications developed in this chapter include the removal of the noise filter, and adaption of the K and G dynamics to more closely match real-life values. Delay components are also added to the model in order to incorporate human reaction time.

6.1 Problem Description

The LPP tracking problem described in Chapter 4 remains, but the model is redefined to avoid the assumption that the noise is dependent system dynamics as in (5.17) and modify the respiratory muscle actuation dynamics.

Recall that during each clinical pressure tracking experiment, the pressure reference, $r(t)$, is displayed to the patient on a screen from time $t = 0$ up until the present time t . The screen also shows the pressure $P(t)$ measured in the breathing tube (N.B. the variable y in Chapter 5 has been reassigned as the variable P in this chapter as y referred only to pressure output, whereas P is a more encompassing approach). Each test runs over the interval $t \in [0, T]$, where T is the overall duration. The target pressure is higher than ambient pressure, so the participant must always be exhaling to maintain a positive pressure gradient. The valve's resistance, $V(t)$, is controlled to adjust airflow out of the tube. The aim of this work is to control $V(t)$ such that $P(t)$ tracks $r(t)$ as closely as possible.

6.1.1 Forced Respiration Dynamics

Figure 6.1a shows the original equivalent circuit (used in Chapter 5) with variable current source (i.e. airflow) Q . This original model proposed that the person controlled the airflow out of their lungs. This would be the equivalent of the person controlling their glottis; with hindsight, this was not the case as the glottis remains fully open. Figure 6.1b shows the modified equivalent circuit introducing variable voltage supply (i.e. pressure), P_l , and corresponding flow variable Q . This modification proposes a more realistic scenario where the person controls the pressure within the lungs, rather than controlling the glottis (i.e. controlling the airflow out of their lungs).

The variable valve resistance is included in the form of a variable resistor $V(t)$. Here laminar flow is assumed, so that the Hagen-Poiseuille equation enables valve resistance $V(t)$ to be related directly to the valve position (which is the controlled variable). The voltage, $P(t)$, is the pressure difference measured across the valve, and corresponds to the pressure at the entrance to the participant's airway. The exhaled airflow rate corresponds to the current $Q(t)$. As mentioned above, the pressure source signal $P_l(t)$ has been added to represent the effect of respiratory muscle movement under the participant's voluntary control (i.e. the pressure in the lungs).

To determine how $P_l(t)$ is generated, there are a variety of models of voluntary human sensorimotor control available as mentioned in Section 5.1. It highlights the necessity of incorporating a feed-forward component (K) and feedback component (H) into a model of forced expiration during LPP tests. A further feature of human motor control, which was not considered necessary in Section 5.1, is a feed-forward predictive component. This is analogous to being able to see an object whilst making appropriate movements to touch it.

Figure 6.2a shows the original closed-loop system (used in Chapter 5) with respiratory muscle actuation component $K(q)$, lung and valve dynamics G , feedback component $H(q)$, and filter $F(q)$. The original closed-loop system assumed a disturbance form with system dynamics. However, the identification procedure could not handle the addition of a general form of noise (e.g. Gaussian). Figure 6.2b shows the modified closed-loop system which removes the filter $F(q)$ to assume a more general disturbance and adds the feed-forward predictive component FP . The predictive component assumes a person can see the entire pressure reference r during LPP testing. Figure 6.2a shows the closed-loop system in discrete-time with shift operator q , whereas Figure 6.2b shows the closed-loop system in continuous-time.

Recall from Chapter 4 that it is also necessary to specify some constraints: limits on the maximum airway pressure, and the total exhaled volume (vital capacity) $\int_{t=0}^T Q(t)$, ensure that a test subject does not overexert during LPP testing. A maximum resistance V_{max} ensures the glottis remains open throughout measurements, and a minimum

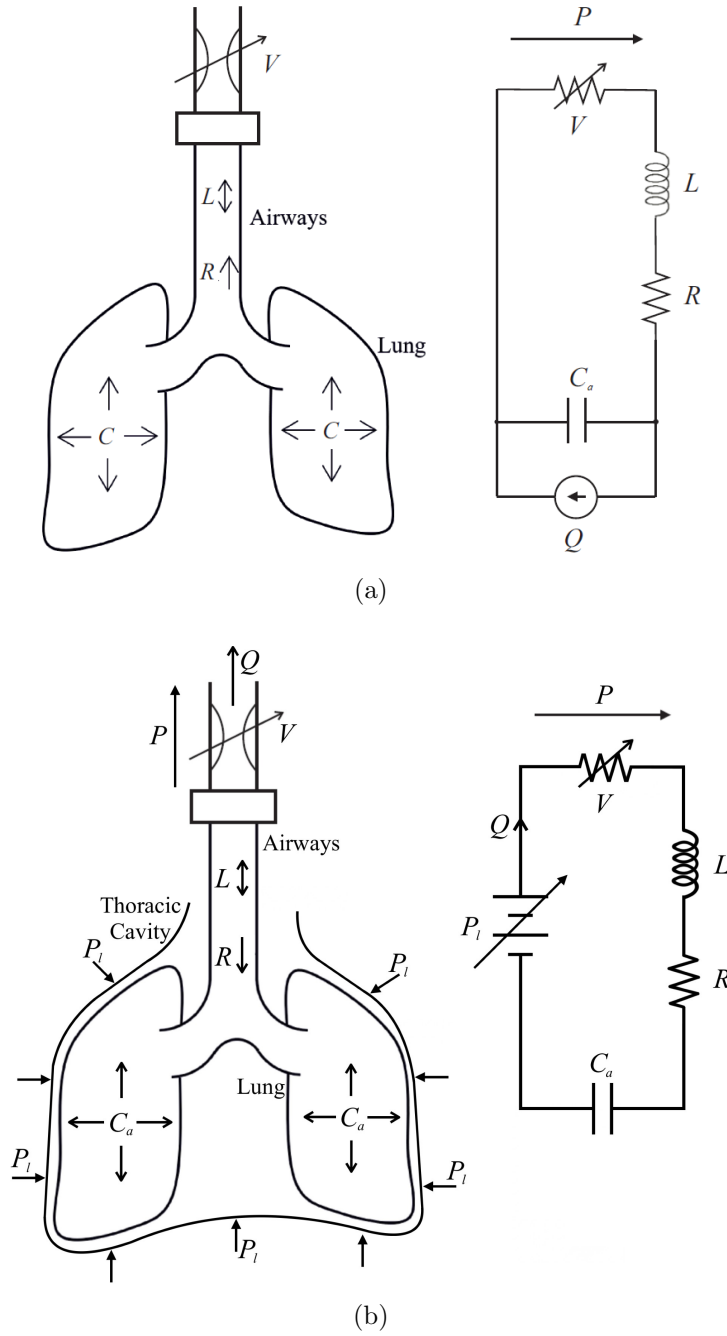


Figure 6.1: (a) Original equivalent circuit with controllable current source (air-flow) Q (repeat of Figure 5.3)
 (b) Modified equivalent circuit with controllable voltage supply (pressure) P_l .

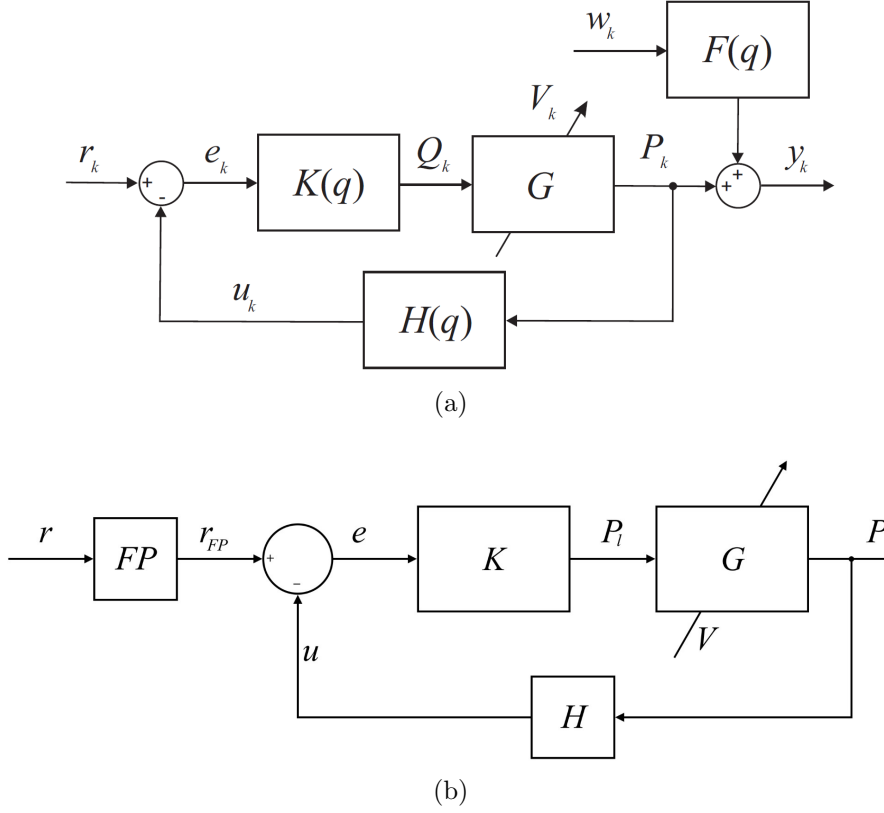


Figure 6.2: (a) Original voluntary pressure reference tracking system with valve resistance V_k (repeat of Figure 5.2)
(b) Modified voluntary pressure reference tracking system with valve resistance V_k .

resistance V_{min} is a physical apparatus limitation. A minimum profile length of $T = 20$ seconds aligns with TMD measurement profiles.

The overall updated system is now described below.

Definition 6.1 (System Description). The assistive pressure tracking system takes the form of Figure 6.2b where operators K and H model voluntary sensorimotor control of the diaphragm and intercostal muscles, and feedback respectively. The LTI discrete time dynamics are represented by the state-space quadruples (A_K, B_K, C_K, D_K) and (A_H, B_H, C_H, D_H) respectively. Operator FP models the feed-forward predictive component of sensorimotor control by the state-space quadruple $(A_{FP}, B_{FP}, C_{FP}, D_{FP})$. The assisted respiration dynamics $G, (P_l, V) \mapsto P$ are shown in Figure 6.1b, where valve resistance, V , is a controlled parameter. The dynamics of G are represented by the

linear parameter-varying (LPV) continuous time state-space system

$$\begin{aligned} \dot{x}_G(t) &= \underbrace{\begin{bmatrix} 0 & \frac{1}{C_a} \\ -\frac{1}{L} & -\frac{(R+V(t))}{L} \end{bmatrix}}_{A_G(V(t))} x_G(t) + \underbrace{\begin{bmatrix} 0 \\ -\frac{1}{L} \end{bmatrix}}_{B_G} P_l(t), \\ P(t) &= \underbrace{\begin{bmatrix} 0 & V(t) \end{bmatrix}}_{C_G(V(t))} x_G(t), \quad t \in [0, T] \end{aligned} \quad (6.1)$$

which converts to the discrete time state-space system

$$\begin{aligned} x_{G,k+1} &= \underbrace{e^{A_G(V(kT_s))T_s}}_{A_G(V_k)} x_{G,k} + \underbrace{A_G^{-1}(V(kT_s))(e^{A_G(V(kT_s))T_s} - I)B_G}_{B_G(V_k)} P_{l,k} \\ P_k &= \underbrace{\begin{bmatrix} 0 & C_G(V(kT_s)) \end{bmatrix}}_{C_G(V_k)} x_{G,k}, \quad k = 1, \dots, N \end{aligned} \quad (6.2)$$

with sample period T_s . The subscript k denotes the sample index, i.e. $P_k = P(kT_s)$ and $N = T/T_s$. The composite G and K dynamics $e \mapsto P$ can then be written as the discrete time state-space triple $(A_{KG}(V_k), B_{KG}(V_k), C_{KG}(V_k))$ where

$$\begin{aligned} A_{KG}(V_k) &= \begin{bmatrix} A_K & 0 \\ B_G(V_k)C_K & A_G(V_k) \end{bmatrix}, \\ B_{KG}(V_k) &= \begin{bmatrix} B_K \\ B_G(V_k)D_K \end{bmatrix}, \quad C_{KG}(V_k) = \begin{bmatrix} 0 & C_G(V_k) \end{bmatrix} \end{aligned} \quad (6.3)$$

which then enables the closed-loop system $r_{FP} \mapsto P$ to be represented as the state-space triple

$$\begin{aligned} A_{cl}(V_k) &= \begin{bmatrix} A_{KG}(V_k) - B_{KG}(V_k)D_H C_{KG}(V_k) & -B_{KG}(V_k)C_H \\ B_H C_{KG}(V_k) & A_H \end{bmatrix}, \\ B_{cl}(V_k) &= \begin{bmatrix} B_{KG}(V_k) \\ 0 \end{bmatrix}, \quad C_{cl}(V_k) = \begin{bmatrix} 0 & C_{KG}(V_k) \end{bmatrix} \end{aligned} \quad (6.4)$$

Incorporating FP then means the overall system $r \mapsto P$ can be represented by the system

$$\begin{aligned} x_{k+1} &= \underbrace{\begin{bmatrix} A_{FP} & 0 \\ B_{cl}(V_k)C_{FP} & A_{cl}(V_k) \end{bmatrix}}_{A(V_k)} x_k + \underbrace{\begin{bmatrix} B_{FP} \\ B_{cl}(V_k)D_{FP} \end{bmatrix}}_{B(V_k)} r_k \\ P_k &= \underbrace{\begin{bmatrix} 0 & C_{cl}(V_k) \end{bmatrix}}_{C(V_k)} x_k, \quad k = 1, \dots, N, \quad x_0 = 0 \end{aligned} \quad (6.5)$$

Note that the G dynamics still use the main passive components of the equivalent circuit in Figure 6.1 of inertance, compliance, and the airway and valve resistance as in (5.2), and The K and H components maintain a general LTI form as in (5.4) and (5.5). Having defined the voluntary pressure reference tracking system dynamics, the control problem can now be defined.

Definition 6.2 (Valve Assistance Problem). Consider the system shown in Figure 6.2b with discrete state-space matrices (6.5) computed over samples $k = 1, 2, \dots, N$. The control problem is to select the sequence of valve resistance values $\bar{V} = (V_1, V_2, \dots, V_N)$ such that the 2-norm of the tracking error is minimised, i.e.

$$\arg \min J(\bar{V}), \quad J(\bar{V}) := \sum_{i=1}^N (r_i - P_i)^2. \quad (6.6)$$

subject to dynamics (6.5) and constraints

$$0 \leq P_k \leq P_{max}, \quad (6.7a)$$

$$V_{min} \leq V_k \leq V_{max}, \quad k = 1, \dots, N \quad (6.7b)$$

$$\sum_{k=0}^N Q_k \leq vc \quad (6.7c)$$

$$N = T/T_s, \quad T \geq 20 \text{ seconds} \quad (6.7d)$$

where Q_k is the airflow at time index k , given by $Q_k = P_k/V_k$ and vc is the vital capacity.

The Valve Assistance Problem cost function (6.6) remains the same as cost function (5.8), however, (6.6) is bound by the hard constraints in (6.7). Recall that the Valve Assistance Problem is fundamentally different to a conventional control problem since it involves changing a parameter within the plant dynamics (i.e. the valve resistance V_k), rather than controlling a secondary input signal (i.e. a pump).

6.2 Modified Model Predictive Valve Control (MPVC)

Section 5.2 introduced the concept of MPVC. To reduce computational load, the set of valve resistances was reduced to a discrete set, \mathcal{V} . The controller used a cost function using the error between reference and measured pressure, and the sample-to-sample change in valve resistance. However, this approach was not optimal as there was a possibility that the resistance could remain low for a period of time. This would be unacceptable for TMD measurements which may be longer than 20 seconds, i.e. constraint (6.7d) would not be adhered to. The modified MPVC adjusts the original sample-to-sample change in resistance, to one that restricts changes from a maximum value.

Definition 6.3 (Model Predictive Valve Control). The Valve Assistance Problem (6.6) with constraints (6.7) is solved by computing the sequence of valve resistances $\bar{V} = (V_1, V_2, \dots, V_N)$ that minimise the finite horizon cost function

$$\arg \min J(\bar{V}), \quad J(\bar{V}) := \sum_{i=1}^N (r_i - P_i)^2 \Phi_i + (V_{max} - V_i)^2 \Psi_i \quad (6.8)$$

where Φ_i and Ψ_i are positive definite and positive semi-definite scalar weights respectively. This is subject to dynamics (6.1)-(6.5), the constraint that V_i is taken from a set of pre-defined valve resistances, i.e.

$$V_i \in \mathcal{V}, \quad \mathcal{V} = \{v_1, v_2, \dots, v_n\}, \quad V_{min} \leq v_i \leq V_{max}, \quad (6.9)$$

and the remaining constraint (6.7a).

To solve (6.8), MPVC replaces it with the receding horizon approximation (i.e. stage cost)

$$\arg \min J(\bar{V}_k), \quad J(\bar{V}_k) := \sum_{i=k}^{k+m-1} (r_i - P_i)^2 \Phi_i + (V_{max} - V_i)^2 \Psi_i \quad (6.10)$$

subject to dynamics (6.1)-(6.5) and constraints (6.7a), (6.9). This is computed at each sample k . Here m is the prediction horizon, and the stage valve resistance sequence on sample k is $\bar{V}_k = (V_k, V_{k+1}, \dots, V_{k+m})$. The first element of \bar{V}_k is then applied: $V_k = [1 \ 0 \ \dots \ 0] \bar{V}_k$.

The cost function (5.10) used in the first approach in Chapter 5 is shown below

$$\arg \min J(\bar{V}_k), \quad J(\bar{V}_k) := \sum_{i=k}^{k+m-1} (r_i - y_i)^2 Q_i + (V_{i-1} - V_i)^2 R_i$$

Comparing this to the updated version in (6.10), the update still considers the minimisation of the tracking error as part of the cost. However, the cost no longer penalises sample-to-sample changes in valve resistance, but penalises the difference in valve resistance from a maximum. The original sample-to-sample change penalisation led to a low resistance being selected for longer periods of time than would be necessary during simulation. This was acceptable in simulation, but if applied in practice, a person would run out of breath within a few seconds. This would make the control efforts non-viable for use during concurrent LPP and TMD measurements.

The overall updated MPVC system is shown in Figure 6.3. Computing cost function (6.10) requires the current state x_k within system (6.5). This is not measurable, but an approximation, \hat{x}_k , can be computed using the Time-Varying Kalman Filter system

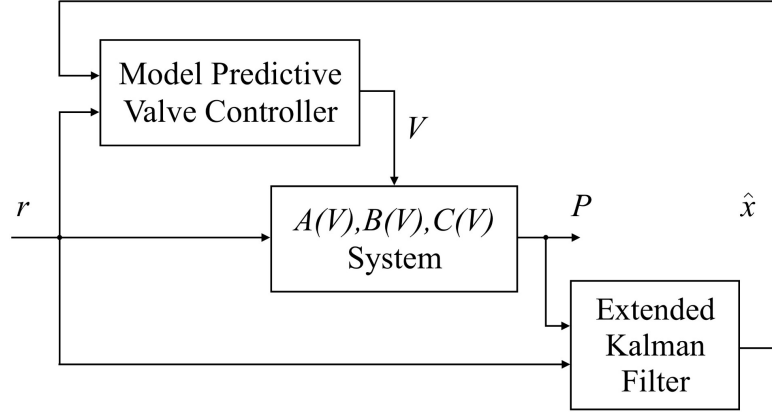


Figure 6.3: Block diagram of the MPVC system where r is the pressure profile input and \hat{x} is the estimated plant state.

[51], given by

$$\begin{aligned}
 M_k &= S_k C^\top(V_k) (C(V_k) S_k C^\top(V_k) + \lambda_m)^{-1}, \\
 \hat{x}_k &= \hat{x}_k + M_k (P_k - C(V_k) \hat{x}_k), \\
 S_k &= (I - M_k C(V_k)) S_k, \\
 \hat{x}_{k+1} &= A(V_k) \hat{x}_k + B(V_k) r_k, \\
 S_{k+1} &= A(V_k) S_k A^\top(V_k) + B(V_k) \mu_p B^\top(V_k),
 \end{aligned} \tag{6.11}$$

with initial values $\hat{x}_0 = 0$ and $S_0 = B_{V_{max}} \mu_p B_{V_{max}}^\top$. Here M_k is the Kalman gain matrix, S_k is the state error covariance matrix, λ_m is the measurement noise covariance matrix, and μ_p is the process noise covariance matrix. Within system (6.11), P_k is the measured pressure, r_k is the known reference profile value, and V_k is the valve resistance value at sample k .

The Kalman Filter equations shown in (6.11) have the same functionality as the equations in (5.16). The differences are purely notational. In order not to confuse R_m and Q_p (i.e. the measurement noise and process noise covariance matrices), with R and Q (i.e. the airway resistance and airflow), the matrix notations have been changed to λ_m and μ_p respectively. Additionally, state-space matrices A , B , and C have been changed to $A(V_k)$, $B(V_k)$, and $C(V_k)$ to show their sample-to-sample variability.

Solving (6.10) (subject to dynamics (6.5), constraints (6.7), and $V_k \in \mathcal{V}$) on each sample k is a non-convex problem and can be addressed using an exhaustive search (specialist solvers such as non-linear or integer programming can also be used).

The cost (6.10) can be written in matrix form as

$$\begin{aligned}
 J(\bar{V}_k) &= (\vec{r}_k - \vec{P}_k)^\top \bar{\Phi} (\vec{r}_k - \vec{P}_k) \\
 &\quad + (V_{max} - \bar{V}_k)^\top \bar{\Psi} (V_{max} - \bar{V}_k)
 \end{aligned}$$

where $\vec{r}_k = [r_k, r_{k+1}, \dots, r_{k+m}]^\top$, $\vec{P}_k = [P_k, P_{k+1}, \dots, P_{k+m}]^\top$, $\bar{V}_{max} = [V_{max}, \dots, V_{max}]^\top$, $\bar{\Phi} = \text{diag}\{\Phi, \dots, \Phi\}$, $\bar{\Psi} = \text{diag}\{\Psi, \dots, \Psi\}$, and

$$\vec{P}_k = \Gamma(\bar{V}_k)\vec{r}_k + \Xi(\bar{V}_k)\hat{x}_k \quad (6.12)$$

with

$$\Gamma(\bar{V}_k) = \begin{bmatrix} 0 & 0 & \cdots & 0 & 0 \\ \gamma(1,0) & 0 & \cdots & 0 & 0 \\ \gamma(2,0) & \gamma(2,1) & \cdots & 0 & 0 \\ \vdots & \vdots & \ddots & \vdots & \vdots \\ \gamma(m,0) & \gamma(m,1) & \cdots & \gamma(m,m-1) & 0 \end{bmatrix}$$

$$\Xi(\bar{V}_k) = [\xi(0), \xi(1), \dots, \xi(m)]^\top$$

where

$$\gamma(a, b) := C(V_{k+a})A(V_{k+a-1}) \times \cdots \times A(V_{k+b+1})B(V_{k+b})$$

and

$$\xi(a) := \begin{cases} C(V_k), & \text{for } a = 0 \\ C(V_{k+a})A(V_{k+a-1}) \cdots A(V_k), & \text{otherwise.} \end{cases}$$

This is the same matrix form as the conventional MPC tracking solution shown in Appendix B but in this instance incorporates the parameter-varying component of the system.

6.3 Modified Parameter Identification

The system parameters within (6.1)-(6.5) must be identified using a procedure suitable for clinical research application. The initial attempt in Chapter 5 using the ARMAX solution created a restrictive form of assumed external disturbance. Therefore, a more general procedure is proposed below that removes assumptions on the system disturbances.

Definition 6.4 (Identification Problem). Consider the parameter-varying discrete closed-loop system shown in Figure 6.2b with dynamics (6.1)-(6.5). Given a set of sampled experimental input-output data $\{\tilde{r}_i, \tilde{P}_i\}_{i=1, \dots, N}$, and corresponding valve resistance sequence $\tilde{V} = (\tilde{V}_1, \tilde{V}_2, \dots, \tilde{V}_N)$, the identification problem is to compute the parameter vector $\hat{\theta}$ containing all the unknown parameters within K , G , and H . This corresponds

to the minimisation problem

$$\min_{\tilde{\theta}} \sum_{k=1}^N (\tilde{P}_k - P_k)^2 \quad (6.13)$$

where θ contains all unknown coefficients of FP , K , G , and H , subject to dynamics (6.1)-(6.5) with input \tilde{r} and valve sequence vector \tilde{V} .

The system parameters can then be identified by simulating the model across an appropriate range of parameters and finding the minimum of (6.13). For example, an appropriate range of resistance, R , would be between 1 and 20. There is always flow resistance in the airways meaning it is not possible for R to be 0, and values above 20 would mean respiratory pathologies are present in which case the person should not be performing the tests.

6.4 Simulation Results and Discussion

6.4.1 Model Structure Selection and Simulation

Since the tracking task is reactive (i.e. the participant cannot see the upcoming reference and possible changes), the predictive component FP can be set equal to a perception delay of 0.2s, corresponding to the average human response time to a sensory stimulus [53]. Based on established models of human motor control [50] K and H are chosen to realise a proportional-integral feedback controller (with respective gains K_p and K_i). An additional delay is incorporated into K to account for the decision delay of 0.1s.

This selection leads to the forms:

$$\begin{aligned} A_{FP} &= \begin{bmatrix} 0 & 0 & \cdots & 0 \\ 1 & 0 & \ddots & \ddots & \vdots \\ 0 & 1 & \ddots & \ddots & \vdots \\ \vdots & \ddots & \ddots & \ddots & \vdots \\ 0 & \cdots & 0 & 1 & 0 \end{bmatrix}, \quad B_{FP} = \begin{bmatrix} 1 \\ 0 \\ 0 \\ \vdots \\ 0 \end{bmatrix}, \\ C_{FP} &= \begin{bmatrix} 0 & 0 & 0 & \cdots & 1 \end{bmatrix} \end{aligned} \quad (6.14)$$

and

$$\begin{aligned}
 A_K &= \begin{bmatrix} 0 & 0 & \cdots & 0 & 0 \\ 1 & 0 & \ddots & \ddots & \vdots \\ 0 & 1 & \ddots & \ddots & \vdots \\ \vdots & \ddots & \ddots & \ddots & \vdots \\ 0 & \cdots & 0 & 1 & 0 \\ 0 & \cdots & \cdots & \cdots & T_s & 1 \end{bmatrix}, \quad B_K = \begin{bmatrix} 1 \\ 0 \\ 0 \\ \vdots \\ 0 \end{bmatrix}, \\
 C_K &= \begin{bmatrix} 0 & \cdots & 0 & K_p & K_i \end{bmatrix}.
 \end{aligned} \tag{6.15}$$

Accepted values of L fall between 0.001 and 0.01 and have negligible effect on the tracking response, therefore will be omitted from the G dynamics. Additionally, the review of models in Chapter 3.3 made it clear that inertance is a respiratory component that is more prominent in high frequency oscillatory airflow between 5-20 Hz. During forced expiration in this research, the dominant frequencies of the oscillations and pressure changes are lower than 5Hz.

Therefore the overall closed-loop dynamics are given by state-space system (6.5) with

$$\begin{aligned}
 A(V_k) &= \begin{bmatrix} 0 & 0 & \cdots & \cdots & \cdots & 0 & \frac{-V_k}{R+V_k} \\ 1 & 0 & \ddots & \ddots & \ddots & \ddots & 0 \\ 0 & 1 & \ddots & \ddots & \ddots & \ddots & \vdots \\ \vdots & \ddots & \ddots & \ddots & \ddots & \ddots & \vdots \\ \vdots & \cdots & 0 & 1 & 0 & \ddots & \vdots \\ \vdots & \cdots & \cdots & 0 & T_s & 1 & 0 \\ 0 & \cdots & \cdots & 0 & K_p T_s & K_i T_s & \exp\left(\frac{-T_s}{(R+V_k)C_a}\right) \end{bmatrix} \\
 B(V_k) &= \begin{bmatrix} 1 & 0 & \cdots & 0 \end{bmatrix}^\top, \quad C(V_k) = \begin{bmatrix} 0 & \cdots & 0 & \frac{V_k}{R+V_k} \end{bmatrix}
 \end{aligned} \tag{6.16}$$

Lung compliance, C_a is set to 0.1 L/cmH₂O as this value accurately fits all healthy subjects [45]. The search parameter vector within (6.13) therefore becomes $\hat{\theta} = (R, K_p, K_i)$.

Chapter 5 presented the simplest model which relied on the RLC circuit dynamics in G and linear gain in K to produce the model response. This led to values of L , R , and V that were less realistic. The introduction of a proportional-integral (PI) feedback controller allows for more realistic values of L , R and V . For simulation, the parameters in $\hat{\theta}$ are selected to be $R = 5$ cmH₂O, $K_p = 7$, and $K_i = 3$ based on the data in Figure 4.2b. Figure 6.4 shows simulations of the model's response to a reference change at different valve resistances. These responses are scalable, i.e. if the reference change was larger the overshoot would be proportionally larger. For example, if the reference changes from 0 to 10 cmH₂O, the peak pressures in Figure 6.4 would be (a) 11 cmH₂O, (b) 12 cmH₂O, and (c) 13 cmH₂O. The responses are also translatable, i.e. the

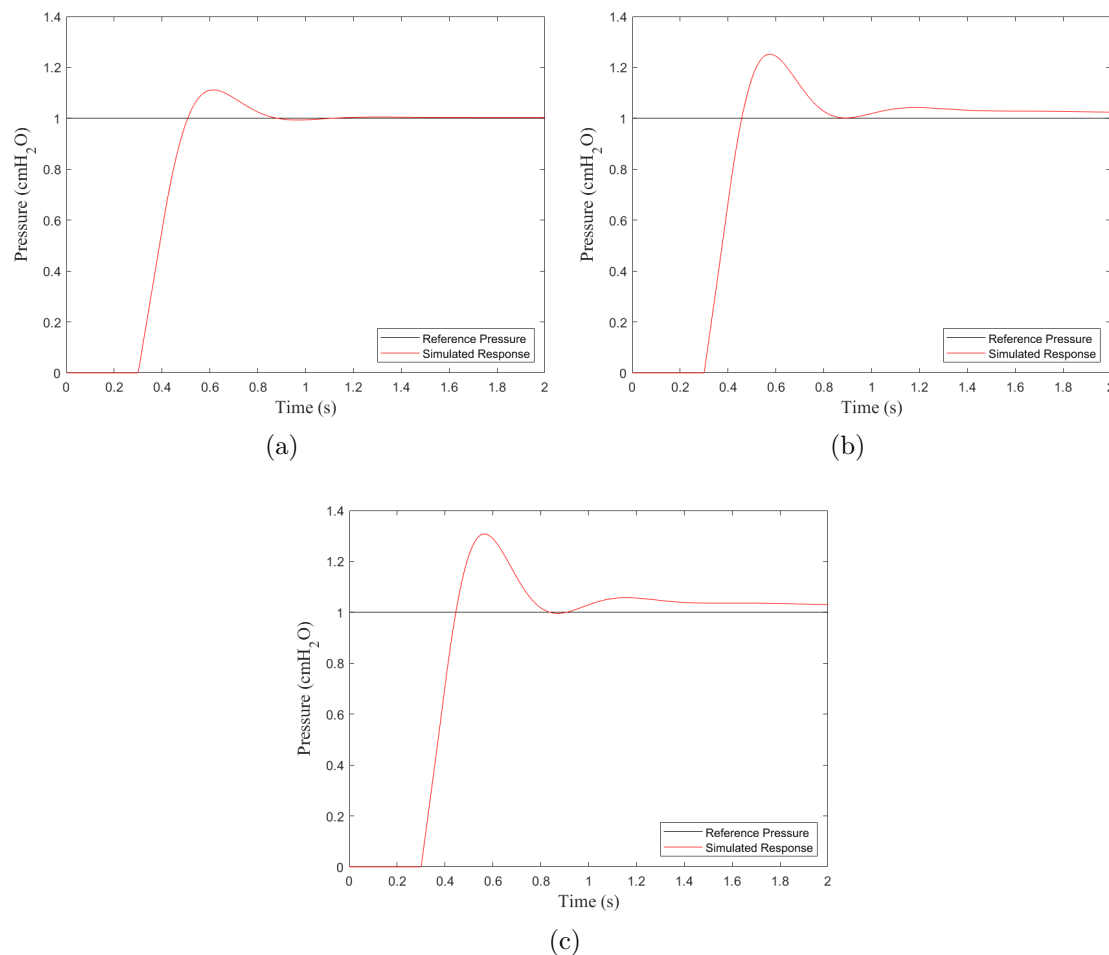


Figure 6.4: Simulated responses to a reference unit step change with a valve resistance of:

- (a) 20 cmH₂O/L/s
- (b) 80 cmH₂O/L/s
- (c) 1000 cmH₂O/L/s.

overshoot would be the same for a reference change from 0 to 10 cmH₂O as it would be for a reference change from 10 to 20 cmH₂O.

Figure 6.5 shows the simulated response to a valve resistance step-change when tracking a constant pressure reference. These responses are proportional to the reference that is being tracked. So a resistance step-change from 1000 to 80 cmH₂O would reduce the generated pressure by $\approx 6\%$ while a resistance step-change from 1000 to 20 cmH₂O would reduce the the generated pressure by $\approx 20\%$. This is dependent on the airway resistance parameter, R , in the closed-loop state-space matrices in (6.16).

6.4.2 Control

The MPVC scheme was tested in simulation alongside *in vivo* preliminary tests. The measurement sampling frequency was set at 100Hz ($T_s = 0.01$ s) to match that of clinical

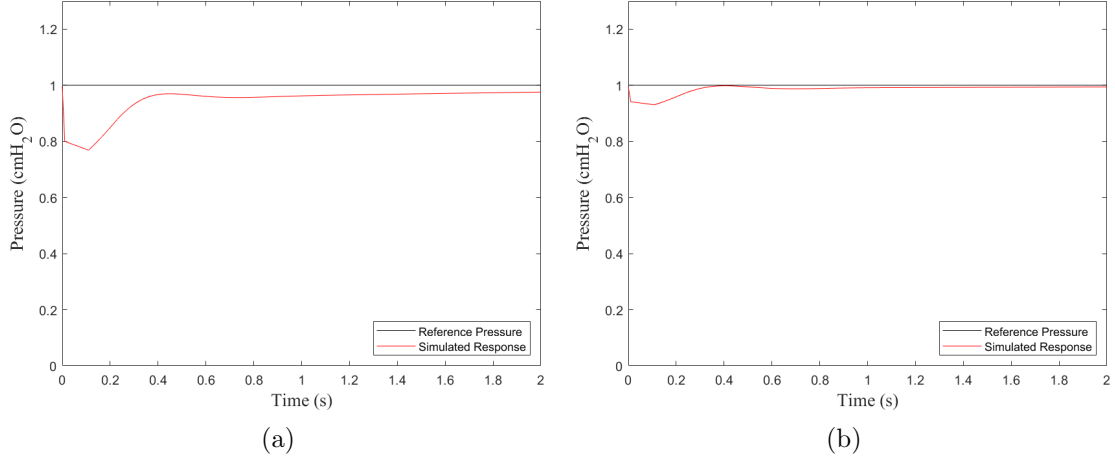


Figure 6.5: Simulated responses at a constant pressure reference to a valve resistance change of:

- (a) 1000 cmH₂O/L/s to 20 cmH₂O/L/s
- (b) 1000 cmH₂O/L/s to 80 cmH₂O/L/s.

TMD measurements and to adhere to the specification presented in Section 4.2.1. The *in vivo* application indicated that a maximum of 2 computations could be performed in the 0.01s time period. This would not be sufficient for practical application of the controller. The control frequency was therefore set to 10Hz i.e. applying a new control input every 0.1s. A maximum of 100 control computations could be performed in the control-time sampling period. To ensure the maximum number of MPVC computations could be performed, the prediction horizon was set to 5 (including the current control-time sample) and number of possible valve resistances set to 3 to allow 81 control computations per sample (3^{5-1}).

Based on the *in vivo* testing, the selected valve resistance values were determined to comprise: a value to release pressure; a value to assist the participant in decreasing lung pressure; a maximum value of resistance which does not allow glottal closure. Based on the testing, this resulted in the permissible set of valve resistances $\mathcal{V} := \{80, 160, 1000\}$. Solving the non-convex MPVC problem (6.10) is then achieved by evaluating the stage cost J for all $|\mathcal{V}|^m$ possible valve resistance sequences. The controller then selects the lowest stage cost and applies the first element of solution \bar{V}_k .

Simulations showed a 3-6% improvement in tracking error with no noise and a 3-10% improvement with additional Gaussian noise. Figure 6.6 shows how the valve resistance changes during the measurement period and the corresponding response of the model to the reference and resistance changes. The key observation to note is when the valve resistance changes from the maximum resistance (1000 cmH₂O/L/s). The drop in resistances mostly correspond to the necessity to reduce pressure during an overshoot and during a pressure reference drop. The drop in resistance before the 8-second mark is an attempt from the controller to increase the pressure when the reference changes at 8 seconds.

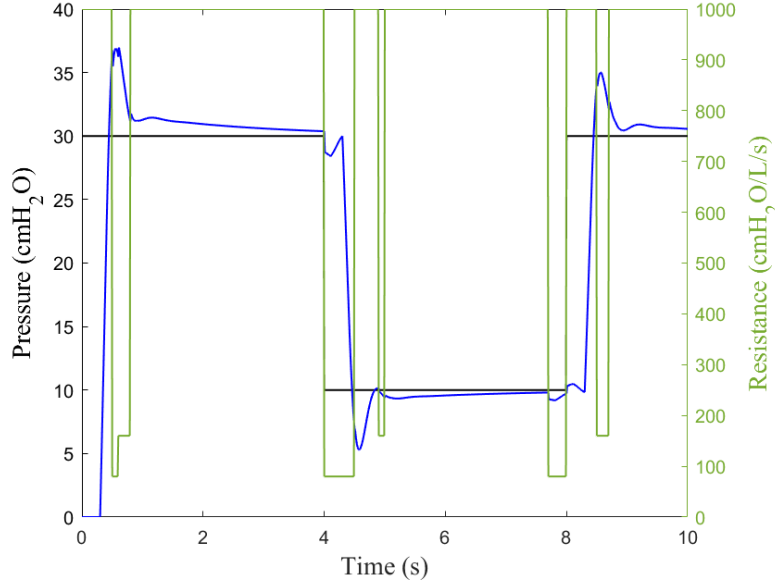


Figure 6.6: Graph showing the model's tracking response (blue) of the reference (left y-axis), with the corresponding resistance values (green, right y-axis).

6.4.3 Identification

The identification procedure was presented in Section 6.3 attempting to minimise cost function (6.13). The search space must have a suitable range for each parameter in $\hat{\theta}$ to ensure all plausible model iterations are explored. Therefore, for both simulation and practical application, the cost function (6.13) is minimised over the search space of suitable parameters

$$\hat{\theta} \in \{(R, K_p, K_i) \mid R \in \{1, 2, \dots, 20\}, K_p \in \{1, 2, \dots, 20\}, K_i \in \{0, 1, \dots, 20\}\}. \quad (6.17)$$

Figure 6.7 shows the simulated response with no noise and the identified model's response. Figures 6.8 and 6.9 show the same simulated response as in Figure 6.7 but with minor and moderate Gaussian noise respectively added to the output. The simulated data is filtered to reduce measurement noise before the identification procedure is performed. The ARMAX identification process in Section 5.3 proved to be unsuccessful when a randomised Gaussian noise was added to the output of the simulated response. This is due to the assumption that the measured noise has a structure similar to the system dynamics and therefore has an implicit solution. As Gaussian noise is randomised, the solution is not implicit and makes the identification non-convex. However, the simplified search algorithm in Section 6.3 can be used to compute an average cost across multiple data sets. This means that the cost function is taken for each model output across all data sets and the minimum of the combined cost functions (i.e. one for each data set) is computed. The more general approach allows for all possibilities of model

to be explored and the best fit model across the data sets is selected. A benefit of this is that measurement noise (the remnants after filtering) has a lower impact than if the identification process was performed on singular data sets.

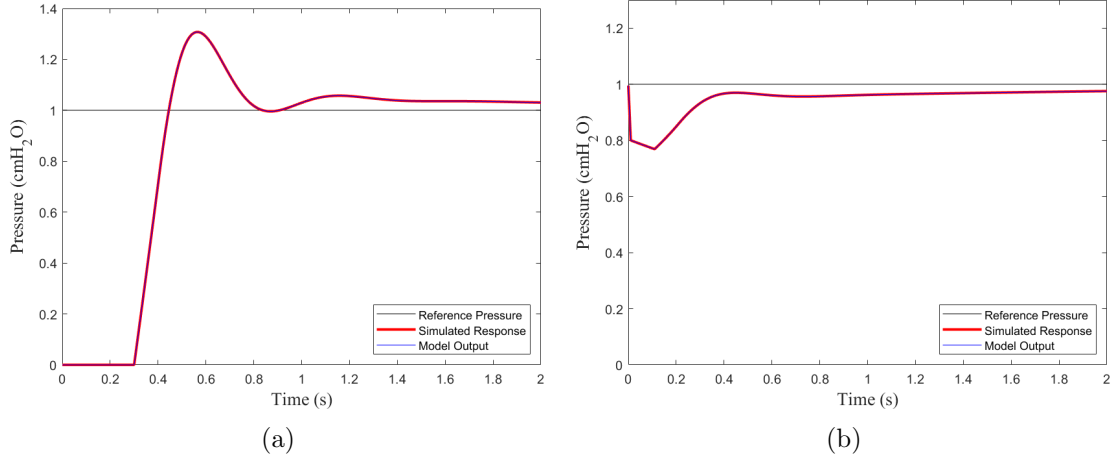


Figure 6.7: Identified model (blue) compared to simulated data (red).

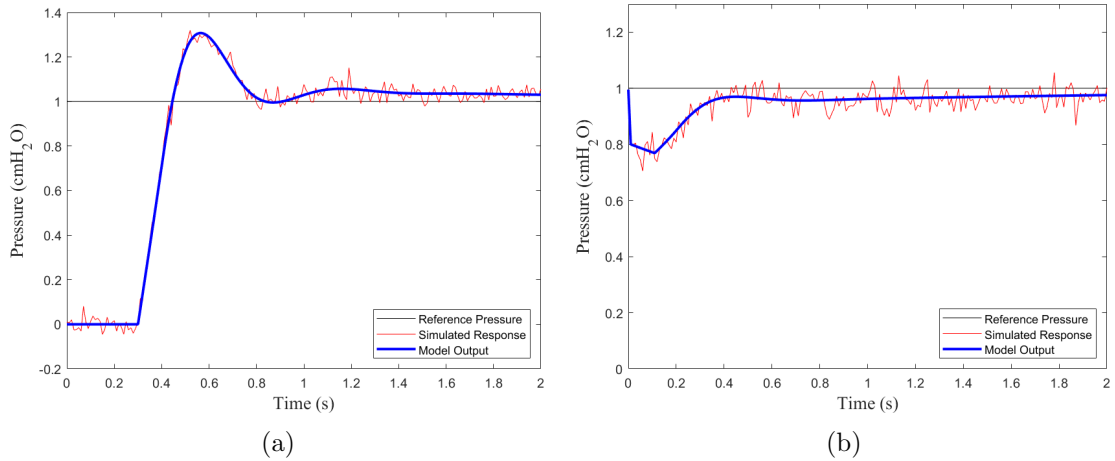


Figure 6.8: Identified model (blue) compared to simulated data with minor Gaussian noise (red).

Figures 6.7, 6.8, and 6.9 demonstrate that the identification procedure is viable for practical application as it can adjust to the noisy data. The procedure was performed on multiple simulated responses (i.e. across a significant range of $\hat{\theta}$ parameters) and the identification procedure correctly identified the $\hat{\theta}$ parameters with an accuracy of $\approx 70\%$. However, the incorrectly identified models had parameters within three units of the correct value a further $\approx 73\%$ of the time (i.e. 73% of the remaining 30%). This means that an appropriate model was identified $\approx 92\%$ of the time. The remaining inaccurate models were due to poor data with excessive noise that would not be considered viable for use in the identification procedure if taken during practical application.

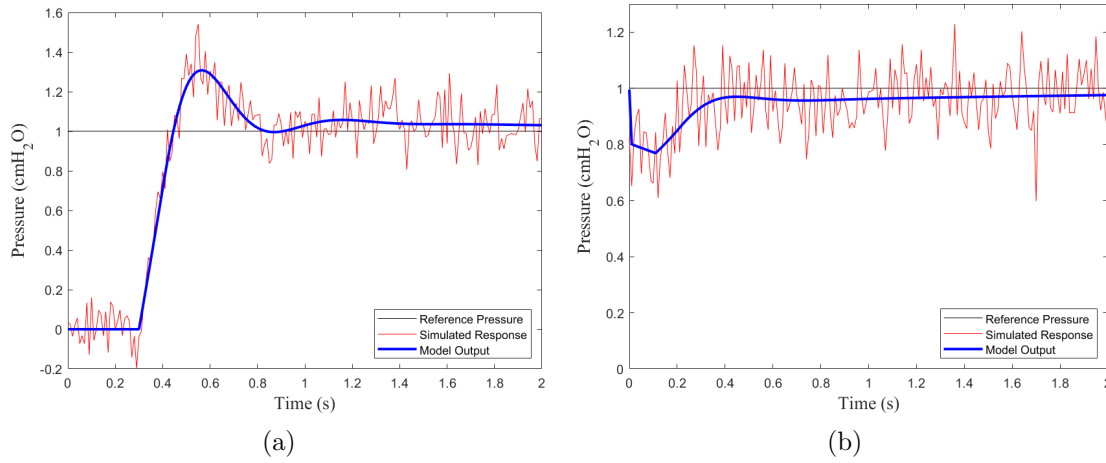


Figure 6.9: Identified model (blue) compared to simulated data with moderate Gaussian noise (red).

6.5 Experimental Application

The simulation results in Section 6.4 showed that the modified model structure could produce similar overshoot and tracking dynamics to the real data in Figure 4.2b. The controller application showed that the resistance of the valve only changed at necessary points such as to reduce pressure or to encourage an increase in pressure. The use of a search identification procedure removed assumptions of the noise dynamics made in Chapter 5 and therefore improved the accuracy of the procedure when noise was present in the identification data. This section applies the model, controller and identification procedure in practical experimentation on 10 healthy participants following approval from the University of Southampton ethical standards committee (**ERGO/F-PSE/62619**). The controller developed in Section 6.2 is compared against comparative proportional and integral forms of control. Additionally, two versions of the Kalman Filter are used for MPVC to observe differences in control dependent on assumptions made about the measurement data.

6.5.1 Comparative Control Methods

MPVC provides a highly accurate solution to the Valve Assistance Problem (Definition 6.2), however, simpler methods may also provide potential solutions. Based on the review in Section 3.2 and following summary in Section 4.3, traditional controllers cannot be directly applied to this parameter control problem, since the controller is adjusting an internal parameter of the system (V) rather than an input signal. However, they motivate simple structure approaches such as PID. To establish its applicability, consider

the dynamics shown in Figure 6.1b

$$P_l(t) = L \frac{dQ(t)}{dt} + (R + V(t))Q(t) + \frac{1}{C_a} \int Q(t), \quad (6.18)$$

$$P(t) = Q(t)V(t) \quad (6.19)$$

which, assuming the rate of change of airflow is small, simplify to

$$P_l(t) - \frac{1}{C_a} \int Q(t) = RP(t)/V(t) + P(t) \quad (6.20)$$

$$\Rightarrow P(t) = \frac{aV(t)}{R + V(t)} \quad (6.21)$$

around an operating point $a = P_l - \frac{1}{C_a} \int Q(t)$. Since a and R are positive, the dynamics $V(t) \mapsto P(t)$ comprise a smooth, monotonically increasing function that passes through $(0, 0)$, with an amplitude that depends on the flow volume. This monotone relationship suggests that a PID-type control action would effectively reduce the error $e_k = r_k - P_k$. This motivates implementing a proportional controller of the form

$$V_k = V_{e_0} - K_{p_e} e_k \quad (6.22)$$

where V_{e_0} is a resistance offset that moves the system to a pressure operating point concurrent to the r operating point. K_{p_e} is set such that constraint (6.7b) is adhered to. A drawback to proportional control is possible valve resistance oscillation due to rapid pressure changes. For example, when the reference pressure has a step decrease, the error will be significantly negative. This will cause the valve to open in order to drop the generated pressure quickly. However, this pressure drop will cause the valve to close up to increase the resistance. This can happen multiple times in a time frame of $\approx 0.5 - 1$ s which is the cause of the oscillations. Large pressure drops may also cause a significant drop in valve resistance creating a high airflow, causing the participant to run out of air in their lungs more quickly.

These issues can be addressed using integral control, which amalgamates valve resistance over time depending on error e_k , taking the form

$$V_k = V_{e_0} - K_{i_e} \sum_{i=k_{ec}}^k e_i \quad (6.23)$$

with limits V_{min} and V_{max} . Here K_{i_e} is the integral coefficient of the error and k_{ec} is the time index when the error most recently changed sign.

6.5.2 Valve Control System

In the preceding sections it has been assumed that the valve resistance, V_k , can be directly set at each time instant k by the controller. However, in reality, the controlled variable is a pulse-width modulation (PWM) duty cycle sent to the valve, which affects the airflow through the valve (thus the valve resistance) in the following indirect manner:

- the PWM signal, ρ , dictates the magnitude of a proportional current (gain κ) that is applied to the valve;
- the resultant current, $\kappa\rho$, changes the flow coefficient, K_v , of the valve by actuating the valve position. These two variables are related by a static non-linear function, $K_v = \eta(\kappa\rho)$, which includes hysteresis;
- the value of K_v relates the pressure and flow via $K_v = Q/\sqrt{P}$.

A resistance-tuning controller is therefore needed to continually adjust the PWM duty cycle signal, ρ , such that the required valve resistance, V_k , is achieved. This is done by measuring the pressure value P_k , and computing the necessary flow rate, denoted $Q_{r,k}$, that achieves V_k at every sample. Then a proportional control loop (gain K_ρ) is applied to force Q_k to track this $Q_{r,k}$. The resulting controller is shown in Figure 6.10.

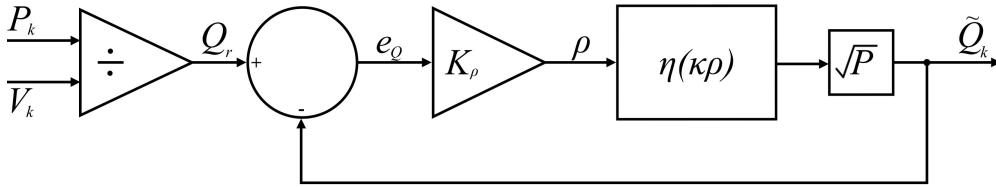


Figure 6.10: Block diagram of the resistance-tuning controller.

The resistance-tuning controller is applied at the same frequency as the measurement sampling frequency of 100Hz. No results were collected to show this controller's function. However, observations were made by the author in which the tuning controller adjusted the resistance to within 5% of the required valve resistance in ≤ 4 sampling periods (i.e. ≤ 0.04 seconds).

6.5.3 Procedure

During testing, all participants were seated in an upright position and used the same equipment (apart from the disposable mouthpieces and filters) in a standardised position. Prior to testing, the pressure and airflow sensors were calibrated by placing them on a flat surface as shown in Figure 4.3 and applying an offset to produce zero-readings.

6.5.4 Identification Data Collection

The next step is to capture the dynamics of the system using the identification procedure in Section 6.3. This requires that the pressure sequences $\{\tilde{r}_i\}_{i=1,\dots,N}$ and corresponding valve resistance sequences $\{\tilde{V}\}_{i=1,\dots,N}$ are sufficiently exciting yet short enough to be practically feasible.

The identification data set is constructed by amalgamating 24 separate identification tests, each lasting at least 2 seconds. The first set of 12 tests capture the participant's response to a step reduction in valve resistance, while they attempt to track a constant reference pressure (such as in Figure 6.5). The reference value r_{id} , is taken from the set $\{10, 20, 30\}$ with units cmH₂O. The valve is initially closed ($V = \infty$), and the participant is required to reach the value of r_{id} . The valve is then opened to a specified resistance V_{id} taken from the set $\{20, 40, 60, 80\}$ with units cmH₂O/L/s. Measurements begin and the participant is required to get the pressure back up to r_{id} as quickly as possible (see Figure 6.12a).

The second set of 12 tests capture the participant's response to a step increase in pressure, starting at a pressure of $P = 0$ cmH₂O (such as in Figure 6.4). Once the valve opens, they have to reach the reference pressure r_{id} as quickly as possible and settle (see Figure 6.12b). The tests are performed with the same combination of references (r_{id}) and resistances (V_{id}) as the first procedure.

The 24 sets of data are then grouped according to the test procedure and valve resistance applied. For each test and resistance level the data are normalised across the three reference pressures and an average is taken. This produces eight groups (two tests types, four resistance values of V_{id} each). These eight data sets are used for identification purposes.

This normalisation is possible since the same change in V_k occurs at each pressure reference r , the dynamics (6.16) remain the same thus superposition applies. Therefore the output can be scaled by dividing by the pressure reference level. Taking an average of each of the eight groups reduces the number of sets used to compare against during identification.

The eight averaged data sets are combined to form the overall set $\{\tilde{r}_i, \tilde{P}_i\}_{i=1,\dots,N}$, $\{\tilde{V}\}_{i=1,\dots,N}$. Then cost function (6.13) is minimised over the same search space of suitable parameters in Section 6.4.3

$$\begin{aligned} \hat{\theta} \in \{ (R, K_p, K_i) \mid R \in \{1, 2, \dots, 20\}, K_p \in \{1, 2, \dots, 20\}, \\ K_i \in \{0, 1, \dots, 20\} \}. \end{aligned} \quad (6.24)$$

To assess how closely the resulting model fits a measured data set $\{\tilde{r}, \tilde{P}, \tilde{V}\}$, the percentage accuracy is computed as

$$\left(1 - \frac{\sum_{i=1}^N (\tilde{P}_i - P_i)^2}{\sum_{i=1}^N \tilde{P}_i^2}\right) \times 100 \quad (6.25)$$

where \tilde{P} is the measured pressure, and P is the output of model (6.1)-(6.5) with input $\{\tilde{r}, \tilde{V}\}$. This will be termed the *fitting accuracy* when using identification data, and *prediction accuracy* when using any other data.

6.5.5 Control Application

Five control schemes were tested with each participant. The first approach employs a constant valve resistance. This replicates the resistance of the red cap in the original clinical research setup, and is therefore the standard experimental approach. This is the baseline approach to LPP tracking.

The second approach is the discrete integral controller presented in Section 6.5.1. This takes the form (6.23) but the gains V_{e_0} and K_{i_e} are adapted such that

$$V_k = \begin{cases} V_{k-1} - 20, & e_k < -2, \\ 160, & -2 \leq e_k \leq 2, \\ V_{k-1} + 20, & e_k > 2. \end{cases}$$

The third approach is the discrete proportional controller (6.22), whose gains V_{e_0} and K_{p_e} are adapted such that

$$V_k = \begin{cases} 20, & e_k \leq -10, \\ 40, & -10 < e_k \leq -8, \\ 60, & -8 < e_k \leq -5, \\ 80, & -5 < e_k \leq -3, \\ 160, & -3 < e_k \leq 5, \\ 300, & 5 < e_k \leq 10, \\ 1000, & e_k > 10. \end{cases}$$

The choice of gains effectively limits the control action to prevent valve oscillation or high airflow.

The fourth and fifth approaches use MPVC with different Kalman Filter covariance scalar parameters, λ_m and μ_p , within (6.11).

As the ratio μ_p/λ_m increases, the process noise assumes more variance compared to the measurement noise. This has the effect of placing more reliance on the measurement data compared to the model in computing the estimated state. Modifying the ratio has a significant effect on the overall control action.

Both MPVC control approaches use a covariance of $\lambda_m = 1$. However, the fourth and fifth control approaches use $\mu_p = 0.1$ and $\mu_p = 1$ respectively.

6.5.6 Pressure Profiles

Participants were required to perform 30 pressure tracking tests in total. These comprised six pressure profiles (cmH₂O), repeated five times (each with a different controller). The six profiles were composed of random steps. Each step size was a multiple of a fixed amplitude Δr , and had a duration of 3 seconds. The profile had to be contained within an overall pressure range (based on constraint (6.7a)). The parameters used to construct each profile type are as follows:

- a) $10 \leq r \leq 30, \Delta r = 5$
- b) $10 \leq r \leq 30, \Delta r = 10$
- c) $10 \leq r \leq 40, \Delta r = 5$
- d) $10 \leq r \leq 40, \Delta r = 10$
- e) $10 \leq r \leq 50, \Delta r = 5$
- f) $10 \leq r \leq 50, \Delta r = 10$

In application, the step sizes are randomised so that participants cannot predict them. Similarly, the order of the controllers is randomised to provide an unbiased assessment of the ability of each controller. Figure 6.11 shows an example of a participant's response to a pressure profile. **N.B.** The profiles used in this research do not correspond to the profiles that would be used alongside TMD measurements. The profiles for this research have been chosen to avoid participant prediction, and to test the controllers across the full range of pressures and pressure changes.

Two safety protocols are employed to identify the lung vital capacity and pressure constraints in (6.7). The vital capacity is measured for each participant 3 times and an average is taken. The limit v_c is then set around 1 litre less than their vital capacity. There is an in-built automatic cut-off when this limit is reached. Participants are also asked to exhale until they reach a maximum pressure that they feel is exerting but still comfortable.

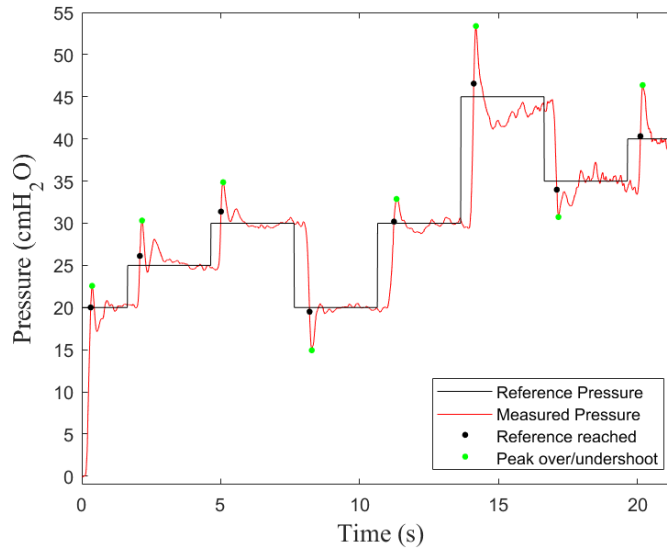


Figure 6.11: Example tracking response (profile type (e)) with constant valve resistance. Black points represent the first point where the reference has been reached after a step change. Green points represent peak overshoot/undershoot.

6.6 Practical Results and Discussion

Following University of Southampton ethics approval (ERGO/FPSE/62619), 10 healthy participants (7 men and 3 women, age range 20-56) with no underlying health conditions were recruited onto this study. The participants will be referred to as P1-P10.

6.6.1 Model Identification

Each participant completed the identification and control tests described in Section 6.5. Figures 6.12a and 6.12b show examples of the measured tracking responses and the model tracking responses for the two types of identification test. Figure 6.13 presents the model identification results in the form of box and whisker plots showing the data fitting accuracy for each participant. Three measures of model fitting accuracy (MFA) are shown:

- MFA1: Fitting accuracy of the model to the averaged identification data (8 data sets, 2 second measurement period, see Section 6.5.4);
- MFA2: Prediction accuracy of the model to all identification data (24 data sets, 2 second measurement period);
- MFA3: Prediction accuracy of the model to all control data (30 data sets, 10-50 second measurement period).

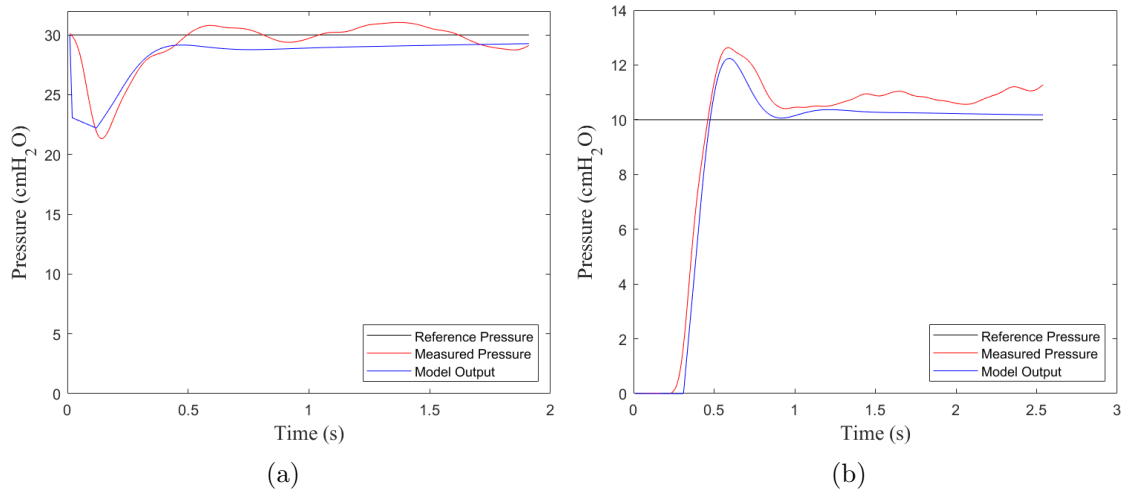


Figure 6.12: (a) Sample tracking response of first identification procedure ($r_{id} = 30$, $V_{id} = 20$)
 (b) Sample tracking response of second identification procedure ($r_{id} = 10$, $V_{id} = 60$).

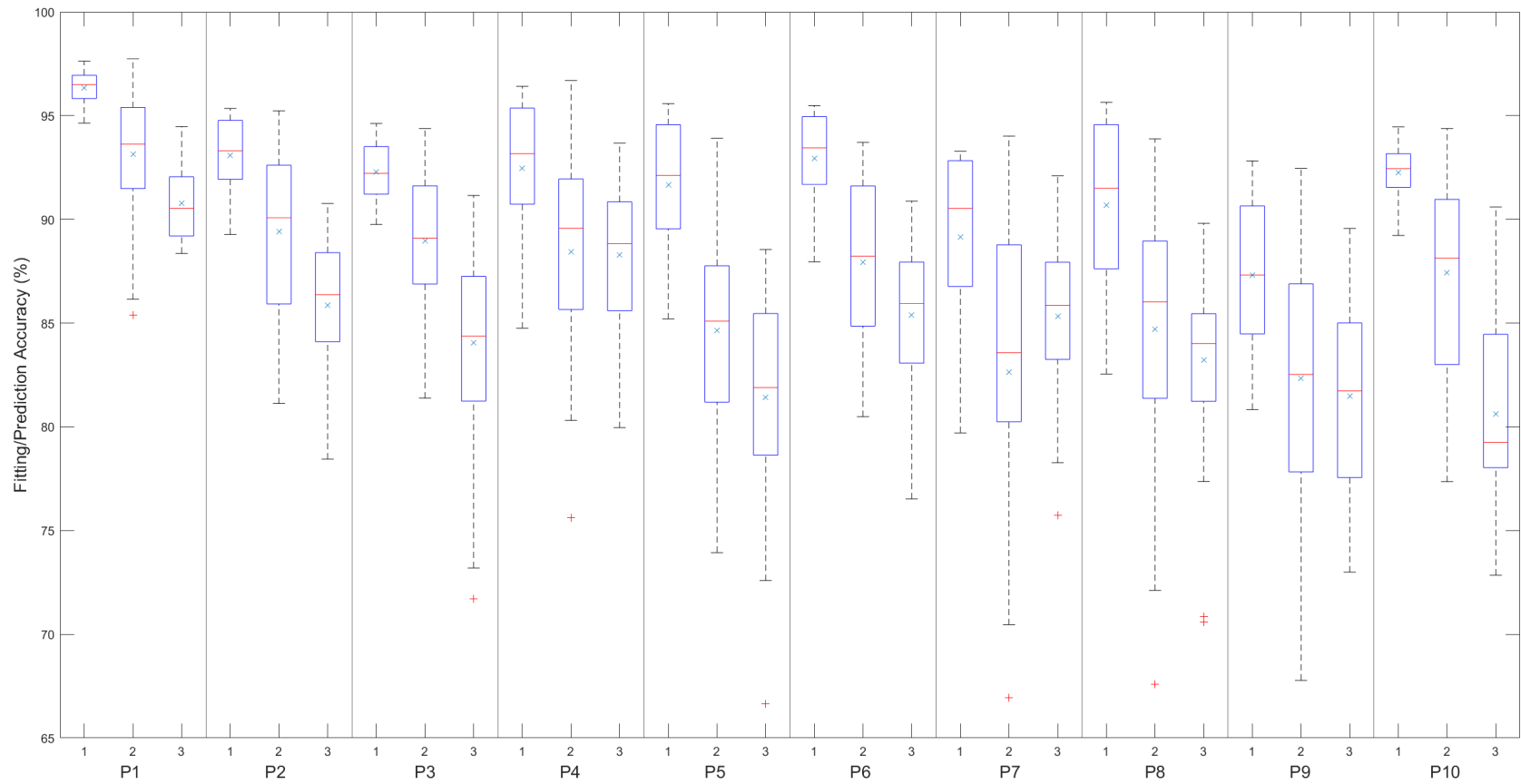


Figure 6.13: Box and whisker plots of model fitting and prediction accuracies of identification and control data corresponding to each participant. Columns labelled: 1 represent MFA1; 2 represent MFA2; 3 represent MFA3. The central line of the boxes represents the median and the 'x' mark represents the mean.

For MFA1, the average of the medians, means, and IQRs over all participants are 92.3%, 91.8%, and 4.0% respectively. This shows that the participants had good consistency after a short practice period, it also shows that the model and identification process is effective for practical use. MFA1 is highest as these data were used to identify the model.

For MFA2, the combined average of the medians, means and IQRs over all participants are 87.6%, 87.0% and 6.8% respectively. This not only shows that the model is accurate but also that the participants are relatively consistent in their pressure reference tracking and response to specific resistance changes.

MFA3 measures the model accuracy during the participants' controlled tracking results. Figure 6.14a shows the same data as in Figure 6.11 but with the predicted output of the identified model overlaid in blue. The combined average of the medians, means and IQRs over all participants are 84.9%, 84.6% and 5.3% respectively. This further confirms the validity of the model and identification procedure.

6.6.2 Control

For control application, eight of the ten participants were comfortable generating a pressure above 50 cmH₂O, the other two participants generated maximums of 40 and 45 cmH₂O. In these cases the pressure profile ranges in Section 6.5.6 were adjusted to 5-25, 10-30, and 5-35 cmH₂O and 10-30, 5-35, and 10-40 cmH₂O respectively.

Figure 6.14a shows an example of the identified model's ability to reproduce the measured pressure generated by a participant during a LPP test with a constant valve resistance. Figure 6.14b shows an example of a participant's LPP tracking ability with MPVC assistance.

The following metrics were computed for each profile tracking test: average airflow; 2-norm of profile tracking error; time taken to reach the profile pressure after a step-down (labelled 'fall time'); 2-norm of profile tracking error after a step-up or step-down; absolute value of overshoot/undershoot to a step change in proportion to the magnitude of the step change. These metrics are defined in more detail below.

Figures 6.15a - 6.15e show box and whisker plots of each metric. Each box and whisker corresponds to the pooled data from all participants for a particular control type and is labelled on the plots as follows:

- 1) Constant valve resistance
- 2) Proportional-integral (PI)

- 3) Proportional
- 4) MPVC with Kalman parameters $\lambda_m = 1$, $\mu_p = 0.1$ (MPVC1)
- 5) MPVC with Kalman parameters $\lambda_m = 1$, $\mu_p = 1$ (MPVC2).

As previously described, Control Type 1 (constant valve resistance) is the baseline approach against which Control Types 2-5 are compared below.

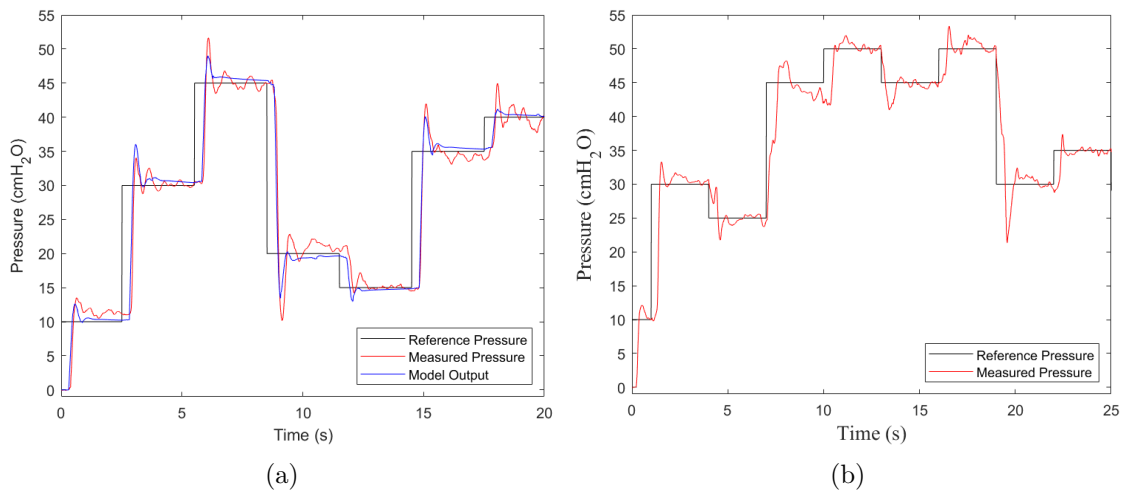


Figure 6.14: (a) Sample tracking response with constant valve resistance (Figure 6.11, profile type (e)) with predicted model output overlaid
(b) Sample tracking response with MPVC assistance (profile type (e)).

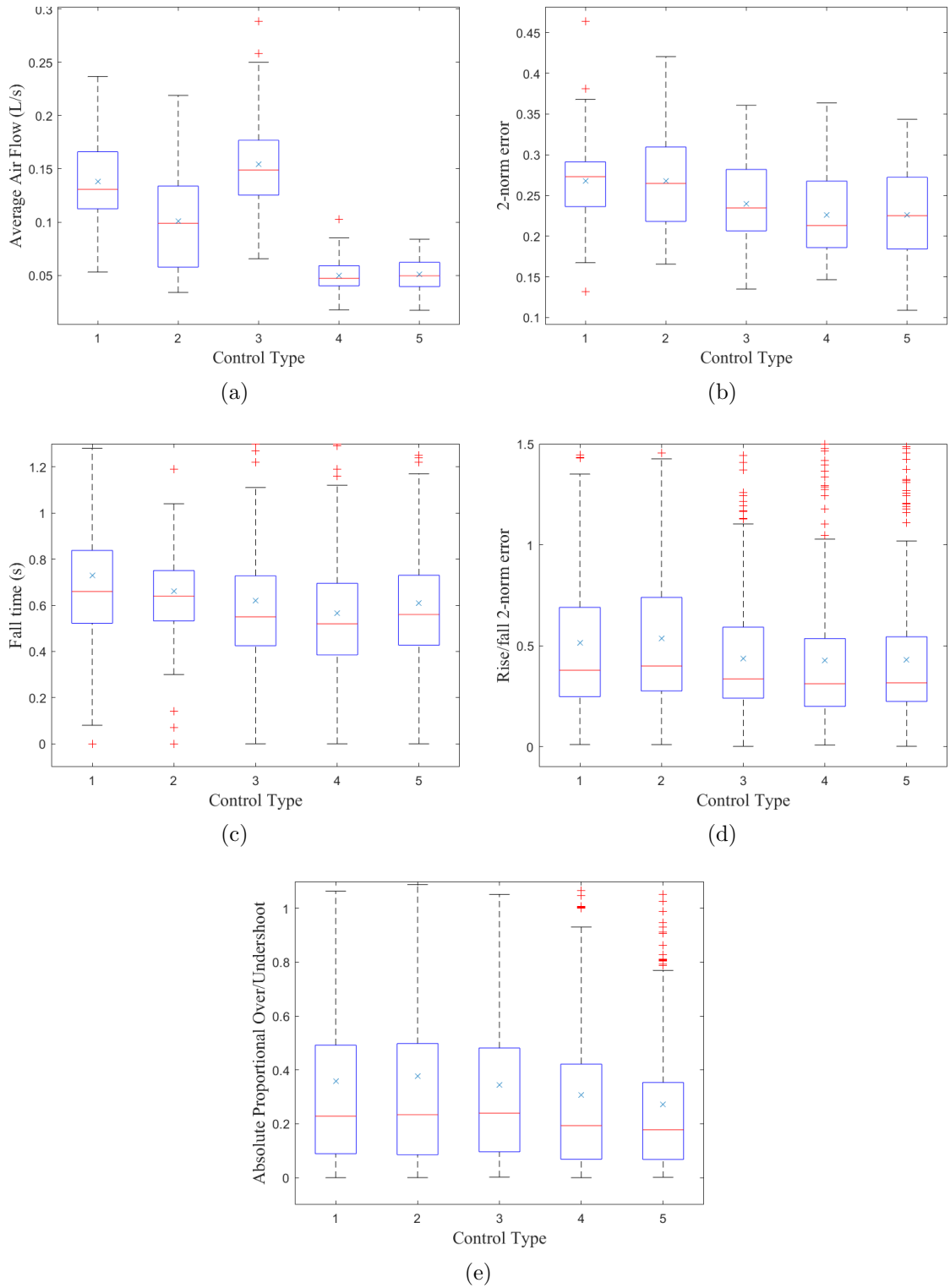


Figure 6.15: Box and whisker plots of combined:
 (a) average airflow data;
 (b) error norm data;
 (c) fall time data;
 (d) rise/fall 2-norm error data;
 (e) absolute proportional overshoot/undershoot data,
 for each control type. Control types are defined in Section 6.6.2.

Table 6.1: Table of medians and means from the metrics in Figures 6.15a-6.15e

| Control Method | Combined Statistical Data | | | | | | | | | |
|-----------------------|---------------------------|--------|--------------|--------|---------------|--------|----------|--------|---------|--------|
| | Average Airflow (L/s) | | 2-Norm Error | | Fall Time (s) | | R/F2-NE* | | APO/U** | |
| | Median | Mean | Median | Mean | Median | Mean | Median | Mean | Median | Mean |
| Constant Resistance | 0.1307 | 0.1378 | 0.2730 | 0.2677 | 0.6600 | 0.7301 | 0.3791 | 0.5155 | 0.2285 | 0.3596 |
| Proportional-Integral | 0.0988 | 0.1007 | 0.2647 | 0.2681 | 0.6400 | 0.6620 | 0.3999 | 0.5364 | 0.2340 | 0.3765 |
| Proportional | 0.1488 | 0.1543 | 0.2347 | 0.2395 | 0.5500 | 0.6204 | 0.3355 | 0.4378 | 0.2400 | 0.3445 |
| MPVC1 | 0.0471 | 0.0498 | 0.2130 | 0.2260 | 0.5200 | 0.5660 | 0.3115 | 0.4277 | 0.1935 | 0.3073 |
| MPVC2 | 0.0495 | 0.0512 | 0.2251 | 0.2259 | 0.5600 | 0.6088 | 0.3168 | 0.4309 | 0.1780 | 0.2729 |

* R/F2-NE refers to Rise/Fall 2-Norm Error
 ** APO/U refers to Absolute Proportional Over/Undershoot

Table 6.2: Table of ranges and number of data points, with outliers in brackets, from the metrics in Figures 6.15a-6.15e

| Control Method | Combined Statistical Data | | | | |
|-----------------------|---------------------------|---------------|---------------|---------------|---------------|
| | Average Airflow (L/s) | 2-Norm Error | Fall Time (s) | R/F2-NE* | APO/U** |
| | Range | | | | |
| Constant Resistance | 0.0530-0.2368 | 0.1320-0.4641 | 0-2.55 | 0.0110-3.0386 | 0-2.3860 |
| Proportional-Integral | 0.0339-0.2189 | 0.1656-0.4206 | 0-2.63 | 0.0106-3.1497 | 0.0003-4.9780 |
| Proportional | 0.0656-0.2886 | 0.1351-0.3607 | 0-2.55 | 0.0020-1.4428 | 0.0023-2.5640 |
| MPVC1 | 0.0176-0.1026 | 0.1466-0.3636 | 0-1.71 | 0.0081-3.2357 | 0-2.5720 |
| MPVC2 | 0.0172-0.0838 | 0.1089-0.3435 | 0-1.87 | 0.0022-2.2928 | 0.0015-3.3800 |
| | Number of Data Points | | | | |
| Constant Resistance | 60(0) | 60(3) | 151(15) | 422(18) | 422(24) |
| Proportional-Integral | 60(0) | 60(0) | 187(16) | 461(21) | 461(30) |
| Proportional | 60(2) | 60(0) | 143(13) | 384(11) | 384(17) |
| MPVC1 | 60(1) | 60(0) | 200(11) | 506(23) | 506(27) |
| MPVC2 | 60(0) | 60(0) | 197(14) | 517(25) | 517(31) |

* R/F2-NE refers to Rise/Fall 2-Norm Error

** APO/U refers to Absolute Proportional Over/Undershoot

Table 6.1 shows the medians and means and Table 6.2 presents the ranges and number of data points from Figures 6.15a-6.15e. In Table 6.1, the highlighted values are the most desirable values.

To ensure the vital capacity constraint (6.7c) and time constraint (6.7d) are both met, average airflow must be less than 0.15 L/s (assuming a minimum vital capacity of 3 litres). PI control shows a small reduction in airflow, proportional control shows a slight increase and both MPVC approaches show a significant decrease as well as a smaller range. Lower average airflow corresponds to longer measurement periods, therefore MPVC is the best approach for this metric, providing a 64% decrease in average airflow.

The 2-norm of the tracking error indicates how well the participants are able to track the profile; the lower the 2-norm, the better the tracking. PI control shows similar levels of tracking error to the constant valve resistance case, but both proportional and MPVC show a reduction in tracking error with the greatest reduction of 22% shown in MPVC1.

Fall time refers to the time it takes for a participant to reach the new pressure reference value after a step-down change (e.g. black points in Figure 6.11). PI control shows a similar fall time to constant valve resistance, proportional and MPVC2 show a significant decrease by about 0.1s, while MPVC1 shows the biggest improvement with a decrease of 0.15s (22% reduction).

The 2-norm of the rise/fall error refers to the 2-norm tracking error in the time window between a step change in reference and when the pressure reference is reached (i.e. same time window as rise/fall time). PI control shows an increase in the error, whilst proportional control and both MPVC approaches decrease the error. MPVC1 shows the most significant reduction (18%) in rise/fall error.

Absolute proportional overshoot/undershoot refers to the maximum error between profile and measured pressure for one second after the reference has initially been reached (green points in Figure 6.11). PI and proportional control show a similar overshoot/undershoot metric while both MPVC approaches show a reduction with MPVC2 showing the greatest reduction (24%).

6.7 Summary

The high median and mean values of MFA1-3 show that the model and the identification process can accurately model the healthy adult human response to pressure profiles whilst maintaining simplicity in design and efficiency in identification.

Inspection of the data revealed that most of the percentage accuracies below 75% were associated with reaction time (the combined perception and decision delays discussed in Section 6.4.1) to a step increase in the reference profile. The model assumed a

0.3 second reaction time, and although most of the reaction delays were between 0.25 and 0.35, some were longer than 0.45 seconds. These longer reactions create a large error between measured and predicted output thus significantly reducing the prediction accuracy (e.g. note the red crosses for P5 MFA3 and P7/P8 MFA2). This is an issue that could be satisfactorily resolved in future work by adding these delays into the identification process. Reaction time was not incorporated into the identification vector $\hat{\theta}$ in this research as the computational load would have been greatly increased, thus extending the identification time making it impractical with current hardware.

Across all metrics shown in Figures 6.15a-6.15e, MPVC demonstrates a clear improvement in performance and reduction in tracking error when compared to not only the existing clinical research setup, but also proportional control and PI control of the valve. Most significantly, it reduces the 2-norm of the tracking error by 22% and the absolute proportional overshoot/undershoot by 24%. This shows that the accuracy of the participants tracking ability both across the profile and in pressure changes is notably improved with assistance from MPVC. This confirms that the model, identification, and control method could be a viable approach to assist LPP tracking during TMD measurements in a clinical research environment.

An important positive aspect of this study was the usability of the setup. The prevailing feedback received from the participants after testing was that with initial instructions the setup was easy to use and they understood what to do; they were mostly able to perform the intended actions (except those mentioned at the start of Section 6.6.2); they found it easier to attain pressures (particularly higher pressures) with MPVC. This shows that the new setup and MPVC are successful both from a technical perspective as well as patient experience perspective.

Chapter 7

Conclusions and Future Work

Control of lung and airway pressure is a crucial component of research into intracranial pressure (ICP). The use of lung pressure profile (LPP) testing alongside tympanic membrane displacement (TMD) measurements could provide a useful means of early diagnosis of brain pathologies (e.g. tumours). LPP tests involve a patient tracking a given lung pressure reference. However, currently the patient's ability may fall short of the tracking accuracy required.

The addition of pressure control assistance should improve this tracking ability. This thesis has presented the first control approach to assist airway pressure tracking. It employs a novel form of model predictive control (MPC) which manipulates an internal parameter of a model rather than a control input. It controls the airflow out of a hand-held clinical research breathing setup, via actuation of an integrated valve, during LPP reference tracking.

This thesis has attempted to develop three novel concepts. The first is the development of a model which can mimic the tracking response of a patient to a LPP reference. The second is a controller which can actuate a model parameter to improve the tracking response. The third is a model identification procedure which can incorporate the parameter-varying nature of the system to produce an appropriate model.

A simple model was developed which assumed the tracking response relied on the dynamics of the model with linear gain of respiratory muscle force. This was unsuccessful in simulation as the parameters were not realistic values of resistance and inertance. The model was modified to use more realistic values and used a proportional-integral gain of respiratory muscle control. Simulation results proved applicability, and practical experimentation results showed that controlling airflow improves profile tracking by 22% compared to the original clinical research setup. Model predictive valve control (MPVC) provided improved assistance across all metrics compared to the baseline and model-free control methods. Participants stated that MPVC was user-friendly.

This thesis has demonstrated that MPVC improves a person's tracking ability of a LPP reference. Future work will expand upon the number of test subjects to further validate the use of MPVC, with the aim of transferring to a clinical research setting. Additionally, the diversity of test subjects will also be expanded to include a wider age range and a range of health conditions, both related to and unrelated to lung, circulatory and brain physiology.

The analysis of the results showed great promise for the application of MPVC in a clinical research environment. However, it also indicated that there were some shortcomings to the approach taken in this thesis - the model identification procedure used in practical experimentation was adequate but could be improved. Future work will incorporate reaction time (i.e. delays) into the set of identified parameters. Additionally, the model could be expanded to incorporate human learning. Participants stated that as they progressed through the test procedure, they became more confident at generating the specific lung pressures required of them, even though they could not observe any upcoming pressure changes.

With regards to control, given the limitation that a pump cannot be used to actively increase pressure, future work will focus on further reducing overshoot/undershoot. If the average value for overshoot/undershoot could be reduced to ≈ 3 cmH₂O (or less) of the reference pressure, then MPVC would be appropriate in a clinical research setting for LPP tests alongside TMD measurements. Mechanisms to achieve this include: increasing the prediction horizon; increasing the number of valve resistances; incorporating reaction time (i.e. delays) into the set of identified parameters; and developing a multiple model adaptive control strategy to modify the model, based on the reference pressure change.

Future work could also research the possibility of use in other medical disciplines. As this is a respiratory control setup, applications may include, for example, spirometry in order to detect pathologies such as asthma or bronchitis. There could also be potential for use in assessments of physical fitness.

The progression of this research provides a solid foundation for controlling lung pressure during forced expiration. The aim is that it will eventually be used to develop an accessible form of non-invasive diagnostics for cranial pathologies.

Appendix A

Specification Document

2020-12-17 PhD Specification Meeting (UHS team)

These notes capture the UHS team's thoughts and considerations regarding a specification for the feedback/control unit.

It is our hope that this provides guidance on what is a good direction and what will help ensure that the project is useful in our further clinical work, but it should not be taken as limiting or restricting the scope of the research, or precluding exploring any new directions that may arise as the project progresses.

Requirements

Electrical/interfacing

- Outputs to include achieved (sensed) pressure and current target pressure
 - Currently, analogue voltages suit our experimental equipment best (can be recorded in sync with other analogue signals from other equipment)
 - Digital outputs may be of use in the future plus the device should digitally record the signals itself
 - The outputs should be near-real time. We think a 1ms delay would be excellent, 10ms acceptable and 100ms too slow.

Feedback & control

- The device must interact with and thus improve the efforts of a volunteer or patient trying to control the pressure within a disposable breathing tube.
- Target range of achievable/controllable pressures: ± 60 cm H₂O
- Target profiles: arbitrary, e.g. read from CSV file, suggest providing for profile points at ideally 100 Hz
- Target pressure profiles may include rest periods when the participant is able to breathe freely. (Ideally through the mouthpiece and without too much dead-space. Alternatively through the nose or by taking the mouthpiece out.)
- Target pressure profiles should be 20s long at minimum and should be capable of being combined into experimental protocols lasting several minutes or more, with free-breathing breaks between them.
- Pressure change rate achievable: suggest it should be capable of relatively fast steps, e.g. 60 cm H₂O change in 0.25 seconds or faster. Applies to both up- and down-steps
 - This timing is estimated, we considered the target to see a step in blood pressure within $\frac{1}{4}$ of a heart beat assuming a heartrate of 60bpm.
 - Steady state (DC) pressures are also required.
- Must provide a selectable minimum flow rate for non-rest periods.
 - This is to ensure that the subject is not able to alter the pressure in their lungs while the pressure in the tube remains constant. Without a minimum flow rate they could

achieve this by closing their glottis. We don't know how important this, it is likely to be more important in profiles that include a long steady state pressure and less important in profiles with constantly changing pressures. The optimal minimum "leak" flow will need to be determined from experiment. It is a compromise between ensuring the glottis remains open and ensuring that the subjects has enough lung capacity to complete the profile. We have estimated from inspired lung capacity that a minimum flow in the order of 5ml/second should provide at least a 20 second duration study.

- It would be good to be able to control this rate, not necessarily dynamically or to a profile but as a constant per-test-run, e.g. could achieve it by having a manual valve with a position encoder. Optimal rate may be patient-specific.

Some additional thoughts

- Consider a UI for the patient/volunteer that is in the 'Super Mario style' where the landscape represents the target and the character has to be controlled by regulating the pressure.
- Consider options that would include a port for an active control over the reference ground pressure— for example bellows. A consideration at least for literature review, and general awareness.
 - Advantages
 - Ability to control airway pressure more actively
 - Likely to give the volunteer better support in achieving the pressure profile
 - Ability to include negative pressures
 - Disadvantages
 - Risks likely to be higher, e.g. risks of harm from over-action and from re-breathing the same air would likely be greater.
 - Greater infection prevention requirements.
 - Significantly more complicated end product may be less affordable and practical for wide scale clinical use. Could be the deluxe research lab option.

Appendix B

Conventional MPC Framework

A general transfer function takes the form:

$$\frac{y(s)}{u(s)} = \frac{b_{n-1}s^{n-1} + b_{n-2}s^{n-2} + \dots + b_1s + b_0}{s^n + a_{n-1}s^{n-1} + \dots + a_1s + a_0} \quad (\text{B.1})$$

where y is the output and u is the control input.

The transfer function can also be represented as a continuous-time state space model which takes the form:

$$\begin{aligned} \dot{x}(t) &= A_c x(t) + B_c u(t) \\ y(t) &= C_c x(t) + D_c u(t) \end{aligned} \quad (\text{B.2})$$

where x is the system state with initial conditions $x(t_0) = x_0$, $\dot{x}(t)$ is the next system state and A_c , B_c , C_c , D_c are the controller-canonical matrices:

$$A_c = \begin{bmatrix} 0 & 1 & 0 & \dots & 0 & 0 \\ 0 & 0 & 1 & \dots & 0 & 0 \\ \vdots & \vdots & \vdots & & \vdots & \vdots \\ -a_0 & -a_1 & -a_2 & \dots & -a_{n-2} & -a_{n-1} \end{bmatrix}$$

$$B_c = \begin{bmatrix} 0 \\ 0 \\ \vdots \\ 0 \\ 1 \end{bmatrix}$$

$$C_c = \begin{bmatrix} b_0 & b_1 & b_2 & \dots & b_{n-2} & b_{n-1} \end{bmatrix}$$

$$D_c = \begin{bmatrix} 0 \end{bmatrix}$$

The states space model can also be in discrete-time in the form

$$\begin{aligned} x_{k+1} &= Ax_k + Bu_k \\ y_k &= Cx_k + Du_k \end{aligned} \tag{B.3}$$

where $k = 0, 1, 2, \dots$ denotes the sample index.

MPC manipulates the control input u . The objective of MPC is to compute the sequence of control inputs $u_0, u_1, \dots, u_{t_{max}}$ that minimise the infinite horizon cost equation:

$$J = \sum_{k=0}^{\infty} (\Delta u_k^T \hat{Q} \Delta u_k + (x_k - d_k)^T \hat{R} (x_k - d_k)) \tag{B.4}$$

However, to handle to constraints and non-linear systems, MPC uses a finite horizon approximation (i.e. stage cost) equation:

$$J = \sum_{k=k_0}^{k_0+N-1} (\Delta u_k^T \hat{Q} \Delta u_k + (x_k - d_k)^T \hat{R} (x_k - d_k)) \tag{B.5}$$

where N is the prediction horizon (index value), $\Delta u_k = u_k - u_{k-1}$ (i.e. the change in control input variable), $x_k - d_k$ is the state error norm, and \hat{Q} and \hat{R} are the control and state error weighting coefficients respectively. The prediction horizon is the number of time indices ahead of the current time index that the controller can predict the system's tracking trajectory.

The state predictions can also take the matrix form

$$\vec{x}_{t_0} = G\vec{u}_{t_0} + Hx_{t_0} \tag{B.6}$$

with

$$G = \begin{bmatrix} 0 & 0 & \cdots & 0 & 0 \\ B & 0 & \cdots & 0 & 0 \\ AB & B & \cdots & 0 & 0 \\ \vdots & \vdots & \ddots & \vdots & \vdots \\ A^{N-2}B & A^{N-3}B & \cdots & B & 0 \end{bmatrix}$$

$$H = [I, A, A^2, \dots, A^{N-1}]^\top$$

Similarly, the output tracking predictions take the matrix form

$$\vec{y}_{t_0} = G_C \vec{u}_{t_0} + H_C x_{t_0} \quad (\text{B.7})$$

with

$$G = \begin{bmatrix} 0 & 0 & \cdots & 0 & 0 \\ CB & 0 & \cdots & 0 & 0 \\ CAB & B & \cdots & 0 & 0 \\ \vdots & \vdots & \ddots & \vdots & \vdots \\ CA^{N-2}B & CA^{N-3}B & \cdots & CB & 0 \end{bmatrix}$$

$$H = [C, CA, CA^2, \dots, CA^{N-1}]^\top$$

References

- [1] M. C. Thompson, C. T. Freeman, N. O'Brien, A.-M. Hughes, T. Birch, and R. Marchbanks, "Model predictive valve control of lung pressure profile tracking," in *2022 Australian & New Zealand Control Conference (ANZCC)*, pp. 132–137, IEEE, 2022.
- [2] M. C. Thompson, C. T. Freeman, N. O'Brien, A.-M. Hughes, R. Marchbanks, and A. Birch, "Model predictive valve control for lung pressure profile tracking assistance," in *2024 IEEE Conference on Control Technology and Applications (CCTA)*, pp. 624–630, IEEE, 2024.
- [3] M. C. Thompson, C. T. Freeman, N. O'Brien, A.-M. Hughes, T. Birch, and R. Marchbanks, "Model predictive valve control to assist lung pressure profile tracking," *IEEE Transactions on Control Systems Technology*, 2025. (Submitted).
- [4] M. Harary, R. G. Dolmans, and W. B. Gormley, "Intracranial pressure monitoring—review and avenues for development," *Sensors*, vol. 18, no. 2, p. 465, 2018.
- [5] P. H. England, "Deaths associated with neurological conditions in England: 2001 to 2014," 2018.
- [6] A. Monro, "Observations on the structure and functions of the nervous system," *London Medical Journal*, vol. 4, no. 2, pp. 113–135, 1783.
- [7] G. Kellie, "An account of the appearances observed in the dissection of two of three individuals presumed to have perished in the storm of the 3d, and whose bodies were discovered in the vicinity of leith on the morning of the 4th, november 1821; with some reflections on the pathology of the brain: Part i," *Transactions. Medico-Chirurgical Society of Edinburgh*, vol. 1, p. 84, 1824.
- [8] S. Munakomi and J. M. Das, "Intracranial pressure monitoring," in *StatPearls [Internet]*, StatPearls Publishing, 2024.
- [9] R. S. Marshall and S. A. Mayer, *On Call Neurology: On Call Series*. Elsevier Health Sciences, 2007.
- [10] S. Imagebase, "Diagram of blood flow in the heart, lungs and body," 2024. Accessed: 20-09-2024.

- [11] F. P. Tiecks, C. Douville, S. Byrd, A. M. Lam, and D. W. Newell, "Evaluation of impaired cerebral autoregulation by the valsalva maneuver," *Stroke*, vol. 27, no. 7, pp. 1177–1182, 1996.
- [12] R. Zhang, C. G. Crandall, and B. D. Levine, "Cerebral hemodynamics during the valsalva maneuver: insights from ganglionic blockade," *Stroke*, vol. 35, no. 4, pp. 843–847, 2004.
- [13] H. Prabhakar, P. Bithal, A. Suri, G. Rath, and H. Dash, "Intracranial pressure changes during valsalva manoeuvre in patients undergoing a neuroendoscopic procedure," *min-Minimally Invasive Neurosurgery*, vol. 50, no. 02, pp. 98–101, 2007.
- [14] L. Hill, *The physiology and pathology of the cerebral circulation: an experimental research*. J. & A. Churchill, 1896.
- [15] A. B. Hansen, J. S. Lawley, C. A. Rickards, E. J. Howden, S. Sarma, W. K. Cornwell 3rd, S. B. Amin, H. Mugele, K. Marume, C. Possnig, *et al.*, "Reducing intracranial pressure by reducing central venous pressure: assessment of potential countermeasures to spaceflight-associated neuro-ocular syndrome," *Journal of Applied Physiology*, vol. 130, no. 2, pp. 283–289, 2021.
- [16] J. Gisolf, J. Van Lieshout, K. Van Heusden, F. Pott, W. Stok, and J. Karemaker, "Human cerebral venous outflow pathway depends on posture and central venous pressure," *The Journal of physiology*, vol. 560, no. 1, pp. 317–327, 2004.
- [17] P. Holmlund, A. Eklund, L.-O. Koskinen, E. Johansson, N. Sundström, J. Malm, and S. Qvarlander, "Venous collapse regulates intracranial pressure in upright body positions," *American Journal of Physiology-Regulatory, Integrative and Comparative Physiology*, vol. 314, no. 3, pp. R377–R385, 2018.
- [18] R. J. Marchbanks, A. Reid, A. M. Martin, A. P. Brightwell, and D. E. Bateman, "The effect of raised intracranial pressure on intracochlear fluid pressure: three case studies.," *British journal of audiology*, vol. 21 2, pp. 127–30, 1987.
- [19] A. Reid, R. Marchbanks, D. Burge, A. Martin, D. Bateman, J. Pickard, and A. Brightwell, "The relationship between intracranial pressure and tympanic membrane displacement," *British journal of audiology*, vol. 24, no. 2, pp. 123–129, 1990.
- [20] C. M. Campbell-Bell, A. A. Birch, D. Vignali, D. O. Bulters, and R. J. Marchbanks, "Reference intervals for the evoked tympanic membrane displacement measurement: a non-invasive measure of intracranial pressure," *Physiological Measurement*, vol. 39, 2018.
- [21] W. K. El-Bouri, D. Vignali, K. G. Iliadi, D. O. Bulters, R. J. Marchbanks, A. A. Birch, and D. M. Simpson, "Quantifying the contribution of intracranial pressure and arterial blood pressure to spontaneous tympanic membrane displacement," *Physiological Measurement*, vol. 39, 2018.

- [22] J. H. Dräger and B. Dräger, “The pulmotor: A device for positive pressure ventilation,” 1907. Historical documentation.
- [23] P. Drinker and L. A. Shaw, “An apparatus for the prolonged administration of artificial respiration: I. a design for adults and children,” *Journal of Clinical Investigation*, vol. 7, no. 2, pp. 229–247, 1929.
- [24] G. Goodwin, S. Graebe, and M. Salgado, “Classical pid control,” *Control system design*, vol. 240, pp. 157–177, 2001.
- [25] F. Tehrani, M. Rogers, T. Lo, T. Malinowski, S. Afuwape, M. Lum, B. Grundl, and M. Terry, “A dual closed-loop control system for mechanical ventilation,” *Journal of clinical monitoring and computing*, vol. 18, pp. 111–129, 2004.
- [26] A. C. Lua, K. C. Shi, and L. P. Chua, “Proportional assist ventilation system based on proportional solenoid valve control,” *Medical engineering & physics*, vol. 23, no. 6, pp. 381–389, 2001.
- [27] J. Reinders, B. Hunnekens, F. Heck, T. Oomen, and N. van de Wouw, “Adaptive control for mechanical ventilation for improved pressure support,” *IEEE Transactions on Control Systems Technology*, vol. 29, no. 1, pp. 180–193, 2020.
- [28] S. Yan, H. ZHANG, and L. Zihao, “Mechanical ventilation intelligent control technology based on fuzzy adaptive pid,” in *2019 IEEE 8th International Conference on Fluid Power and Mechatronics (FPM)*, pp. 156–163, IEEE, 2019.
- [29] I. M. Mehedi, H. S. Shah, U. M. Al-Saggaf, R. Mansouri, and M. Bettayeb, “Adaptive fuzzy sliding mode control of a pressure-controlled artificial ventilator,” *Journal of Healthcare Engineering*, vol. 2021, no. 1, p. 1926711, 2021.
- [30] H. Hazarika and A. Swarup, “Application of an optimal ilc algorithm for flow rate tracking of a ventilator system,” in *2020 First IEEE International Conference on Measurement, Instrumentation, Control and Automation (ICMICA)*, pp. 1–6, IEEE, 2020.
- [31] S. Sakthiya Ram, C. Kumar, A. Ramesh Kumar, and T. Rajesh, “Hybrid optimization techniques based automatic artificial respiration system for corona patient,” *Automatika*, vol. 63, no. 2, pp. 226–243, 2022.
- [32] T. Nemoto, G. E. Hatzakis, C. W. Thorpe, R. Olivenstein, S. Dial, and J. H. Bates, “Automatic control of pressure support mechanical ventilation using fuzzy logic,” *American journal of respiratory and critical care medicine*, vol. 160, no. 2, pp. 550–556, 1999.
- [33] M. Scheel, A. Berndt, and O. Simanski, “Iterative learning control: An example for mechanical ventilated patients,” *IFAC-PapersOnLine*, vol. 48, no. 20, pp. 523–527, 2015.

- [34] A. F. de Castro and L. A. B. Tôrres, “Iterative learning control applied to a recently proposed mechanical ventilator topology,” *IFAC-PapersOnLine*, vol. 52, no. 1, pp. 154–159, 2019.
- [35] G. Perchiazzi, C. Rylander, M. Pellegrini, A. Larsson, and G. Hedenstierna, “Monitoring of total positive end-expiratory pressure during mechanical ventilation by artificial neural networks,” *Journal of clinical monitoring and computing*, vol. 31, pp. 551–559, 2017.
- [36] A. Peine, A. Hallawa, J. Bickenbach, G. Dartmann, L. B. Fazlic, A. Schmeink, G. Ascheid, C. Thiemermann, A. Schuppert, R. Kindle, *et al.*, “Development and validation of a reinforcement learning algorithm to dynamically optimize mechanical ventilation in critical care,” *NPJ digital medicine*, vol. 4, no. 1, p. 32, 2021.
- [37] G. Männel, C. Hoffmann, and P. Rostalski, “A robust model predictive control approach to intelligent respiratory support,” in *2018 IEEE Conference on Control Technology and Applications (CCTA)*, pp. 12–17, IEEE, 2018.
- [38] D. Acharya, S. K. Pradhan, and D. K. Das, “Explicit model predictive control design for artificial respiratory ventilation system,” *International Journal of Dynamics and Control*, vol. 12, no. 6, pp. 1851–1859, 2024.
- [39] B. Fuerst, T. Mansi, F. Carnis, M. Sälzle, J. Zhang, J. Declerck, T. Boettger, J. Bayouth, N. Navab, and A. Kamen, “Patient-specific biomechanical model for the prediction of lung motion from 4-d ct images,” *IEEE transactions on medical imaging*, vol. 34, no. 2, pp. 599–607, 2014.
- [40] C.-L. Lin, M. H. Tawhai, and E. A. Hoffman, “Multiscale image-based modeling and simulation of gas flow and particle transport in the human lungs,” *Wiley Interdisciplinary Reviews: Systems Biology and Medicine*, vol. 5, no. 5, pp. 643–655, 2013.
- [41] A. Ben-Tal, “Simplified models for gas exchange in the human lungs,” *Journal of theoretical biology*, vol. 238, no. 2, pp. 474–495, 2006.
- [42] B. Hunnekens, S. Kamps, and N. Van De Wouw, “Variable-gain control for respiratory systems,” *IEEE Transactions on Control Systems Technology*, vol. 28, no. 1, pp. 163–171, 2018.
- [43] L. Hao, Y. Shi, M. Cai, S. Ren, Y. Wang, H. Zhang, and Q. Yu, “Dynamic characteristics of a mechanical ventilation system with spontaneous breathing,” *IEEE Access*, vol. 7, pp. 172847–172859, 2019.
- [44] K. Y. Volyanskyy, W. M. Haddad, and J. M. Bailey, “Pressure-and work-limited neuroadaptive control for mechanical ventilation of critical care patients,” *IEEE transactions on neural networks*, vol. 22, no. 4, pp. 614–626, 2011.

- [45] B. Diong, A. Rajagiri, M. Goldman, and H. Nazeran, “The augmented ric model of the human respiratory system,” *Medical & biological engineering & computing*, vol. 47, no. 4, pp. 395–404, 2009.
- [46] M. Schmidt, B. Foitzik, O. Hochmuth, and G. Schmalisch, “Computer simulation of the measured respiratory impedance in newborn infants and the effect of the measurement equipment,” *Medical engineering & physics*, vol. 20, no. 3, pp. 220–228, 1998.
- [47] B. Juroszek and J. Stanisławski, “Synthesis of the structure of the respiratory system in forced expiration,” 2003.
- [48] A. Rajagiri and B. Diong, “Evaluation of augmented ric model of child respiratory impedance based on impulse oscillometry data,” in *2006 IEEE Region 5 Conference*, pp. 291–295, IEEE, 2006.
- [49] NHS, “Spirometry,” 2024. Accessed: 03-09-2024.
- [50] D. M. Wolpert, Z. Ghahramani, and J. R. Flanagan, “Perspectives and problems in motor learning,” *TRENDS in Cognitive Sciences*, vol. 5, no. 11, pp. 487–494, 2001.
- [51] M. B. Rhudy, R. A. Salguero, and K. Holappa, “A kalman filtering tutorial for undergraduate students,” *International Journal of Computer Science & Engineering Survey*, vol. 8, no. 1, pp. 1–9, 2017.
- [52] L. Ljung, *System identification: Theory for the user*. Prentice Hall, 2nd ed., 1998.
- [53] G. R. Grice, R. Nullmeyer, and V. A. Spiker, “Human reaction time: Toward a general theory,” *Journal of Experimental Psychology: General*, vol. 111, no. 1, p. 135, 1982.